UNIVERSITA' VITA-SALUTE SAN RAFFAELE

CORSO DI DOTTORATO DI RICERCA INTERNAZIONALE IN MEDICINA MOLECOLARE

CURRICULUM IN GENE AND CELL THERAPY

Characterisation of Mucopolysaccharidosis murine models to develop pre-clinical gene therapy strategies

DoS: Dr. Maria Ester Bernardo

Second Supervisor: Dr. Francesco Dazzi

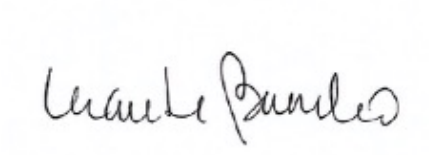
Tesi di DOTTORATO di RICERCA di Margherita Berti

Matr: 017572

Ciclo di dottorato XXXVI

SSD: MED/03 - BIO/11 – BIO/13

Anno Accademico 2022/2023



CONSULTAZIONE TESI DI DOTTORATO DI RICERCA

Il/la sottoscritto/*I Margherita Berti*

Matricola / *registration number 017572*

nata a/ *born at Florence*

il/*on 02/03/1994*

autore della tesi di Dottorato di ricerca dal titolo / *author of the PhD Thesis titled*

Generation, characterisation, and selection of a newly developed CRISPR-Cas9 murine model of Mucopolysaccharidosis type IVA

AUTORIZZA la Consultazione della tesi / AUTHORIZES *the public release of the thesis*

X NON AUTORIZZA la Consultazione della tesi per 12 mesi /DOES NOT AUTHORIZE *the public release of the thesis for* 12 *months*

a partire dalla data di conseguimento del titolo e precisamente */ from the PhD thesis date,*

specifically Dal / *from* 15/11/2023 Al / *to 15/11/2024*.

Poiché /*because*:

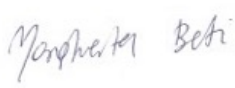
□ l'intera ricerca o parti di essa sono potenzialmente soggette a brevettabilità/ *The whole project or part of it might be subject to patentability;*

X ci sono parti di tesi che sono già state sottoposte a un editore o sono in attesa di pubblicazione/ *Parts of the thesis have been or are being submitted to a publisher or are in press;*

□ la tesi è finanziata da enti esterni che vantano dei diritti su di esse e sulla loro pubblicazione/ *the thesis project is financed by external bodies that have rights over it and on its publication.*

Si rende noto che parti della tesi sono indisponibili in relazione all'utilizzo di dati tutelati da segreto industriale **(da lasciare solo se applicabile)** /*Please Note: some parts of the thesis are not available in relation to the norm of the use of information protected by trade secret* ***(To leave only if relevant)***

E' fatto divieto di riprodurre, in tutto o in parte, quanto in essa contenuto / *Copyright the contents of the thesis in whole or in part is forbidden*

Data /Date 14/11/2023 Firma /Signature 

DECLARATION

This thesis has been:

- composed by myself and has not been used in any previous application for a degree.

Throughout the text I use both 'I' and 'We' interchangeably.

- has been written according to the editing guidelines approved by the University.

Permission to use images and other material covered by copyright has been sought and obtained. For the following image/s (specify), it was not possible to obtain permission and is/are therefore included in thesis under the "fair use" exception (Italian legislative Decree no. 68/2003).

All the results presented here were obtained by myself, except for:

1) pQCT and histomorphometrical data *were performed in collaboration with Dr Simona Bolamperti and Isabella Villa,* Osteoporosis and bone and mineral metabolism Unit, San Raffaele Scientific Institute, Milan, Italy

2) Immunohistopathological stainings *were performed in collaboration with Dr Francesca Sanvito, Dr Rossana Norata and Dr Martina Rocchi from the* Pathology Unit, Department of Experimental Oncology, IRCCS San Raffaele Scientific Institute, Milan, Italy

3) Behavioural experiments were *were performed in collaboration with Dr Patrizia D'Adamo from the* Mouse Behavior Facility, San Raffaele Scientific Institute, Milan, Italy.

4) *Computed-Tomography Scan were performed in collaboration with Dr Antonello Spinelli from the* Preclinical imaging Facility, San Raffaele Scientific Institute, Milan, Italy.

All sources of information are acknowledged by means of reference.

Acknowledgements

For the purpose of this project, I would like to thank Prof. Maria Ester Bernardo, Prof. Alessandro Aiuti and their teams for the practical support in the everyday laboratory duties. In particular, I would like to thank Dr. Stefania Crippa for her mentorship and support throughout this project. I would like to acknowledge all of our collaborators at Ospedale San Raffaele. In particular, we would like to thank Dr Simona Bolamperti and Isabella Villa for performing the pQCT analyses present in this study. Special thanks to Dr Francesca Sanvito and her team for performing the immunohistochemical stainings on all of our samples. We would like to acknowledge Dr Antonello Spinelli for his support with the Computed tomography scan and Dr Patrizia D'Adamo and her team for performing the open field tests on our models, alongside our technician Raisa Jofra-Hernandez. Finally, we would like to thank our external collaborators at the University of Modena, Prof. Nicola Volpi and Dr. Fabio Galeotti for helping us setting up a protocol for keratan sulphate detection in mouse samples, on Mass Spectrometry.

"Nevertheless, she persisted".
Senator Mitch McConnell

Alla mia famiglia, ai miei nonni.

Abstract

Mucopolysaccharidoses (MPSs) are a group of 11 diseases affecting ~0.1% children with genetic disease. Symptoms develop from enzymatic deficiencies disrupting glycosaminoglycans' (GAGs') degradation. Among different types, MPS IVA arises from deficient N-acetylgalactosamine-6-sulphate sulphatase (GALNS), causing accumulation of undegraded substrates and severe skeletal and growth impairment, dramatically impacting on patients' quality of life. Standard treatment for MPS combines enzyme replacement therapy and, in selected cases, allogeneic haematopoietic stem cell transplant that limit GAGs accumulation and alleviate symptoms, though without achieving a full correction of the skeletal phenotype. Recent studies have proven *ex-vivo* gene therapy with haematopoietic stem progenitor cells (HSPC-GT) a safe therapy in 8 paediatric patients of Mucopolysaccharidosis type I Hurler (MPSIH), with supranormal enzyme levels and initial clinical response, also at the skeletal level (Gentner et al., 2021). Based on these promising results, HSPC-GT may be considered a potential treatment option for other lysosomal storage disorders with skeletal involvement such as MPSIVA. This diseases, however, still lacks an appropriately representative model. For this reason, we have characterised a new model generated by CRISPR-Cas9, using gRNAs targeting the *Galns* locus in C57BL6/J mice. We have obtained four different genotypic variants for *Galns* deletion (*Galns*$^{-/-}$), which have undergone a biochemical morphological, behavioural, and histopathological characterisation to select the *Galns*$^{-/-}$ (knock-out, KO) model with the most representative skeletal phenotype. Biochemical analyses have confirmed all KO mice to have no GALNS activity, though only one variant out of four showed clear signs of skeletal disease, with reduced weight gain over time and shorter long bones on CT-scan analysis. In line with these results, the same KO variant showed differences in bone resistance and bone composition on pQCT and appeared the weakest on grip-strength test. Additionally, a number of pro-inflammatory markers appeared upregulated in our selected mouse model, on RT-qPCR. In this study, we achieved the generation of a novel murine model for MPSIVA and completed its all-round characterisation. Production of this new mouse model will favour the development and testing of innovative treatments for MPSIVA, including HSPC-GT approaches

Table of Contents

Abstract *6*

1. Introduction *13*

1.1 Lysosomal Storage disease **13**

1.2 The Lysosome **14**

1.3 Lysosomal storage disease **19**

1.1 *SUMF1* mediated activation of Galns **20**

1.2 Mucopolysaccharidoses (MPSs) **20**

1.2.1 Clinical Manifestations 20

1.2.2 MPS classification 21

1.2.1 MPS IVA 24

1.2.2 Genetic Background 25

1.2.3 MPSIVA diagnosis 27

1.2.4 GALNS activity in KS and C6S degradation 28

1.3 Glycosaminoglycans **30**

1.4 Keratan sulphate **31**

1.5 LSD-associated inflammatory pathways **34**

1.5.1 MMPs elevation in pathological context 34

1.5.2 Reduced antioxidant defence in MPS 35

1.5.3 TGF-β hyperactivity 35

1.5.4 Fibroblast growth factors signalling altered by GAGs accumulation 36

1.5.5 GAGs accumulation stimulate Toll-like receptor signalling pathways 37

1.5.6 Inflammasome-mediated response can be activated by lysosomal dysruption 38

1.6 ER-stress in MPSs **43**

1.7 Skeletal manifestations in man and available mouse MPSIVA models **45**

1.8 Current therapeutic options **49**

1.8.1 Enzyme Replacement Therapy 49

1.8.2 Surgery 51

1.8.3 HSCT 52

1.9 Proposed novel therapies and preliminary data. 54

2 Aim of the work 57

3 Results 58

3.1 Generation of a murine model of MPSIVA by CRISPR-Cas9 58

3.1.1 Whole Blood composition 59

3.1.2 GALNS protein detection and activity in KO mice 60

3.1.3 KS in plasma and urine samples at different timepoints 62

3.2 Morphological characterisation of MPSIVA mouse models 63

3.2.1 KO7 appear smaller in weights than all other groups. 63

3.2.1 Reduced length of femurs and tibiae of KO7 mice. 64

3.2.2 Reduction in Cortical Area and SSI of KO7s compared to WTs. 65

3.3 Histopathological findings 66

3.4 Motor and behavioural functions 67

3.5 Confirmatory analysis on selected model 70

3.5.1 Genetic mechanisms 70

3.5.2 Histo-morphometry analyses of tibiae 70

3.5.3 Pro-inflammatory markers appear upregulated in KO7 mouse organs 71

3.5.4 ER-Stress evaluation. 72

4 Discussion 74

5 Limitations of the study 84

6 Material and Methods 85

6.1 Model generation by sgRNA CRISPR-Cas9 85

6.1.1 Genotype 86

6.1.2 Off-target pathogenic variants evaluation on selected model 87

6.1.3 Back-crossing 88

6.1.4 RNA extraction 88

6.1.5 RT-qPCR pre-amplification (pre-Amp) 89

6.1.6 Protein extraction 90

6.1.7 Western Blot 90

6.2 Biochemical analysis 91

6.2.1 Complete Blood Count 91

6.2.2 Enzymatic Activity Assay....91
6.2.3 KS accumulation detection by ELISA....92
6.2.1 KS accumulation detection by HPLC-MS(SIR) 92
6.2.2 Creatinine measurement....93
6.3 Inflammatory profiling 93
6.3.1 Quantification of inflammatory markers by RT-qPCR 93
6.4 Morphological analysis 95
6.4.1 Computed tomography scan 95
6.4.2 Histo-morphometry....96
6.5 Histopathological analyses 97
6.6 Motor and Behavioural tests 98
6.6.1 Open field test. 98
6.6.2 Rotarod....98
6.6.3 Grip-Strength test....99
6.7 Statistical analysis 99
7 Appendix 100
7.1 CBC analysis of whole blood samples from female mice models at different time points 100
7.2 WB of GALNS expression in liver samples from 5-months-old mouse models, full picture of analysed membranes.....101
7.3 Off-target pathogenic variants screening 102
7.4 Alternative Open Reading Frame sequences 103
7.4.1 Murine Galns ORF1 (WT) plasmid sequence: 103
7.4.2 Murine Galns ORF2 plasmid sequence:....104
7.5 Complete results of Inflammatory profiling of mice. 105
7.6 CT scan measurements 106
7.7 pQCT complete analysis....108
7.8 Histo-morphometry on female WT and KO7 models 109
7.9 Motor and Behavioural tests complete....109

8 References 110

Acronyms and abbreviations

4MU	4-Methyl-umbellyferone
AAV9	Adeno-associated virus serotype 9
ACK	Ammonium-chloride-potassium
ATF6	Activating transcription factor 6
ADL	Activity of daily living
ARSB	Arysulphatase B
ATF6	Activating transcription factor 6
BM	Bone marrow
BMD	Bone mineral density
BMP	Bone morphogenetic proteins
BSA	Bovine serum albumin
BSAP	bone alkaline phosphatase
C4S,	Chondroitin 4 sulphate
C6S	Chondroitin 6 sulphate
CBC	Complete blood count
CBCT	Cone beam computed tomography
CCV	Clathrin-coated vesicles
CDS	Coding sequence
CHOP	C/EBP homologous protein
CNS	Central nervous system
CRISPR	Clustered regularly interspaced short palindromic repeats
CREB	Camp response element-binding protein
CS	Chondroitin sulphate
CT	Computed tomography
DAMP	Danger-associated molecular pattern
DBS	Dried blood spot
DR4	Death domain-containing receptor 4
DR5	Death domain-containing receptor 5
DcR2	Decoy receptor 2
DMEM	Dulbecco's modified eagle medium
DNA	Deoxyribonucleic acid
DS	Dermatan sulphate
ECM	Extra-cellular matrix
EDEM	ER-degradation-enhancing-α-mannidose-like protein

EDTA	Ethylenediaminetetraacetic acid
eIF2α	Eukaryotic initiation factor 2
ELISA	Enzyme-linked immunosorbent assay
EMA	European medical agency
ER	Endoplasmic reticulum
ERAD	Endoplasmic-reticulum-associated protein degradation
ERN2	Endoplasmic reticulum to nucleus signalling 2
ESCs	Embryonic stem cells
ERT	Enzyme replacement therapy
FBS	Foetal bovine serum
FDA	Food and Drug Administration
FEV1	Forced Expiratory Volume in the 1st second
FGF	Fibroblast growth factors
FP	Forward primer
FVC	Forced vital capacity
FXR	Farnesoid X receptor
G418	Geneticin^{tm}
GAG	Glycosamminoglycans
GALNS	N-acetylglucosamine-6-sulphate sulphatase
GE	Gene editing
GLB1	Galactosidase beta 1
GlcNac	N-acetylglucosaminyl-1
GLP	Good laboratory practice
GM	Ganglioside monosialic acid
GM2	Ganglioside monosialic acid 2
GM3	Ganglioside monosialic acid 3
GNS	N-acetylglucosamine-6-sulfatase
GP	Growth plate
GT	Gene therapy
GUSB	Glucuronidase beta
GvHD	Graft-vs-Host disease
HA	Hyaluronic acid
HEK293T	Human embryonic kidney 293T
HGB	Haemoglobin
HGSNAT	Heparan-alpha-glucosaminide N-acetyltransferase
HLA	Human leukocyte antigen

HRP	Horseradish peroxidase
HS	Heparan sulphate
HSCT	Haematopoietic stem cell transplant
HSPC	Haematopoietic stem progenitor cells
HPLC	High-performance liquid chromatography
HYAL1	Hyaluronidase 1
IDS	Iduronate 2-sulfatase
IDTE	1X TE solution
IDUA	Alpha-L-iduronidase
IGHM	Immunoglobulin heavy constant mu
IHC	Immunohistochemistry
IL	Interleukin
IL-1	Interleukin-1
IMDM	Iscove's modified Dulbecco’s medium
IRE1	Inositol requiring 1
iPSC	Induced pluripotent stem cell
IRAK1	Interleukin-1 receptor-associated kinase 1
IRAK2	Interleukin-1 receptor-associated kinase 2
IRAK	Interleukin-1 receptor-associated kinase 4
IRCCS	Istituto di Ricovero e Cura a Carattere Scientifico
ITI	Intertrial interval
JNK	Jun N-terminal kinase
KO	Knock-out
KS	Keratan sulphate
LAMP	Lysosome-associated membrane protein
LC-MS	Liquid Chromatography Mass Spectrometry
LIMP-2	Lysosomal integral membrane protein 2
LSD	Lysosomal storage disease
LV	Lentiviral vector
LYMP	Lymphocytes
M6P	Mannose-6-phosphate
M6PR	Mannose-6-phosphate receptor
MCP	Monocyte chemoattractant protein
MIP	Macrophage inflammatory protein
MITF	Melanocyte inducing transcription factor
MMP	Matrix metalloproteinases

MON	Monocyte
MPS	Mucopolysaccharidosis
MPSI	Mucopolysaccharidosis type I
MPSIH	Mucopolysaccharidosis type I-Hurler
MPSIIA	Mucopolysaccharidosis type IIA
MPSIIB	Mucopolysaccharidosis type IIB
MPSIII	Mucopolysaccharidosis type III
MPSIIIA	Mucopolysaccharidosis type IIIA
MPSIV	Mucopolysaccharidosis type IV
MPSIVA	Mucopolysaccharidosis type IVA
MPSIX	Mucopolysaccharidosis type IX
MPSVI	Mucopolysaccharidosis type VI
MPSVII	Mucopolysaccharidosis type VII
MRI	Magnetic resonance imaging
MS	Mass spectrometry
MSC	Mesenchymal stromal cells
MSD	Multiple sulphatase deficiency
NAGLU	N-acetyl-alpha-glucosaminidase
NEUT	Neutrophil
NLRP3	Nlr family pyrin domain containing 3
NO	Nitric oxide
NPC2	Npc intracellular cholesterol transporter 2
OA	Osteoarthritis
OBs	Osteoblasts
OD	Optical density
OMIM	Online Mendelian Inheritance in Man
OPG	Osteoprotegerin
ORF	Open-reading frame
PAM	Protospacer adjacent motif
PAPS	Phosphoadenosine 5’-sulphate
PB	Peripheral blood
PBMC	Peripheral blood mononuclear cell
PBS	Phosphate buffered saline
PCR	Polymerase chain reaction
PG	Proteoglycan
PGC-1α	Proliferator-activated receptor gamma coactivator 1-alpha

PGK	Phosphoglycerate kinase
PLT	Platelet
Pre-AMP	Pre-amplification
PERK	PKR-like ER kinase
PNS	Peripheral nervous system
PQCT	Peripheral quantitative computed tomography
RANK	Receptor activator of NF-κb
RANKL	Receptor activator of NF-κb ligand (RANKL)
RER	Rough endoplasmic reticulum
RNA	Ribonucleic acid
ROS	Reactive oxygen species
RP	Reverse primer
RT-qPCR	Quantitative reverse transcription polymerase chain reaction
SGSH	N-sulfoglucosamine sulfohydrolase
SSI	Stress-strain index
StD	Standard deviation
TAB1	Transforming growth factor-β (TGF-β)-activated kinase 1 binding protein 1
TAB2	Transforming growth factor-β (TGF-β)-activated kinase 1 binding protein 2
TAK1	Transforming growth factor-β (TGF-β)-activated kinase 1
TBS	Tris buffered saline
TF	Transcription factor
TFE3	Transcription factor binding to IGHM enhancer 3
TFEB	Transcription factor EB
TFEC	Transcription factor EC
TGF	Transforming growth factor
TGX	TRIS-glycine buffer solution 10X
TIGET	Telethon-Institute for Gene Therapy
TIMP	Tissue inhibitors of metalloproteinase
TK	Thymidine kinase
TLR4	Toll-like receptor 4
TNF	Tumour necrosis factor
TRAF6	TNF receptor associated factor 6
TRAIL	TNF-related apoptosis-inducing ligand
TRAIL2	TRAIL-receptor 2
TGN	*Trans*-Golgi network
UDP	Uridine diphosphate glucose

UPR	Unfolded-protein response
USA	United States of America
WB	Western blot
WBC	White blood cell
WT	Wild-type
XBP1	X-box binding protein 1

Table of Figures

Figure 1 The discovery of LSDs, a timeline. 14
Figure 2 Lysosomal enzymes' biosynthesis and transport. 18
Figure 3 The lysosome under physiological or pathological conditions. 19
Figure 4 Main symptom of MPSIVA. 25
Figure 6 Overview of the principal pathogenic variants associated with GALNS. 27
Figure 6 KS degradation process and related disorders. 29
Figure 7 Keratan Sulphate structure and function. 33
Figure 8 Effect of TRAIL on bone development. 38
Figure 9 Inflammatory pathways associated with GAG accumulation and lysosomal disruption. 40
Figure 10 Effect of IL-1B on OCs and OBs 41
Figure 11 Higher HGF secretion inhibit OBs formation and activities, while increasing bone resorption. 43
Figure 12 UPR mechanism of action. 44
Figure 13 Summary of available mouse and rat models for MPSIVA. 49
Figure 14 Schematic representation of standard HSCT procedure. 53
Figure 15 HSPC-GT strategy. 56
Figure 16 Obtained variants of the pathogenic mutation induced by CRISPR-Cas9. 58
Figure 17 Characterisation experimental plan of MPSIVA mouse model. 59
Figure 18 Complete Blood Count analysis of whole blood of male mice. 60
Figure 19 Evaluation of Galns expression and activity in KO and WT. 61
Figure 20 Genetic analysis of KO mice. 62
Figure 21 ELISA Assay to detect KS accumulation in plasma. 62
Figure 22 Comparison between KS detection on ELISA Assay vs. HPLC-MS(SIR). 63
Figure 23 Weight growth over time. 64
Figure 24 Measures of the tibiae and femurs' length on CT-scan. 65
Figure 25 pQCT results at 5 months endpoint. 66
Figure 26 Haematoxylin and Eosin staining of the knee joint. 67
Figure 27 Open field test results. 68
Figure 28 Grip strength test results at 5 months of age. 69
Figure 29 Summary of results from models' characterisation 69
Figure 30 Example of potentially mutated region sequence, aligned with the genome of a representative KO7 mouse. 70
Figure 31 Histomorphometry results of males at 3 and 5 months. 71
Figure 32 Representative results of inflammatory markers in kidney, liver, and spleen tissues from our mouse models. 72

Figure 33 RT-qPCR analysis of the expression of biomarkers of ER-stress in samples of kidney retrieved from WT and KO7 mice. 73
Figure 34 Experimental plan of transduction of hMSCs with mutated or WT GALNS. 83
Figure 35 Schematic representation of CRISPR-Cas9 strategy employed to generate a KO pathogenic variant on the Galns-encoding sequence of C57BL/6J mice. 85
Figure 36 Measurements retrieved from total body CT-Scans of mice models. 96
Figure 37 Representative picture of pQCT scan on tibia. 97
Figure 38 Results from CBC in female mice at time points of 2, 4 and 8 months of age. Analysis performed on samples retrieved from WT and KO female mice at 2 (n=6) and 4 months of age (n≥5). Only WT (n=6) and KO7 (n=6) mice were evaluated at 8 months timepoint. Data are represented as single values with means +/- StD. Empty symbols represent the females. Two-Way ANOVA (non-parametric; *p-value<0.03; **p-value<0.0021; Bonferroni test for correction). 100
Figure 39 Results from 5-months-old liver samples evaluated by WB. 101
Figure 40 RT-qPCR results of inflammatory markers screening on spleen samples of WTs and KOs mice. 105
Figure 41 RT-qPCR results of inflammatory markers screening on Liver samples of WTs and KOs mice 105
Figure 42 Gender-matched results from CT-scan analysis of the anterior paws. 106
Figure 43 Gender-matched measurements of the craniofacial bones on CT scan. 107
Figure 44 Analysis on pQCT of the bone structure of the tibia of our female mouse models. 108
Figure 45 Histo-morphometrical analysis on the tibia of WT and KO7 female mice. 109
Figure 46 Complete analysis of Rotarod and Grip Strength test at 3 and 5 months timepoint 109

Table 1 Summary of recognised MPS types and subtypes. 21
Table 2 PCR protocol for MPSIVA mouse models' genotyping 86
Table 3 PCR Protocol for off-target pathogenic variants. 87
Table 4 Pfu Taq Polymerase PCR protocol to screen for off-target pathogenic variants. 87
Table 5 RT-qPCR protocol for pre-amplification of Galns 89
Table 6 RT-qPCR protocol for gene expression quantification, after pre-Amp. 89
Table 7 Panel of Biomarkers for inflammatory profiling. 94
Table 8 List of ER-stress associated biomarkers evaluated in two representative organs of WT and KO7 mice. 95
Table 9 Panel of genes potentially affected by off-target mutations. 102

1. Introduction

1.1 Lysosomal Storage disease

Lysosomal storage disease (LSD) is an umbrella definition for 70 genetic diseases that arise from altered lysosome function. The largest portion of LSDs is composed of autosomal recessive conditions, though a minority of three diseases are inherited in an X-linked manner. The pathogenic mechanism underlying LSDs involves variants to genes encoding for lysosomal proteins, including enzymes like proteases and glycosidases, transporters, integral membrane proteins, enzyme modifiers or activators. Alterations to such proteins lead to a faulty degrading mechanism and substrate accumulation in the lysosomes, which, in turn, alters cellular metabolism and may induce apoptosis (Platt et al., 2018).

However, the identification of LSDs and their underlying mechanisms has required many years (Figure 1). Although lysosomes were identified towards the mid 1950s, the first clinical descriptions of LSD's phenotypes date back to the 19th century, as reviewed by Mehta *et al.* (Mehta et al., 2006). The organelle is the principal proteolytic structure aimed at processing extra- and intra-cellular macromolecules, to discard or recycle them. Lysosomes act by means of endosomes and autophagosomes' fusion with the molecules to be disposed and activation of autophagic mechanisms (Trivedi et al., 2020). Details of the lysosomes' activity are described later in this chapter.

Shortly after lysosome recognition, the biochemical alterations at the basis of LSDs were also unveiled and the organelles were described as cellular catabolic stations (De Duve et al., 1955; Novikoff et al., 1956). This led to further in depth studies that clarified the association between specific diseases, their relative deficient enzymes and the primary storage substances (Hers, 1963; van Hoof, 1974). In the following twenty years, understanding the mechanisms of action of protein trafficking became the main effort of researchers, in the attempt of unravelling the pathophysiological mechanisms behind LSDs and developing novel therapeutic strategies to tackle these conditions. Results from this effort provided essential information about extra- and intercellular trafficking of lysosomal enzymes, contributing to the development of innovative therapies like the first enzyme replacement therapies (ERTs) (Barton et al., 1991, 1990; Beck, 2001; Kroos et al., 2012; Sly and Fischer, 1982). More recently, the advent of innovative technologies to directly modify the genome, such as gene editing (GE), has allowed scientists to develop new animal models of diseases

by creating knock-out (KO) organisms. At the same time, the refinement of Mass Spectrometry (MS) has improved the study and characterisation of lysosomal proteins (Sleat et al., 2005). These innovations altogether have allowed the in-depth study of LSDs' pathophysiology and progression as well as the testing of innovative therapies (Pastores et al., 2013). The accessibility to effective models, however, is still not possible for all conditions, limiting the extent and rapidity of improvements in terms of treatment and disease management.

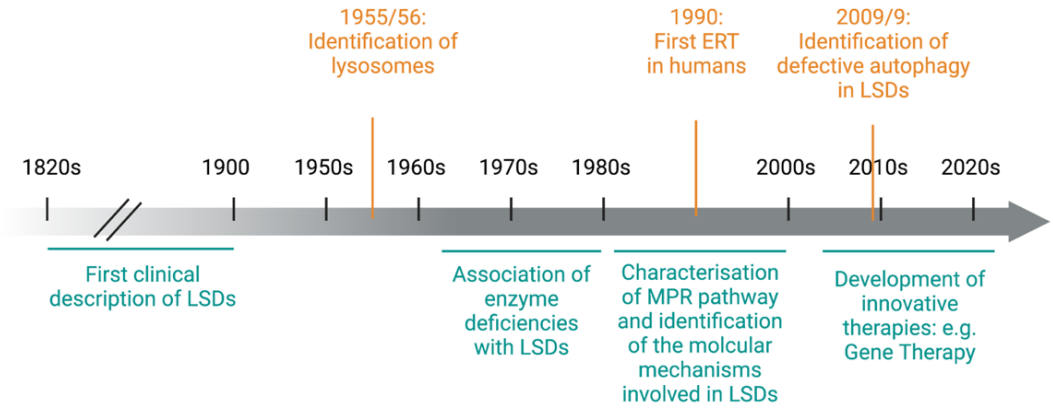


Figure 1 The discovery of LSDs, a timeline.
The first clinical description of LSD is registered during the 19th century, though it was only in the mid 1950s that lysosomes could be identified and in 1963 when the organelles' malfunction could be associated with the disease development. In the following period spanning from the 1970s to the 1990s, the mechanisms of action of mannose-6-phosphate (M6P) receptor gained importance in the eyes of researchers, as well as the mechanisms underlying lysosomal sorting and their involvement in LSDs. Starting from the 1990s, scientific research has shifted towards a more therapeutic investigation, in order to develop innovative treatments for these conditions (Adapted from Parenti, Medina and Ballabio, 2021)

1.2 The Lysosome

Key organelles in LSDs development are the lysosomes. Lysosomes are highly dynamic cytoplasmic organelles capable of responding to stimuli to regulate several cell functions (Ballabio and Bonifacino, 2020; Perera and Zoncu, 2016; Settembre et al., 2012). They predominantly derive from the Golgi apparatus and span between 0.2 and 0.3μm in diameter (Trivedi et al., 2020). Their primary function is the degradation of macromolecules like proteins, carbohydrates, lipids, and nucleic acids after absorption via phagocytic, endocytic and autophagic paths. Once absorbed, macromolecules are degraded by more than 60 acidic hydrolases into smaller components, to be used in cellular metabolism (Ballabio and Bonifacino, 2020). Due to this highly acidic luminal environment, an isolating membrane poor in cholesterol and a thick glycocalyx ensures isolation from the rest of the cell and preserves the lysosomal membrane from degradation (Schulze et al., 2009). However, the

lysosomal membrane also plays an essential role in mediating lysosomal activities. For example, it actively regulates the fusion of the lysosome with other compounds and the transport of metabolites, ions and soluble substrates (Settembre et al., 2013b).

The organelle originates from the Golgi apparatus, following four different potential pathways, all involving the maturation from early endosomes (EEs) to mature lysosome, through a late endosome (LE) stage. In the first mechanism, maturation of EEs into lysosomes is mediated by recycling vesicles released by the Trans-Golgi apparatus (Luzio et al., 2007, 2005). A second model of lysosomal biogenesis relies on vesicular transport of intraluminal vesicles (ILVs) by vesicle/multivesicular bodies (ECV/MVBs). ILVs mediate the mobilization of molecules from EEs to LEs and finally to lysosomes or directly from LEs to lysosomes (Luzio et al., 2007, 2005). The third model describes the lysosomes and late endosomes contact ("kiss") followed the by cargo transfer and separation ("run") of LEs from lysosomes (Luzio et al., 2007, 2005). The final model, also known as the 'fusion-fission' model, involves a heterotypic fusion of LEs-lysosomes to create a hybrid organelle, instead of an LE, that later reforms a mature lysosome.

Overall, the group of lysosomal proteins is a vast collection of luminal, membrane and peripherally associated proteins. More in detail, luminal proteins include acid hydrolases aimed at degrading substrates or activating enzymes and protein factors to breakdown and transport macromolecules from the lysosome. These enzymes include members of the sulphatase, glycosidase, peptidase, phosphatase, lipase and nuclease families, which ensure the targeting of many and different substrates (Settembre et al., 2013b). An example can be found in lipid transfer Niemann-Pick type C2 protein (NPC2), responsible for the transportation of cholesterol and lipids. Further examples of luminal proteins are highly glycosylated lysosome-associated membrane proteins (LAMPs) that exert a protective effect towards the lysosomal membrane and its metabolic components (i.e. ion channels and transporters), among other functions (Ballabio and Bonifacino, 2020). The lysosomal cytosol homes the association of proteins and complexes that regulate lysosomal biogenesis, metabolic processes, and the communication with other organelles.

Among several key regulators of lysosomal activities, transcription factor EB (TFEB) is fundamental for physiological biogenesis of the organelle as well as for correct autophagic activity, exocytosis, and macromolecules processing. At

physiological state, TFEB is located in the cytoplasm, but starvation conditions induce its translocation into the cell nucleus and a transient reduction of its molecular weight, suggesting TFEB activation to be regulated by nutrients and growth factors (Sardiello et al., 2009). Similar starvation studies have revealed TFEB to be regulated by several factors, such as peroxisome proliferator-activated receptor gamma coactivator 1-alpha (PGC-1α) a master coactivator of mitochondrial development and a direct target of TFEB (Settembre et al., 2013a). Other transcriptional regulators of TFEB include farnesoid X receptor (FXR) and cAMP response element-binding protein (CREB), a fed-state sensing nuclear receptor and a fasting transcriptional activator, respectively (Ghosh et al., 2015).

Overexpression of TFEB in HeLa and COS7 cells has been observed to increase the amount of autophagosomes, whilst treatment of mouse embryonic fibroblasts with lysosomal inhibitors following transduction with LV vectors encoding for TFEB, maintained autophagosome formation unaltered (Mizushima et al., 2010; Sun et al., 2021). On the other hand, RNA interference of TFEB in HeLa cells, reduced LC3-II and TFEB levels, suggesting co-regulation of biogenesis and autophagosomes by TFEB (Settembre et al., 2011). TFEB's upregulation has been observed to increase autophagy-mediated substrates' degradation and clearance of lipid drops and damaged mitochondria (Settembre et al., 2013a). Collectively, studies on the regulatory elements of TFEB's activity have revealed its fundamental role in autophagy, lipophagy and mitophagy, as well as its ability to modulate various degradative pathways, revealing its essential role for correct lysosomal activity.

Under the regulatory effect of TFEB and other modulators of the microphthalmia/transcription factor E family (e.g. transcription factor EC (TFEC), transcription factor binding to IGHM (Immunoglobulin Heavy Constant Mu) enhancer 3 (TFE3), and melanocyte inducing transcription factor (MITF)), lysosomal enzyme precursors are generated in the rough endoplasmic reticulum (RER) and further modified in the Golgi apparatus (Woychik et al., 1986). Both soluble and membrane lysosomal proteins require recognition by sorting receptors, hence novel enzymes are first tagged with mannose-6-phosphate (M6P) residues, to ensure selective binding to the mannose-6-phosphate receptors (M6PRs) in the *trans*-Golgi network (TGN) (Braulke and Bonifacino, 2009; Ghosh et al., 2015). Enzymes tagged with M6PRs are further condensed into plasma membrane, or clathrin-coated vesicles (CCVs), for direct or indirect biosynthetic transport (Trivedi et al., 2020). CCVs budding and fusion initiate lysosomal sorting process, in which the transported cargos

are delivered and selected (Sachse et al., 2002; Saftig and Klumperman, 2009). Understanding the cell capacity to recognise lysosomal enzymes via M6PR has been exploited to develop ERTs against LSDs (Neufeld, 1980).

Lysosomal enzymes biosynthesis is initiated by the insertion into the RER of a signal sequence, that undergoes cleavage and glycosylation (Braulke and Bonifacino, 2009). Once processed, the soluble hydrolase is released into the cytoplasm, from where it reaches the *cis*-Golgi. Here, the enzyme can either be depleted of an oligosaccharide chain and be substituted by a complex sugar residue, or specific mannose residues/oligosaccharides can be changed with phosphate groups (Amaral et al., 2023). The latter process yields the M6P residues, catalysed by two consequential enzymes N-acetylglucosaminyl-1-phosphotransferase (GlcNac-1-phosphotransferase) and N-acetylglucosamine-1-phosphodiester α N-acetylglucosaminidase, a type I membrane protein localized in the TGN (Amaral et al., 2023). This exposes the M6P residue through hydrolysis. Hence, when hydrolyses reach the TGN, the M6P residue is recognised by M6PR, a type I transmembrane glycoprotein (Saftig and Klumperman, 2009). Enzyme sorting in the TGN is mediated by the adaptor-protein complex AP-1 and Golgi localized, γ-ear-containing, ARF-binding family of proteins (GGA)(Amaral et al., 2023). These proteins work in parallel to produce M6PR-containning vesicles that leave the TGN structure to fuse with the EEs (van Meel and Klumperman, 2008). Here, the acidic environment leads the dissociation of the enzyme from M6PR and the freed hydrolase can be transported to the lysosomes by endosomal intermediates (Saftig and Klumperman, 2009). A summary of this process is schematised in Figure 2. In addition to the M6P-mediated transport, some protein follow independent pathways, led by alternative receptors, such as sortilin (or neurotension receptor 3), prosaposin, lysosomal integral membrane protein 2 (LIMP-2) (Amaral et al., 2023).

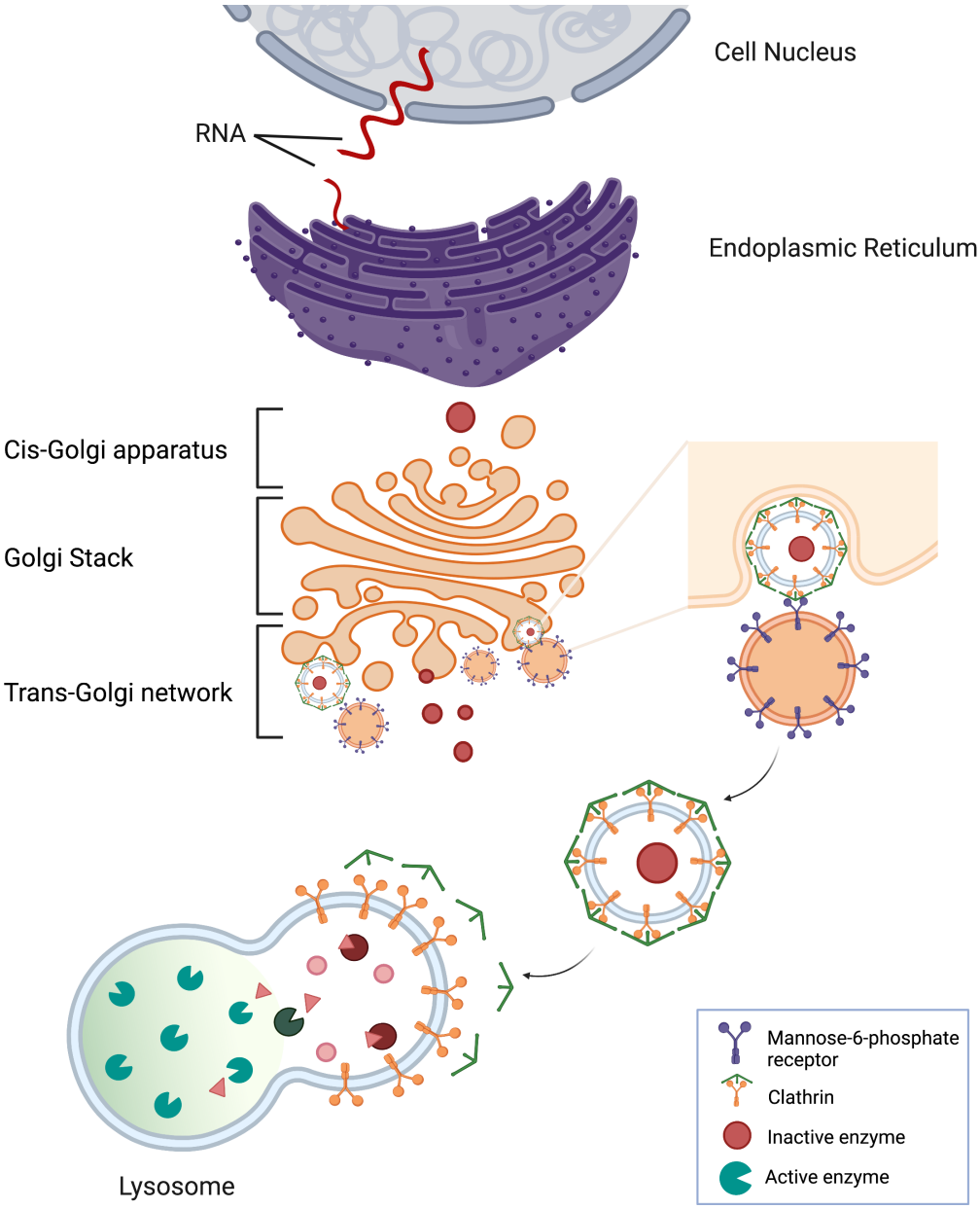


Figure 2 Lysosomal enzymes' biosynthesis and transport.
Proenzymes RNA is processed in the rough ER to generate a proenzyme that enters the Cis-Golgi structure. Here, the mannose residue present on the proenzyme is phosphorylated to form M6P. This structural change allows the trans-Golgi network to recognize M6P and be released into budding vesicles. Such vesicles translocate to the pre-lysosomal endosome where ion pumps activate to lower the pH of the endosome. This environmental trigger allows the dissociation of M6P and recognition by the M6PR. M6PRs recycle back into the Trans-Golgi network.

1.3 Lysosomal storage disease

Between 50-1000 lysosomes are present in the cytoplasm of single mammalian cells. Thus, alterations to genes encoding for lysosomal proteins dramatically impact on lysosomes' physiological activities and give rise to LSD, multi-system disorders associated to a variety of phenotypes. LSDs manifestation spans from early-onset, more severe diseases with a high mortality rate, to milder late-onset conditions, with a more limited impact on patients' quality of life (QoL) and life expectancy. Though considered rare, the family of LSDs affects 5-7,500 livebirths collectively, an estimation likely due to increase thanks to the spreading of the most recent advances in prenatal and pre-implantation genetic screening techniques (Hopkins et al., 2018; Spada et al., 2006; Wasserstein et al., 2019). Among the genes involved in LSDs pathophysiology, there are those encoding for glycosidases, proteases, integral membrane proteins, modulators of lysosomal activity and transporters. Alterations of these proteins result in the corruption of the lysosome's degrading capacities and in progressive accumulation of substrate in the lysosome. This triggers a cascade effect impairing the cell's correct functions and ultimately leads to cell death (Figure 3). Among all genes involved in LSDs, several have been associated with enzyme deficiencies, classified on the basis of accumulated substrate: sphingolipidoses, glycoproteinoses and mucopolysaccharidoses (MPSs) (Platt et al., 2018).

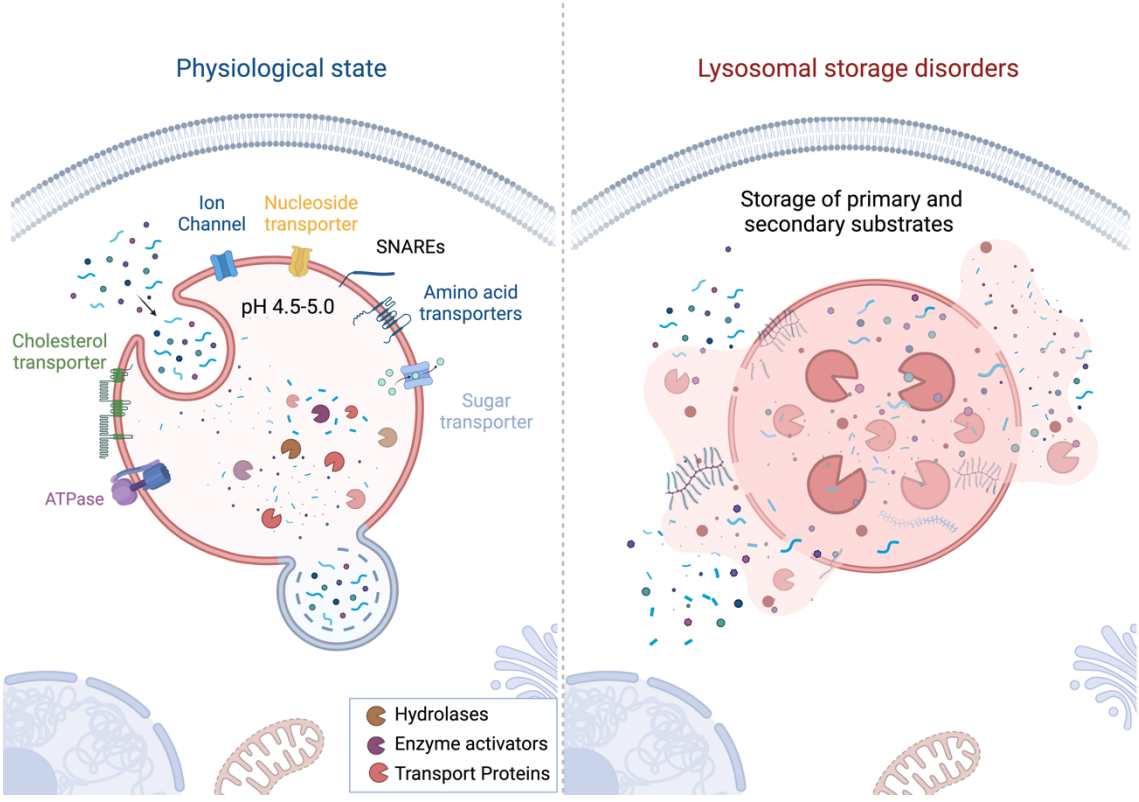


Figure 3 The lysosome under physiological or pathological conditions.

1.1 *SUMF1* mediated activation of GalNs

Among the enzymes active in the lysosome, sulphatases is a category including prokaryotic and eukaryotic enzymes responsible for the hydrolysis of ester sulphates (Hopwood and Ballabio, 2001). Such enzymes are essential for the correct lysosomal functioning, as shown by the detrimental effects in the case of these molecules' alteration or deficiency. This occurs not only in the case of MPSs, but also in that of X-linked ichthyosis, metachromatic leukodystrophy, chondrodysplasia punctata, and multiple sulphatase deficiency (MSD) (Hopwood and Ballabio, 2001). The latter disease presents with impaired activity of all sulphatases and develops from mutations affecting the *SUMF1* gene (Cosma et al., 2003; Dierks et al., 2003; Hopwood and Ballabio, 2001). In order to activate and hydrolyse natural substrates, sulphatases required post-translational modification by changes in their catalytic domain. The region contains cysteine that is switched into formylglycine (FGly), within the ER. The enzyme encoded by *SUMF1* exerts an essential role by generating FGly (Cosma et al., 2003; Dierks et al., 2003). Thus, mutations to *SUMF1* leads to the accumulation of sulfatides, sphingolipids, sulphated glycosaminoglycans, and steroid sulphates (Zilberman and Bibi, 2016). Hence, an involvement of this regulatory gene, should be taken into account in the context of diseases of accumulation.

1.2 Mucopolysaccharidoses (MPSs)

MPSs are a group of inherited metabolic conditions affecting ~0.1% children with genetic illnesses (Gaffke et al., 2021). Collectively, MPS diseases affect 1 in 25,000 live births, with variable incidence depending on the specific type and, interestingly, with geographical location being associated with specific MPS variants (Celik et al., 2021; Lowry et al., 1990; Tomatsu et al., 2019; Voskoboeva et al., 2022). MPSs are caused by enzymatic deficit impairing the degradation of glycosaminoglycans' (GAGs), aimed at regulating extracellular matrix (ECM) assembly and cell signalling (Caterson and Melrose, 2018; Gaffke et al., 2021; Garantziotis and Savani, 2019; Karamanos et al., 2018). Altered degradation leads to intra- and extra-cellular accumulation of undegraded GAGs in tissues of various type (Nagpal et al., 2022).

1.2.1 Clinical Manifestations

Clinically, build-up of GAGs leads to multi-organ dysfunction involving all major systems, such as the nervous, skeletal, cardiac, respiratory and gastrointestinal systems (Nagpal et al., 2022). Hence, MPSs appear as a heterogeneous group and

are distinguished into 13 diseases. MPS I to IX (7 types and 6 subtypes) are classified by the altered enzyme and can show analogous phenotype (*e.g.* MPS type I, II, IVA and B, prevalently skeletal) or differ (*e.g.* MPSIII, primarily neurological) (Zhou et al., 2020). Across different diseases, the age of onset and severity is highly variable, though systemic manifestations commonly include growth and cognitive impairment, skeletal alterations, cardiac valves and coronary artery dysfunctions, hepatosplenomegaly, umbilical hernias, dental conditions, hearing loss, obstruction of the airways and visual impairment (Tomatsu et al., 2019). Additional evidence of musculo-skeletal involvement is observed with a number of ocular abnormalities such as corneal clouding, elevated intraocular pressure, retinopathy and optic nerve damage (Nagpal et al., 2022). MPSs, summarised in Table 1, are generally inherited in an autosomal recessive manner with the exception of MPSII, which appears to be X-linked. Molecular mechanisms causing MPSs are still largely unknown and related to GAG accumulation, which, in fact, functions as diagnostic biomarker for the diseases, together with insufficient or absent enzymatic activity (EA)(Kubaski et al., 2017).

Table 1 Summary of recognised MPS types and subtypes.
Associated enzymes are also listed, together with the substrates left undegraded by the deficient enzyme.

MPS	**Defective gene**	**Accumulated substrate**
Type I	*IDUA*	Dermatan and heparan sulphate
Type II	*IDS*	Dermatan and heparan sulphate
Type III	*SGSH* (IIIA), *NAGLU* (IIIB), *HGSNAT* (IIIC) and *GNS* (IIID)	Heparan sulphate
Type IV	*GALNS* (IVA) *GLB1* (IVB)	Keratan and Chondroitin-sulphate
Type VI	*ARSB*	Dermatan and chondroitin-4 sulphate
Type VII	*GUSB*	Dermatan, heparan, chondroitin-4 and -6 sulphate
Type IX	*HYAL1*	Hyaluronan
Type X	*ARSK*	Dermatan and heparan sulphate

1.2.2 MPS classification

1) MPS type I (MPSI) develops from pathogenic variants to the *IDUA* gene, located on chromosome 4p16, leading to insufficient α-l-iduronidase activity. Enzyme deficiency causes accumulation of dermatan and heparan sulphates (DS and HS) in organ tissues and multisystemic dysfunction. MPSI exists in

three forms, known as Scheie, Hurler-Scheie and Hurler (MPSIH) syndromes, from the mildest to the most severe (Ganesh et al., 2013). Significant clinical manifestations in MPSI include skeletal anomalies, neurological disease, compromission of the respiratory capacity, organomegaly, and cardiac disease, with the most severe patients showing progressive neurodegeneration and disabling skeletal compromission (Muenzer, 2004). Failure to treat MPSI effectively, leads to very premature mortality within patients' first 10 years of life.

2) MPS type II (MPSII), also known as Hunter syndrome, is an X-linked condition affecting 1 in 60-150,000 patients, with higher incidence observed in the population of Ashkenazi Jews (Nelson et al., 2003). As an X-linked disease, it is predominant in males, though it can be observed in females, in rare occasions. It arises from alterations to idunorate-2-sulphatase encoding sequence (*IDS*) located on Xq28. As for MPSI, this pathogenic variant also leads to accumulation of DS and HS and is distinguished into the more common and severe type A and a milder type B form (Wraith et al., 2008). MPSII presents with short stature, coarse facial feature, valvular dysfunction, hepatosplenomegaly but while MPSIIA patients also present with progressive cognitive and behavioural alterations, MPSIIB patients do not suffer from neurological impairment (Wraith et al., 2008).
3) MPS Type III (MPS III, Sanfilippo syndrome) is distinguished into 4 subtypes that develops from pathogenic changes to the *SGSH* (IIIA), *NAGLU* (IIIB), *HGSNAT* (IIIC) and *GNS* (IIID) genes, located on chromosome 17q25.3, 17q.21.1, 8p11.21-p11.1 and 12q14.3 respectively (Wagner and Northrup, 1993). Each subtype of MPSIII is, in fact, associated with a different enzyme: heparan-N-sulfatase in IIIA, α-N-acetylglucosaminidase in IIIB, α-glucosaminide acetyltransferase in IIIC, and N-acetylglucosamine-6-sulfatase in the IIID form, all contributing to HS accumulation (Ganesh et al., 2013; Ozkinay et al., 2021; Yogalingam and Hopwood, 2001). Clinical presentation of MPSIII varies depending on the subtype, though neurological, behavioural and developmental progressive degeneration appear the common denominators of MPSIII syndromes (Jakobkiewicz-Banecka et al., 2016; Nijmeijer et al., 2019).
4) MPS type IV, or Morquio Syndrome is distinguished between the type A, caused by pathogenic mutation of the *GALNS* gene (on chromosome 16q24) and type B, arising from pathogenic variants to the *GLB1* gene (on chromosome 3p21). These pathogenic alterations lead to insufficient activity

of N-acetylgalactosamine-6-sulphatase and of b-galactosidase enzymes and to consequential accumulation of keratan sulphate (KS) and, in the case of MPSIVA only, of chondroitin-6-sulphate (C6S) in several tissues, with severe impairment of the skeletal development. Morquio Syndrome will be described in depth in the next chapter.

5) MPS type VI (MPSVI or Maroteax Lamy disease) clinical manifestations are a consequence of DS and chondroitin-4-sulphate (C4S) accumulation. This occurs due to pathogenic variants of *ARSB* gene, on chromosome 5q11, impairing the correct functioning of N-acetylgalactosamine-4-sulfatase (Harmatz and Shediac, 2017). The main clinical features in MPSVI involve severe malformation of the skeleton and joints, though characterized by a slow symptom progression (Thümler et al., 2012). Further neurological symptoms appear inherent to MPSVI, including hydrocephalus and cerebral atrophy (Azevedo et al., 2013). Nevertheless, symptoms require prompt surgical intervention without which patient may die within the age of 20 due to heart failure, pulmonary infection or airways obstruction (Lin et al., 2016, 2013).
6) The type VII of MPS (MPSVII), also known as Sly syndrome arises from inefficient degradation of C4S, C6S, DS and HS due to β-galactosidase impairment. Enzymatic deficiency is due to pathogenic mutations to the *GUSB* gene, on 7q11 (Montaño et al., 2016). Phenotypic appearance is heterogeneous and involves multiple systems in the organism, though characteristic symptom includes short stature, coarse face, corneal clouding cardiac malfunction and skeletal deformation as well as hydrops fetalis and abnormal accumulation of body fluids (Montaño et al., 2016). Although the age of onset is variable, a limited number of MPSVII patients can reach adulthood, due to the presence of hydrops.
7) MPS type IX, or Natowicz syndrome, arises from pathogenic variants of *HYAL1* gene (chromosome 3p21). This causes deficient activity of hyaluronidase, responsible for the correct degradation of hyaluronan, a polymer aimed at modulation of cell proliferation, migration and differentiation, contributes to cartilage composition and acts as a lubricant for joints (Kiykim et al., 2015). Common symptom of MPSIX include growth alterations such as skeletal and joint disease, short stature, and cleft palate as well as infections and cysts development. Natowicz syndrome is the rarest form of MPS (Kiykim et al., 2015).

8) MPS type X, a recent addition to the group of diseases, has been associated with pathogenic alterations to the *ARSK* gene, usually encoding for arysulphatase-K enzyme. In two patients identified in 2022, a variant was localised in the penultimate exon of the encoding sequence (NM_198150.3:c.1251C > G p.(Tyr417*) (Rustad et al., 2022). On liquid chromatography-tandem mass spectrometry (LC-MS), accumulation of DS and a milder storage of HS were noted in these and previously identified patients (Verheyen et al., 2022). The biallelic pathogenic alteration of *ARSK* is associated with thickening of skull, platyspondyly, beaking of the thoracolumbar vertebrae, widening of clavicles and ribs, narrowing of lower parts of iliac bones, reduced epiphyses, metaphyseal striae, and hypoplastic carpal bones (Verheyen et al., 2022). Non-skeletal alterations include cardiac anomalies and ophthalmological complications, sleep apnoea and ear infections, comparable as to other MPS types (Galimberti et al., 2018; Verheyen et al., 2022).

In this project, we have focused on MPSIV and its devastating effects on patients' QoL as well as the limitations still associated with current standard of care.

1.2.1 MPS IVA

MPSIVA (Morquio disease, OMIM #253000) is an autosomal recessive disease, resulting from faulty activity of the hydrolase N-acetylglucosamine-6-sulphate sulphatase (GALNS) (Zhou et al., 2020). Such deficiency causes keratan sulphate (KS) and chondroitin-6-sulphate (C6S) accumulation mainly in bone, cartilage, cornea and heart valves (S. Khan et al., 2017; Peracha et al., 2018; Tomatsu et al., 2016). In particular, undegraded substrate tends to concentrate in chondrocytes and ECM of cartilage, altering the correct development of both cartilage and bone, due to abnormal chondrogenesis and endochondral ossification processes (Tomatsu et al., 2014). As a consequence, MPSIVA patients present altered ossification, joint hypermobility, skeletal dysplasia, and impaired growth (Goldberg et al., 2017; Jiang and Tuan, 2015; Tomatsu et al., 2010). The condition was first described in 1929 by L. Morquio (Morquio, 1929) and J. F. Brailsford (Brailsford, 1929), and is currently believed to affect very young children, with variable incidence according to country (Hendriksz et al., 2013; S. A. Khan et al., 2017; Lee et al., 2022; Moreno Giraldo et al., 2018; Nelson et al., 2003). To date, the prevalence in Italy is of 1 livebirth every 300,000, 1 in 270,000 births in Germany, whilst in the UK affects 1 in 599,000 newborns (Baehner et al., 2005; Caciotti et al., 2015).

Though children suffering from MPSIVA are born with a healthy appearance, they begin to manifest disease phenotypes within the first 3 years of life (Figure 4). After the initial appearance, symptom progress rapidly and strongly impairs these children's growth and developmental capabilities. The most prominent manifestations of MPSIVA include skeletal dysplasia, short stature and short neck, compression of the spinal cord and kyphoscoliosis, tracheal obstruction, *pectus carinatum, genu valgum* and laxed joints (Montaño et al., 2016, 2007; Tomatsu et al., 2016, 2011). Additional non-skeletal symptom are respiratory complications and valvular heart disease (Tomatsu et al., 2011).

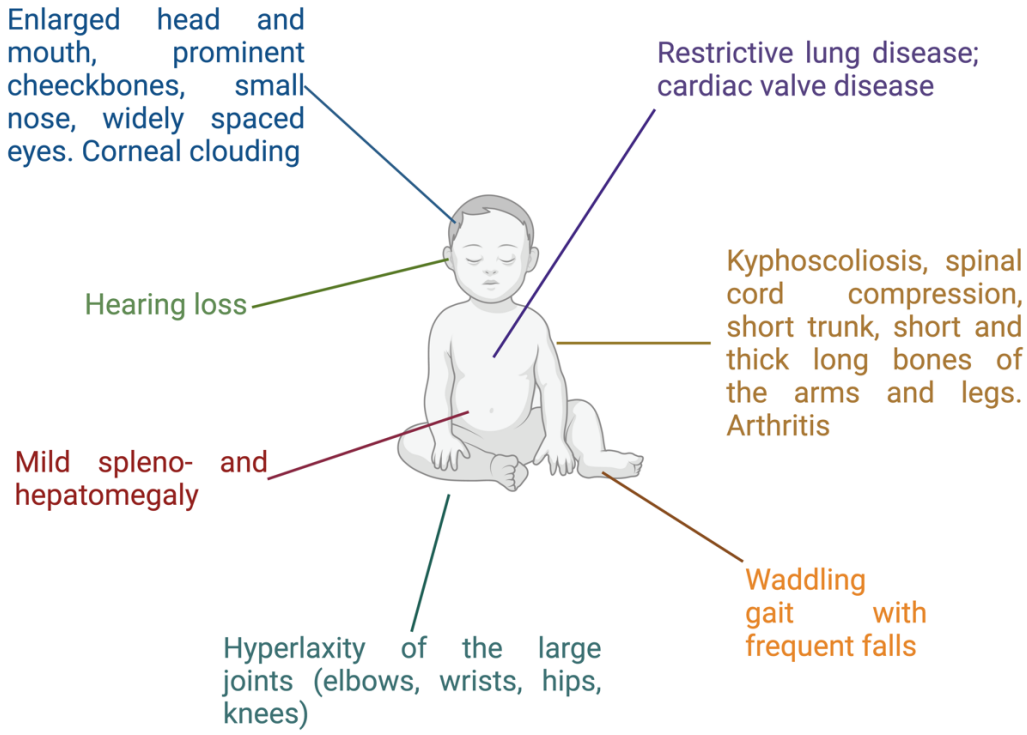


Figure 4 Main symptom of MPSIVA.

Typical manifestations of MPSIVA belong to a broad spectrum of phenotypical evidences that appear between 1 and 3 years of age and variably progress over time. The main symptom of the disease include skeletal anomalies involving all bones and cartilagineous insertions leading to scoliosis as well as deformation of the knees, chest and trachea and general growth retardation. Additional anomalies of the skeletal structure include symptom of arthritis, while non-skeletal phenotypes may be events of sleep apnea, vision and hearing impairment or loss, organlomegaly, dental anomalies, heart vales thickening and spinal cord compression. This reflects negatively on the toddlers' walking abilities.

1.2.2 Genetic Background

Depending on the pathogenic variant at the basis of the condition, symptom appearance varies, producing a spectrum of phenotypes ranging from an early-onset more severe form of MPSIVA to a late-onset, slowly progressing disease (Montaño et al., 2007; Tomatsu et al., 2005). About 327 pathogenic variants to *GALNS* have been

linked with the disease, the majority of which (242) are missense or nonsense pathogenic variants (Celik et al., 2021). While >100 mutations are associated with severe manifestations, only 30 pathogenic variants appear to cause the milder forms of MPSIVA (Dũng et al., 2013; Montaño et al., 2007; Tomatsu et al., 2005). Disease progression severely impacts on patients' QoL, affecting their ability to move and walk independently, often restraining them to the use of a wheelchair. MPSIVA patients with more severe forms of the disease often die within the first 30 years of life, most commonly due to airways obstruction and heart valve failure (Lavery and Hendriksz, 2014; Montaño et al., 2007). Among the root-cause pathogenic mutations of MPSIVA, the most frequent and severe human missense variant c.1156C>T leads to p.Arg386Cys in the GALNS protein, causing a clear correlation between genotype and phenotype in human patients (Dũng et al., 2013; Fukuda et al., 1996; Tomatsu et al., 2005). In general, different geographical areas show specific pathogenic variants prevalence. For example, missense alteration p.Ser287Leu account for 8.82%, p.Phe216Ser for 7.35%, p.Asn32Thr for 7.24%, and pAla291Ser for 5.88%, in India with most pathogenic variants targeting exon 1, 7 and 8 (Bidchol et al., 2014). In Brazil, 1652 MPS patients have been identified between 1982 and 2019, with 12.41% being affected by MPSIV (96.45% type IVA; 3.55 type IVB) (Celik et al., 2021). The most common pathogenic variant detected in Brazil was p.Ser341Arg (22%), also associated with an identical haplotype among patients, suggesting a founder effect (Bochernitsan et al., 2018). Other pathogenic alterations included p.Gly301Cys (13.4%), p.Arg386Cys (12.6%), p.Arg94Leu (11%), and p.Gly116Ser (8.6%) (Celik et al., 2021). 18% British and Irish MPSIVA patients had p.Ille113Phe muations, whilst 14% p.Thr312Ser (Tomatsu et al., 1995; Yamada et al., 1998). 40% of Turkish patients owned a c.334delG deletion and 20% a c.708delT (Terzioglu et al., 2002). Finally, in Italy, the most prevalent pathogenic variants detected in the early 2000s included p.Met1? (26.7%) and p.Arg386Cys (20%), p.Trp10X (13.3%) and p.Ala107Thr (10%) (Tomatsu et al., 2004). A summary of the distribution of the main pathogenic variants associated with MPSIVA can be seen in Figure 5.

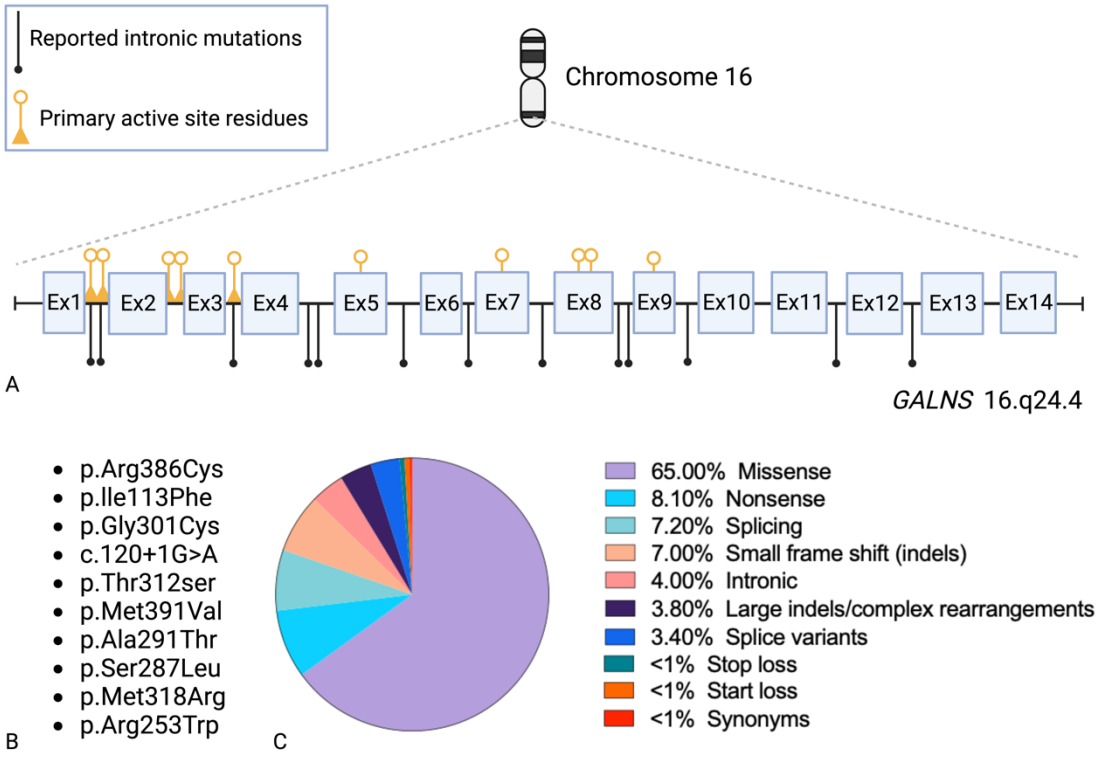


Figure 5 Overview of the principal pathogenic variants associated with GALNS. *Summary of previously reported pathogenic alterations to GALNS gene, associated with MPSIVA. A) Overview of the gene structure and hotspots. B)* The ten genetic alterations most reported worldwide (Morrone et al., 2014). C) Frequency of different types of alterations associated with GALNS gene (Zanetti et al., 2021).

1.2.3 MPSIVA diagnosis

Clinically, the disease is diagnosed via quantification of excessive KS in patients' urine samples (Wood et al., 2013). Additionally EA can be evaluated from dried blood spot (DBS) samples for confirmation (Wood et al., 2013). Other sources for EA can be cultured fibroblasts and leukocytes (Wood et al., 2013). Molecular analysis of potential pathogenic variants of *GALNS* also contributes to diagnose MPSIVA. In Italy, MPSs can be included in the extended newborn screening test by DBS, together with other 48 diseases, including metabolic and lysosomal conditions. Early diagnosis is fundamental to delay symptom arousal or start life-saving treatments, though many rare diseases still lack appropriate therapies. Overall, there has been a broad spectrum of pathogenic variants associated with *GALNS*, and the distribution of the alleles varies from one geographic region to another. However, some of the pathogenic variants have still been recorded with the highest rates.

1.2.4 GALNS activity in KS and C6S degradation

GALNS gene is located on chromosome 16q24.3 and is composed of 14 exons spanning 50 kb (Baker et al., 1993; Nakashima et al., 1994). It generates a 1566-nucleotide long mRNA and encodes for 522-amino acid protein GALNS (Dũng et al., 2013; Regier et al., 1993). The protein is a lysosomal hydrolase enzyme, responsible for the removal of sulphate groups from a terminal N-acetylgalactosamine-6-sulphate (or galactose-6-sulphate) in mucopolysaccharides. These include KS and C6S (Rivera-Colón et al., 2012). Studies on recombinant GALNS revealed the glycoprotein to be a homodimer, with an N-terminal domain on each monomer and composed of domain 1 (residues 28-379), or active site, a domain 2 (residues 380-481) with anti-parallel β-strands and a C-terminal meander (residues 482-510) (Rivera-Colón et al., 2012). Domain 1 is a core ten-stranded β-sheet, central to a six α-helices structure, whilst domain 2 consists of a four anti-parallel stranded β-sheet perpendicular to a long α-helix and is followed by a C-terminal meander threading back to domain 1 (Rivera-Colón et al., 2012). GALNS active site is located in a pocket in the middle of the N-terminal α/β domain, where a calcium molecule is bound to the catalytic nucleophile and the chains of four additional residues (Figure 6) (Rivera-Colón et al., 2012). In depth details of the protein structures are described by Rivera-Colón and colleagues.

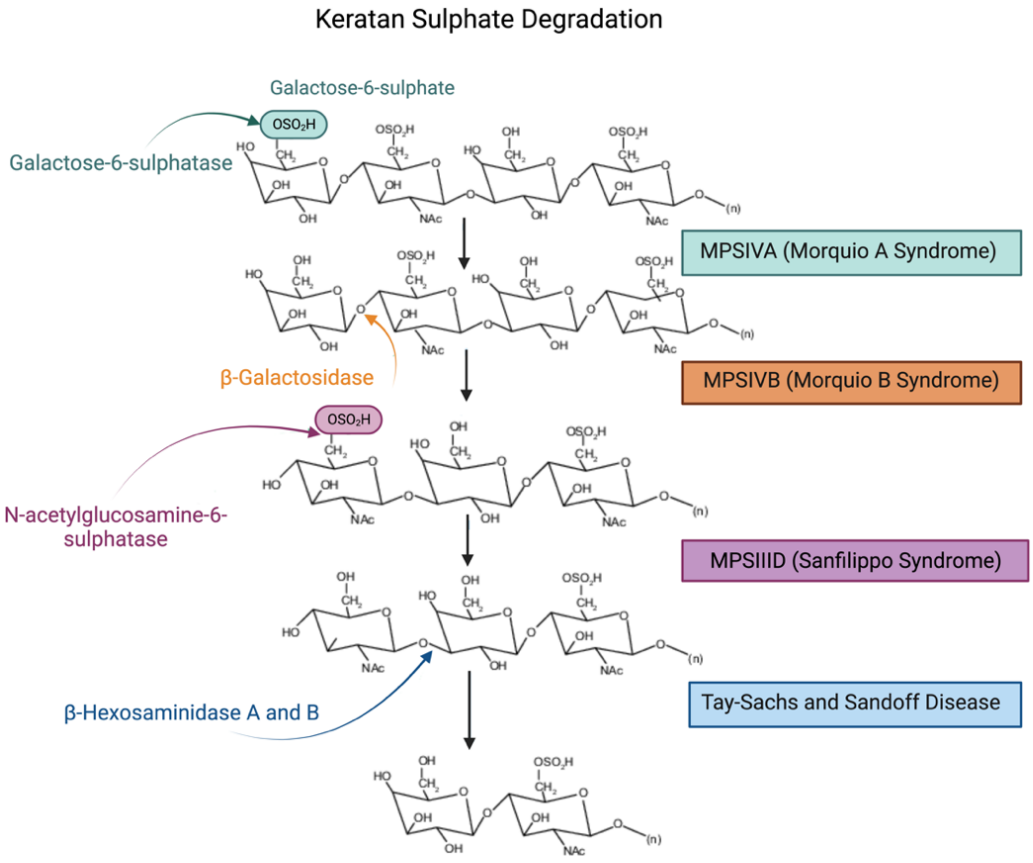


Figure 6 KS degradation process and related disorders.
Schematic representation of KS degradative process. At each stage, deficiency or malfunctioning of the responsible enzyme (listed on the left side of the figure) can lead to a specific disease development (listed on the right side of the picture). The arrows indicate the site of action of each relative enzyme.

In order to elucidate the mechanisms triggered in MPSIVA, the location of 120 pathogenic variants associated with the disease have been mapped, highlighting that a very limited proportion (5%) affects the active side residues. Instead, 27% of mapped pathogenic mutations appear to tackle surface residues, whereas the remaining 65% affect the protein core residues (Rivera-Colón et al., 2012). In human patients, ~148 pathogenic variants on *GALNS* have been highlighted (Khedhiri et al., 2011; Wood et al., 2013). Further analysis on 37 Italian patients has revealed 14 additional pathogenic variants (Caciotti et al., 2015). Several different variants have been recorded over the years, with the most recent studies reporting two patients carrying p.Asn164Thr and p.Gly301Cys pathogenic variants and three siblings heterozygous for p.Asn204Thr and p.Ala322Pro (Erazo-Narváez et al., 2020; Ficicioglu et al., 2020). In total, 446 variants have been recorded, with a proportion of 169 being at the protein level (Zanetti et al., 2021). Evaluation of pathogenic variants associated with MPSIVA has revealed the disease to arise from protein misfolding, due to most gene alterations' disruptive effect of the protein's

hydrophobic core (Rivera-Colón et al., 2012). Corroborating this, the vast majority of *GALNS* variants appear to involve domain 1 hydrophobic core, revealing the protein active residue essential role for the overall structural integrity of the protein (Rivera-Colón et al., 2012). At the same time, domain 2 has been observed to contribute to intermolecular interactions required for protein functioning (Rivera-Colón et al., 2012). Evaluation of the protein activity in animal models may contribute to clarify GALNS protein alterations in MPSIVA.

1.3 Glycosaminoglycans

Originally isolated from mucous membranes, glycosaminoglycans (GAGs), or mucopolysaccharides, are complex sugar molecules structured as linear polysaccharides composed of repeated disaccharide repeats, containing uronic acid (either β-d-glucuronic acid (GlcA) or its C5 epimerised version, α-l-iduronic acid (IdoA)) or galactose, alternated to hexosamine subunits. The amino units, instead, can be either glucose- (α-d- or β-d-glucosamine, GlcN) or galactose-based (Gal) (Pomin and Mulloy, 2018). GAGs are complex and heterogeneous structures distinguished among each other on the basis of their monomeric units, found mainly but not exclusively in connective tissues such as skin, cartilage, cornea as well as the liver, spleen, and vascular tissue (Morla, 2019). In addition, different GAGs families are characterised by the links between their monomeric components, the position of their sulphate groups and the extent of sulphation. Such characteristics define four different classes of GAGs: 1) heparin/heparan sulphate (HS), 2) chondroitin sulphate (CS)/dermatan sulphate (DS), 3) hyaluronan (HA), and 4) KS. Both GAGs and proteoglycans (PGs), which are highly glycosylated macromolecules composed of one core protein and covalently attached GAGs, have been associated with modulation of several signalling pathways, including the TGF-β and the Jun N-terminal kinase (JNK)/p38 pathways (Chen et al., 2006; Koehler et al., 2017; Ma et al., 2019). Among all PGs, HS is the most abundant and has been shown to mediate the activation of signalling pathways involved in cell proliferation, adhesion, and migration within the ECM environment (Iozzo and Schaefer, 2015). Furthermore, HS has been linked with regulation of inflammatory and angiogenetic processes (Iozzo and Schaefer, 2015).

Each GAG is biosynthesized depending on the oligosaccharide linker it contains. For example, chondroitin sulphate, dermatan sulphate and heparan sulphate are O-linked to serine residues in the core protein and their biosynthesis requires three

main steps. First monosaccharides are activated to nucleoside diphosphate sugars and of sulphated 3'-phosphoadenosine 5'-phosphosulphate (PAPS), in the cytoplasm. Once activated, these molecules are transferred to the ER or to the Golgi apparatus to finally be incorporated into the polysaccharide chain by glycotransferases, in the case of sugars, and to be used for sulphation, in the case of PAPS (Anthony J. Hayes and Melrose, 2020). The exception to the abovementioned mechanisms is HA. Contrarily to the other GAGs, HA's precursor sugars (UDP-glucuronic acid and UDP-*N*-acetylglucosamine) are transported to the plasma membrane to undergo further processing, without the need of sulphation of functional groups within the Golgi apparatus (Ghiselli, 2017). Details of KS biosynthesis are described in the next chapter.

Importantly, GAGs constitute the biggest structures of PGs, which persist in the ECM. When PGs are degraded by proteolysis, they are disrupted into GAGs, that, in turn, can be up-taken by lysosomes and broken down intracellularly (Coutinho et al., 2012). Lysosomal degradation process differs depending on the target substrate that is degraded, though overall, up to 10 different enzymes are required to successfully complete the process. These include four glycosidases, five sulfatases, and one nonhydrolytic transferase that, if deficient or abnormally functioning, lead to the development of MPSs (Giugliani et al., 2011). Understanding the effect of specific enzyme deficiencies has played a pivotal role to understand GAGs' catabolism. This, in turn, has allowed the discovery and characterisation of each enzyme-substrate relationship and consequential disease pathogenetic mechanism, providing essential information to develop potential therapeutic strategies. Though our knowledge on the subject has significantly expanded, the task of treatment development remains a challenge for many LSDs.

1.4 Keratan sulphate

Among the different GAGs altered in MPSs, is keratan sulphate (KS). It is composed of β1-4 glycosidically-linked disaccharide repeats alternating *N*-acetyl-glucosamine (GlcNAc) without uronic acid subunits (Funderburgh, 2000; Pomin, 2015). GlcNAc and Gal are sulphated at C6, leading to regions with mono- or di-sulphation (Anthony J. Hayes and Melrose, 2020). Initially identified in the corneal tissue and defined as a linear poly-*N*-acetylactosamine of varying sulphation, KS is a widespread member of the GAG family as a structural component of proteoglycans (PGs) (Meyer et al., 1953; Suzuki, 1939). Poly-*N*-acetylactosamine chains form during embryogenesis from GlcNAc and Gal first as non-sulphated linear structures

and then variably sulphated at C6 of Gal and GlcNAc by glycosyltransferases (Caterson and Melrose, 2018). KS attaches to the core proteins of the PGs structure, as schematised in Figure 7. These molecules contribute to the tensional resistance of connective tissues like cornea, cartilage and the intervertebral discs, as well as the components of the peripheral and central nervous system (PNS, CNS) (Melrose, 2019). The mechanisms of attachment of KS to PGs were clarified by comparative studies between KS in the cornea and in cartilaginous tissues in several species and appeared to be enabled by *N*-linked Asparagine (Asn) or *O*-linked Serine (Ser), Threonine (Thr) or Mannose (Man) residues (Caterson and Melrose, 2018; Choi and Meyer, 1975).

Thus, three types of KS have been classified. KS type I (KS-I), prevalent in the cornea, is conjugated by N-linked glycosylation to an asparagine residue to its core protein. The cartilaginous KS type II (KS-II), instead, presents an O-linked glycosylation to a serine or threonine residue of the core protein. Usually, the chain structures formed in KS-II are shorter and more sulphated than those of KS-I (Li et al., 2012). Similarly, type III KS (KS-III), constitutive of the nervous system, shows O-linked mannosylation to serine (Uchimura, 2015). Despite differences in chain length, sulphation and linkage groups have been observed among the different types of KS, all forms display similar structures, such as stretches of non-sulphated poly-*N*-acetylactosamine, variable areas of mono- and di-sulphated regions of 6-sulphated d-galactose and *N*-acetylglucosamine, which characteristically compose the repeat disaccharide unit of KS (Caterson and Melrose, 2018).

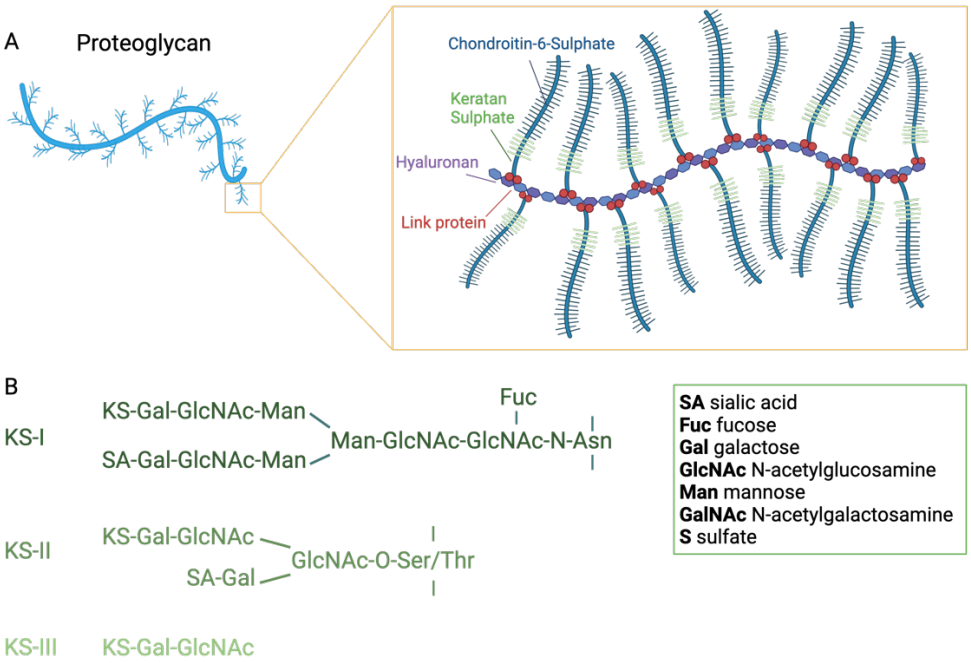


Figure 77 Keratan Sulphate structure and function.
A) Gross structure of KS in relation to PGs. B) Chemical composition of KS subtypes (I, II and III), adapted from (Uchimura, 2015). KS and C6S contain both carboxyl and sulphate residues conferring a negative charge to these molecules. KS and C6S negative charge enables water retention in the ECM, which ensures resistance to compressive forces, characteristic of connective tissue (Hayashi et al., 2011).

KS is biosynthesized in the cytosol after the activation of sugars by bonding to nucleotide diphosphate. The process continues in the endoplasmic reticulum first and then in the Golgi apparatus. One of the three potential linkers, specific for each type of KS (I, II or III) can be synthesized and expanded by addition of saccharides (Sasarman et al., 2016) and lead to KS polymerization (Funderburgh, 2002). The polymerization process of KS is carried out by glycotransferases that alternately add GlcNAc and galactose (Gal) to the polymer (Funderburgh, 2002). The elongation process needs to be coordinated to sulphation of the added GlcNAc and Gal units (Caterson and Melrose, 2018; Funderburgh, 2000).

Studies on mice have highlighted greater fragility of cartilage, accompanied by harsher antibody-induced arthritis, in those models lacking KS compared to WT controls (Hayashi et al., 2011). Similarly, GAG release from explants was higher in mice deficient for KS (Hayashi et al., 2011). Such inflammatory-mediated damage, potentially stimulated by cartilage fragments, can be corrected by administering exogenous KS, suggesting a chondroprotective effect of KS against cartilage degradation (Ghosh et al., 2006; Hayashi et al., 2011). Hence, understanding of the

extent to which the immune system is stimulated in MPSIVA appears necessary to monitor the disease development and patients' prognosis.

1.5 LSD-associated inflammatory pathways

As previously stated, lysosomes play a regulatory role in immune response by controlling autophagy, lipid metabolism, GAGs degradation and regulation of cytokine release. Though GAGs accumulation in tissues has been previously linked to elevated cytokine levels, the inflammatory mechanisms underlying LSDs still need to be fully understood (Abdulkhaleq et al., 2018). While more studies have focused on neuroinflammation, the inflammatory pathways associated with more skeletal MPSs, like MPSIVA, are still largely unknown. In part, the poor characterisation of MPSIVA pathophysiology, particularly under an inflammatory point of view, has contributed to the low availability of effective therapies against the disease. Previous studies have highlighted similarities between the cartilage of MPS patients with that observed in rheumatoid and osteo-arthritis (RA; OA). The conditions appear similar in terms of pro-inflammatory cytokines secretion, including tumour necrosis factor-alpha (TNF-α) and IL-1 beta (IL-1β), as well as for production of nitric oxide (NO). Furthermore, upregulation of matrix metalloproteinases (MMP)-2 and -9, commonly observed in the synovial fluid of RA patients, has been seen in animal models of MPS (Simonaro et al., 2005; Yoshihara et al., 2000). Alterations to cartilage composition is also comparable among these illnesses, with higher chondrocyte apoptosis and diminished PGs in the ECM (Simonaro et al., 2005).

1.5.1 MMPs elevation in pathological context

MMPs enzymes are primarily involved in ECM degradation, regulated by tissue inhibitors of metalloproteinases (TIMPs). Among several types, MMP-2 (gelatinase A, type IV collagenase) and -9 (gelatinase B, type IV collagenase) are aimed at proteolytically degrading the joint matrix by digesting denatured collagen and other substrates, that accumulate in cartilage (Itoh et al., 2002). MMP-9, secreted by macrophages and neutrophils (NEUTs), is thought to be essential for the migration of these cells in inflammatory diseases, contributing to the erosion of cartilage in RA and OA, as well as to fibroblasts' survival, proliferation, migration and invasion of the synovial fluids of RA patients (Nagase et al., 2006; Takaishi et al., 2008; Xue et al., 2014). In arthritis, these gelatinases are the primary cause of degenerative chondrolytic process, making them fundamental to maintain a balanced bone turnover process (Simonaro et al., 2005). Both animal models and human samples

of MPS display alterations in the expression of MMP-2, -9 but also -1, -12 and -13 (Di Natale et al., 2008; Ma et al., 2008; Richard et al., 2008; Simonaro et al., 2008, 2005). In MPSI mice, increased expression of both MMP-2 and -9 was associated with degenerative changes in the joint, involving loss of collagen and PGs (de Oliveira et al., 2013). Thus, evaluation of these enzymes' activity may clarify whether MPSIVA models also suffer from the damaging effects of MMPs imbalance.

1.5.2 Reduced antioxidant defence in MPS

Previous studies have also demonstrated the link between inborn errors of metabolism and oxidative stress. In MPSI, increased lipid peroxidation has been associated to altered activity of antioxidant enzymes after enzyme replacement therapy (ERT), whereas MPSII patients present elevated lipid peroxidation, DNA and protein damage, prior to ERT (Filippon et al., 2011; Pereira et al., 2008). In MPSIVA patients, enzymatic antioxidant activities appear altered, with consequential oxidative damage of lipids, proteins, and leukocytic DNA (Donida et al., 2015; Fujitsuka et al., 2019). This pro-oxidant and -inflammatory state persist in MPSIVA patients undergoing ERT, with decreased glutathione and increased superoxide dismutase activity, mirroring lower antioxidant defence (Donida et al., 2015). In 2023, results from the ERT long-term evaluation in MPSIVA patients have shown a protective effect against both inflammatory and oxidative damage (Aguilar Delgado et al., 2023). This contributes to improving patients' inflammatory state on post-therapy follow-ups, though skeletal manifestations persist. Thus, development of novel therapies should consider evaluating the effect on the oxidative stress of MPSIVA patients, in addition to correct their primary skeletal symptoms.

1.5.3 TGF-β hyperactivity

The dysregulation of TGF-β's known mitogenic effect has been associated with disease of primary skeletal involvement. In MPSVI, for instance, TGF-β overexpression reduces apoptosis and stimulates fast proliferation of chondrocytes, which, however, are maintained in an immature, quiescent state (Simonaro et al., 2005; Wang et al., 2014). TGF-β acts by preventing chondrocytes from differentiating and undergoing the hypertrophic stage of bone development. Hence, persistence of chondrocytes in their immature state may be a marker of abnormal mineralization process in MPS. Previous studies on BM-derived MSCs have highlighted the prolonged exposure to TGF-β1 upregulates several biomarkers of chondrogenesis and hypertrophy, both *in-vitro* and *in-vivo* (Futrega et al., 2021). In health, TGF-β, bone

morphogenetic protein (BMP), and hedgehogs act in concert to ensure correct bone development, by targeting distinct cell populations of the growth plate (GP) at specific stages of development. For example, they promote chondrocytes' anabolic activity, while preventing calcification (Wang et al., 2014). Signalling activity, however, depends on several factors, including the availability of chondroitin sulphate isoforms. Both accumulation and depletion of this GAG have been associated with disruption of correct GP organisation, cell proliferation and apoptosis (Alliston, 2010). In the case of MPSVI, for example, accumulation of C4S leads to a shift in the balance between TGF-β and BMP, towards a hyperactivation of TGF-β and inhibition of BMP (Klüppel et al., 2005). Despite further studies should be performed to clarify their interaction, the expression of both TGF-β and BMP can be used to monitor correct bone development process. Specifically, the known accumulation of C6S in addition to KS in MPSIVA, may implicate an alteration in TGF-β activity with detrimental consequences. This is an aspect that should be investigated in the future.

1.5.4 Fibroblast growth factors signalling altered by GAGs accumulation

Additional important regulators of cell proliferation, migration and differentiation, in development are fibroblast growth factors (FGFs) (Ornitz and Itoh, 2001; Ornitz and Marie, 2015). Though very important in embryogenesis, FGFs regulate growth and tissue maintenance, repair and regeneration processes, in postnatal and adult tissues (Ornitz and Marie, 2015). Accumulation of GAGs has been shown to perturb this regulatory process. For example, uncontrolled GAG accumulation has been shown to alter FGF2-HS interactions and signalling pathway, in mouse models of MSD and MPSI patients (Pan et al., 2005; Settembre et al., 2008). Dysregulated FGF2 signalling response to lysosomal storage has been found in chondrocytes from murine models of MPSI (Kingma et al., 2016). Furthermore, HS accumulation in MPSIH and MPSIIIB affects the capacity of primitive progenitors to respond to mitogenic effect, resulting in a lower proliferation of neural progenitors (Gritti et al., 1996; Li et al., 2002). Further evidence of FGF2 impairment was observed in animal models of MPSII, where the signalling pathway appeared dysregulated at early stages of bone development and differentiation (Bellesso et al., 2018). It is thus believed that accumulation of GAGs alters the response of cell to cytokine activity, leading to impaired bone and neural development. However, though data on different MPSs are available, its role in MPSIVA still needs to be described.

1.5.5 GAGs accumulation stimulate Toll-like receptor signalling pathways

Further insights on the inflammatory mechanisms associated with MPS have revealed GAGs direct triggering of Toll-like receptor-4 (TLR4) signalling pathway. *In-vitro* and *in-vivo* studies have shown neuroinflammation, characteristic of several MPSs, to be associated with activation of the TLR4 pathway, due to stimulation of the adaptor protein myeloid differentiation primary response 88 (MyD88). This results in a surge of pro-inflammatory cyto- and chemokines in many diseases of accumulation (Ausseil et al., 2008; Goodall et al., 2014; Wiesinger et al., 2022). For instance, interleukin-1 (IL-1), TNF-α, monocyte chemoattractant protein-1 (MCP-1) and macrophage inflammatory protein-1α (MIP-1α) are all overexpressed in MPSIIIA and Gaucher Disease mouse models (Arfi et al., 2011; Ausseil et al., 2008; Vitner et al., 2016; Wilkinson et al., 2012). Similarly, MPSI murine models have shown elevated MCP-1, MIP-1 and IL-1 in their CNS (Guo et al., 2019; Holley et al., 2018), whilst MIP-α upregulation has been confirmed in MPSIIIA and B mouse models (Arfi et al., 2011; Ausseil et al., 2008). Accumulation of HS in MPSI, can be detected by TLR4 and stimulate the release of TNF-α and IL-1β, by acting as a TLR4 agonist (Goodall et al., 2014). However, HS interaction with TLR4 appears multi-faceted, with the substrate acting as a danger-associated molecular pattern (DAMP) and triggering TLR4-mediated inflammatory response, via the nuclear factor kappa-light-chain-enhancer of activated B cells (NF-κB) pathway. Though results mainly refer to HS accumulation, a similar mechanism is believed to be triggered by other storage molecules, such as GM gangliosides (Parker et al., 2020; Walkley, 2004). In healthy individuals, TLR4 signalling pathway in mature osteoblasts (OBs) is believed to support load-induced bone formation (Rajpar et al., 2023). In MPS, instead, local inflammation can boost skeletal degeneration. As a proof, MPSVII mice KO for TLR4 have shown a normalisation of GP development, long bone and craniofacial morphology (Simonaro et al., 2010). Hence, attenuating TLR4 expression could help reduce the skeletal damage observed in MPSs.

In light of the role of TLR4 and NF-κB signalling pathways in response to GAGs uncontrolled storage, associated markers should be monitored to evaluate disease state and progression. TNF-related apoptosis-inducing ligand (TRAIL) is a type II transmembrane protein aimed at triggering apoptosis by interacting with its two death domain-containing receptors 4 and 5 (DR4 and DR5) (Brunetti et al., 2013). It contributes to physiological Caspase-8-mediated apoptosis and can activate osteoprotegerin (OPG) and NF-κB pathway (van den Broek et al., 2021). In the

context of bone homeostasis, TRAIL is believed to limit OBs differentiation by increasing the rate of cell death in OBs precursors (Brunetti et al., 2013). This is due to pre-osteoblast higher expression of DcR2 receptor, increasing the cells' sensitivity to TRAIL and triggering the activation of the NF-κB pathway. Higher expression of TRAIL has been linked with increased cell apoptosis and a decreased NEUTs count (Yang et al., 2018). This makes TRAIL a good marker of the inflammatory state in MPSs with skeletal phenotypes and monitoring of this biomarker could help us trace disease progression. A summary of TRAIL effects can be seen in Figure 8.

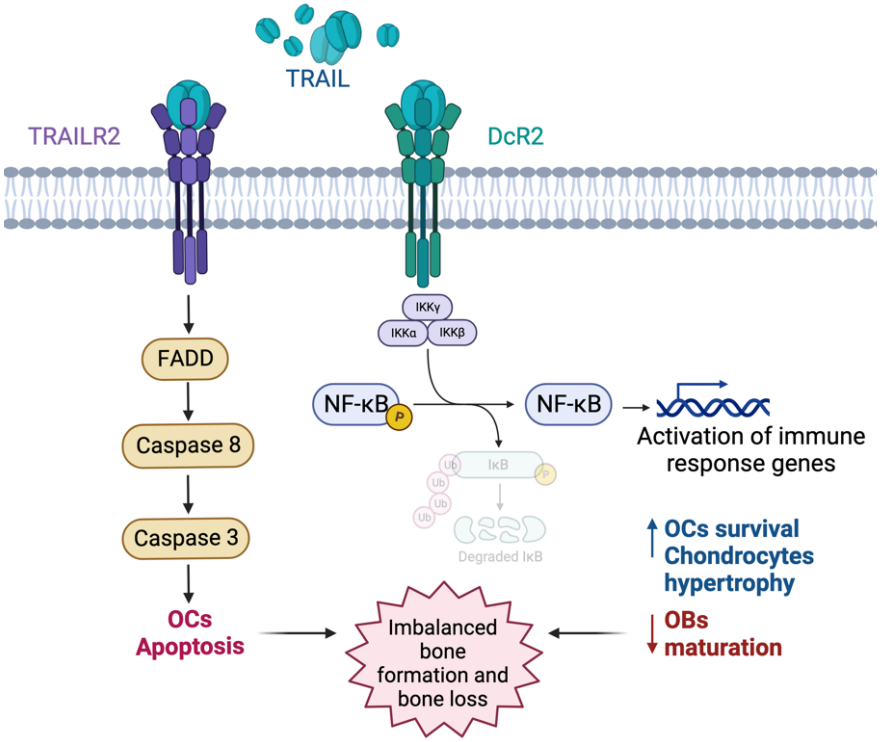


Figure 8 Effect of TRAIL on bone development.
Upregulation of TRAIL leads to a higher rate of OCs destruction due to over-activation of Caspase-8 mediated apoptosis. At the same time, TRAIL also causes the NF-κB pathway activation and impedes the correct maturation process of OBs, while compensating for OC destruction with a supportive and protective effect. This causes an imbalance between OCs and OBs and anomalies in bone turnover.

1.5.6 Inflammasome-mediated response can be activated by lysosomal dysruption

As mentioned earlier, lysosomes play an important role in regulating autophagy, which in turn, works as an inhibitor of IL-1β release (Saitoh et al., 2008). Impairment of correct lysosomal activity is believed to induce a loss of such inhibiting capacity and to activate an inflammasome-mediated response (Latz et al., 2013). Inflammasome complex can be activated by many recognition receptors, triggered by external and internal stimuli to oligomerise into a Caspase-1 complex, which is

then cleaved and induces the release and activation of IL-1β (Song et al., 2017). NLR family pyrin domain containing 3 (NLRP3) is a component of the inflammasome complex, mainly expressed by macrophages. It is aimed at detecting the products of damaged cells and trigger immune response. Among the several inducer stimuli, destabilization of the lysosomal membrane is a known activator of the NLRP3 inflammasome complex (Parker and Bigger, 2019). This was highlighted by studies on Gaucher Disease macrophages, demonstrating impaired autophagy stimulation of NLRP3 inflammasome activation and cytokine release, due to the dependency of inflammasome turnover on correct autophagic process (Aflaki et al., 2016). Impaired autophagy results in the polarization of macrophages towards an M1 phenotype (active state) and a secretion of pro-inflammatory cytokines, such as IL-1β and IL-6 (Aflaki et al., 2016). This activation is suggested to be triggered even by minimal glucosylceramide accumulation in macrophages and in iPSC-derived cells (Mizukami et al., 2002; Panicker et al., 2014). Thus, considering the sensitivity of NLRP3-complex activation, KS and C6S accumulation could likewise trigger it. Thus, monitoring of markers associated with this mechanism, such as IL-1β, could provide information about the activation of this pathway. Though inflammasome activation had not been associated with MPS before, recent studies have suggested the involvement of cathepsin B, a known inflammasome activator, in MPSI and MPSIII pathogenesis. For example, cathepsin B inhibition in MPSI mouse models has achieved a reduction in aortic dilatation and heart valve thickening, improving the general cardiac function (Gonzalez et al., 2018). Instead, in MPSIIIA mice, cathepsin B gene appears upregulated in the brain tissue (Arfi et al., 2011). While a common inflammasome mechanism has not been identified among different types of MPS, results from previous works clearly suggest its involvement in the inflammatory state generated by these LSDs. A summary of the main signalling pathways activated by GAGs accumulation is represented in Figure 9.

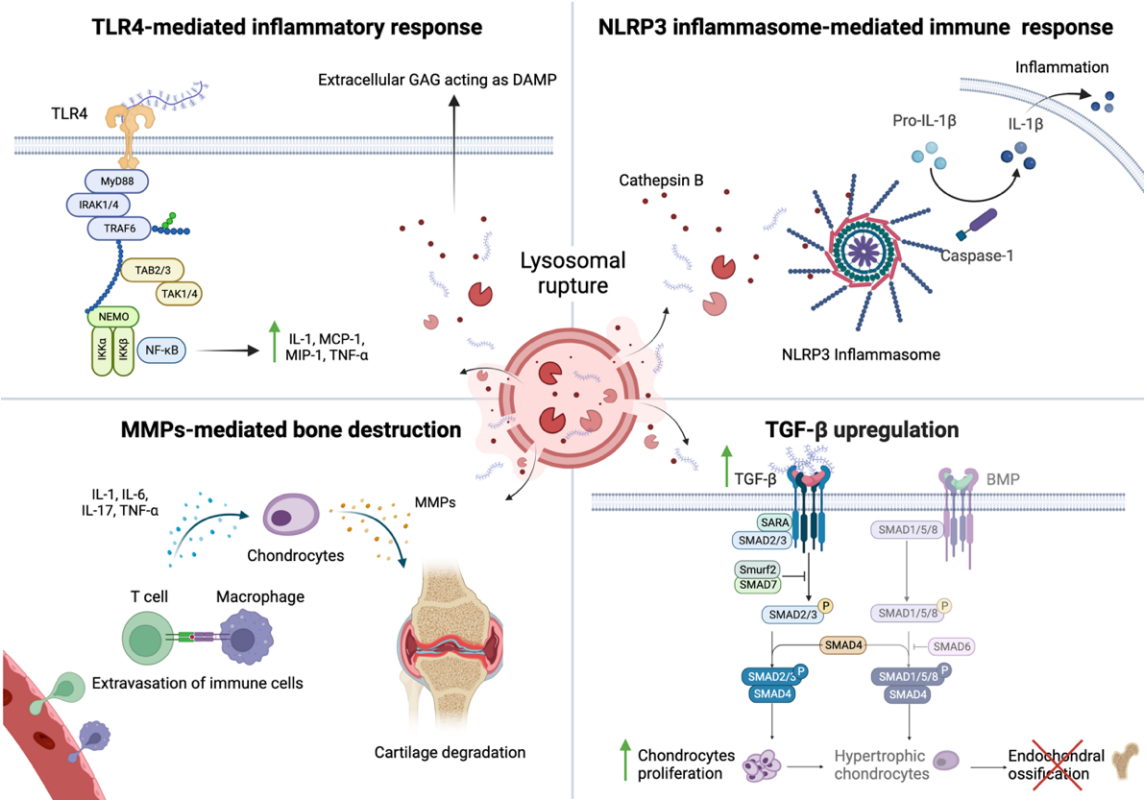


Figure 9 Inflammatory pathways associated with GAG accumulation and lysosomal disruption.

Several pathaways of inflammation are believed to be triggered by uncontrolled storage of undegraded GAGs. Lysosomal storage of this material can trigger lysosomal rupture and release of large amounts of GAGs in the ECM. From here, GAGs can act as DAMPs and activate TLR4 signalling pathway, which, by secondary activation of the NF-κB pathway can induce skeletal damage. Similarly, the released cathepsin-B from burst lysosomes interacts with NLRP3 inflammasome activating its activity and the release of IL-1β. Inflammation-driven bone detriment is also associated with extravasation of immune T- and B-lymphocytes and MMP gelatinases-mediated degenerative chondrolysis. Finally, GAGs accumulation can further damage bone formation by triggering hyperstimulation of TGF-β and chondrocytes proliferation. This leads to an imbalance between TGF-β and BMP signalling pathways, that act in concert to ensure correct endochondral ossification.

In general, IL-1 is a regulatory cytokine with pro-apoptotic and -inflammatory activity. It exists in two isoforms, α and β, that show similar biological activity but differ in their functions (Dinarello, 1997, 1996; Nakae et al., 2003). Of importance, IL-1 regulates correct bone formation and resorption processes, by activating and regulating OCs activity (Lee et al., 2010). It modulates OCs formation by stimulating prostaglandin E_2 production, enhancing receptor activator of NF-κB ligand (RANKL) and OPG expression by OBs and stromal cells (Lee et al., 2010). Though, IL-1, particularly IL-1β, is fundamental to initiate the repair of traumatic damages to the bone, its sustained expression is associated with bone destruction, in pathogenic conditions. As an example, IL-1β has been observed to activate RANKL secretion, while reducing OPG production, stimulating osteoclastogenesis (Nakashima et al.,

2000; O'Gradaigh et al., 2003). At the same time, persistent exposure of OBs to IL-1β diminishes the migratory capacities of these cells towards chemotactic factors, suggesting inhibition of migration-relevant adhesion proteins and MMPs (Figure 10) (Hengartner et al., 2013). Importantly, IL-1β appears elevated also in the synovial fluid of MPSVII dogs, and in fibroblast-like synoviocytes of MPSVI rats, confirming its role as a biomarker of skeletal disease (Simonaro et al., 2010, 2008, 2001). Thus, IL-1β expression is believed to efficiently mirror the effects of skeletal disease and bone formation process. Hence, by evaluating its expression, we could monitor the balance or imbalance of bone formation and remodelling, in MPSIVA models.

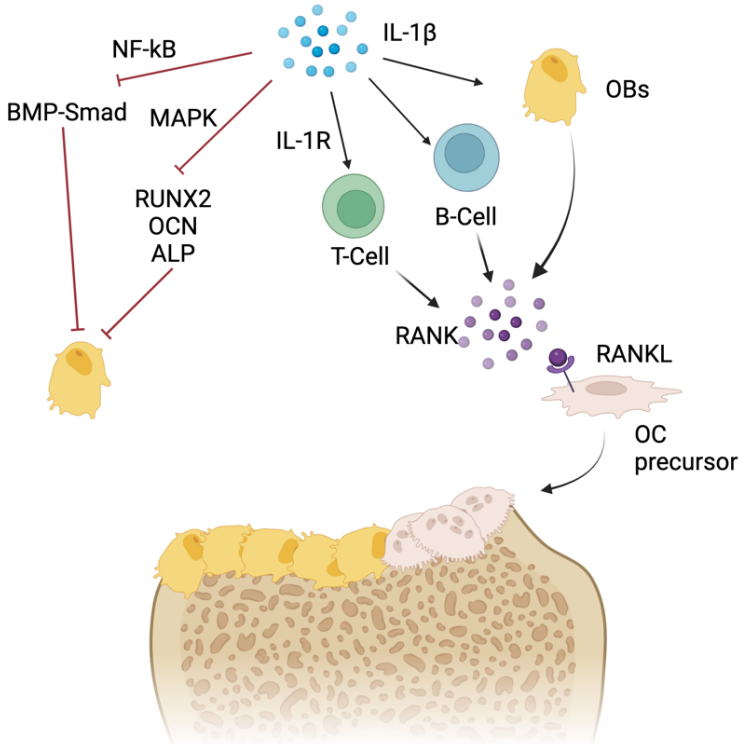


Figure 10 Effect of IL-1β on OCs and OBs
Overexpression of IL-1β correlates with an indirect stimulation of OCs differentiation and a simultaneous inhibition of OBs activities. This causes an imbalance between Ocs and OBs, resulting in the altered bone formation process and in higher fragility of the structure (Adapted from Jiang et al., 2021).

Recently, a comparative study between MPS patients receiving HSCT and an untreated control group have added more details to the impact of inflammation and the magnitude of residual disease after treatment. In a pool of patients suffering from different MPS types, several biomarkers, mainly pro-inflammatory, appeared upregulated on OLINK analysis of dried blood spot samples, prior to HSCT (van den Broek et al., 2021). As observed with ERT, the pro-inflammatory state appears to persist at short-term follow-ups, though inflammation ameliorates after 5-10 years of treatment (Aguilar Delgado et al., 2023; van den Broek et al., 2021). However,

whilst inflammation appears to improve, expression of markers of bone homeostasis remains abnormal, suggesting their potential role as biomarkers for residual skeletal disease. So far, a similar investigation has yet to be performed on MPSIVA patients alone or animal models of the disease and may provide essential information on the pathophysiology and progression of this disease. The limited number of both MPSIVA patients and available animal models, however, makes this task challenging.

One of the upregulated markers of inflammation in MPS patients is HGF (van den Broek et al., 2021). Previous studies have shown an increase in the systemic levels of HGF in RA patients, though its mechanism of action is still debated (Huang et al., 2020; Kontny and Prochorec-Sobieszek, 2013; Rabquer and Koch, 2013). Nevertheless, HGF supportive effect on osteoclastogenesis is known. The GF sustains OCs formation by promoting the maturation of precursor OCs (Adamopoulos et al., 2006; Huang et al., 2020; Taylor et al., 2012). At the same time, the GF inhibits Smads activation and, in turn, morphogenetic protein-induced osteoblastogenesis, reflected by a decrease in systemic bone alkaline phosphatase (BSAP) concentration (Tsubaki et al., 2020). Furthermore, HGF is believed to inhibit BMPs, promotors of OBs differentiation. This mechanism is exacerbated in patients suffering from multiple myeloma, in which serum levels of HGF have been inversely correlated with bone formation (Standal et al., 2007). Hence, increased HGF activity results in a stimulation of osteoclastogenesis and a simultaneous hampering of OBs differentiation, as summarised in Figure 11. These aspects should be monitored in our mouse models of MPSIVA and could highlight impaired mineralisation process.

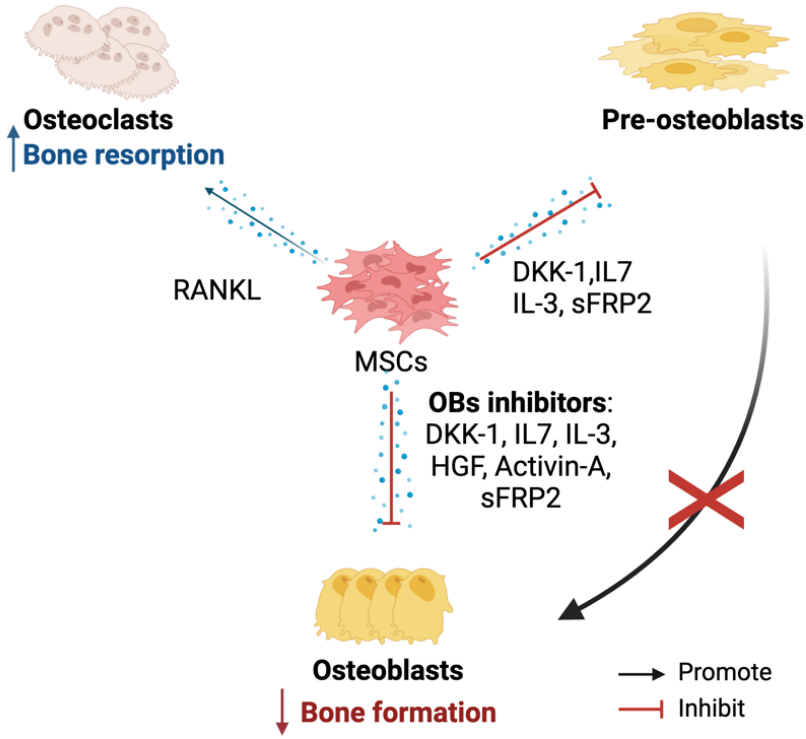


Figure 11 Higher HGF secretion inhibit OBs formation and activities, while increasing bone resorption.

Upregulation of HGF is believed to negatively impact on the appropriate bone formation mechanism by limiting OBs activities of bone formation and maturation of pre-osteoblasts into mature OBs.

1.6 ER-stress in MPSs

In addition to systemic inflammation, the effects of GAGs on the ER should also be considered. In the ER, proteins normally fold into their original conformations to undergo post-translational modifications. Should this process fail, misfolded proteins accumulate in the ER lumen and activate the unfolded protein response (UPR) (Vitner et al., 2010). UPR is started by three transmembrane proteins: activating transcription factor 6 (ATF6), IRE1, and PKR-like ER kinase (PERK). At physiological state, immunoglobin binding protein (BiP), an ER chaperone, binds to the luminal domains of the three master regulators to maintain them inactive. In the case of stress cues, BiP dissociates to activate the transmembrane proteins and their cascade signalling pathways, summarised in Figure 12. For example, TLRs activity can stimulate infiltrating myeloid cells, recognised as significant promotors of inflammatory reaction, which in turn can trigger NF-κB activation via inositol requiring 1 (IRE1) and eukaryotic initiation factor-2α (eIF2α) (Martinon et al., 2010; Martins et al., 2016; Muralidharan and Mandrekar, 2013). Once active, the UPR pursues adaptive response, feedback control, and cell fate regulation (Oslowski and Urano, 2010). The adaptive response mechanism stimulates the upregulation of proteins

aimed at enzyme processing, to increase folding and reduce amassing of unfolded proteins. In addition, clearance of misfolded proteins is promoted by ER-associated protein degradation (ERAD) and autophagy (Oslowski and Urano, 2011). Feedback control limits UPR excessive activation as the clearing process takes place. Cell fate regulation is essential to avoid ER-stress associated pathogenesis, directing cells towards survival or apoptosis, depending on whether the previous mechanisms can resolve ER-stress or not (Oslowski and Urano, 2011). Hence, the effect of KS/C6S accumulation in MPSIVA models should be investigated to understand the ER response.

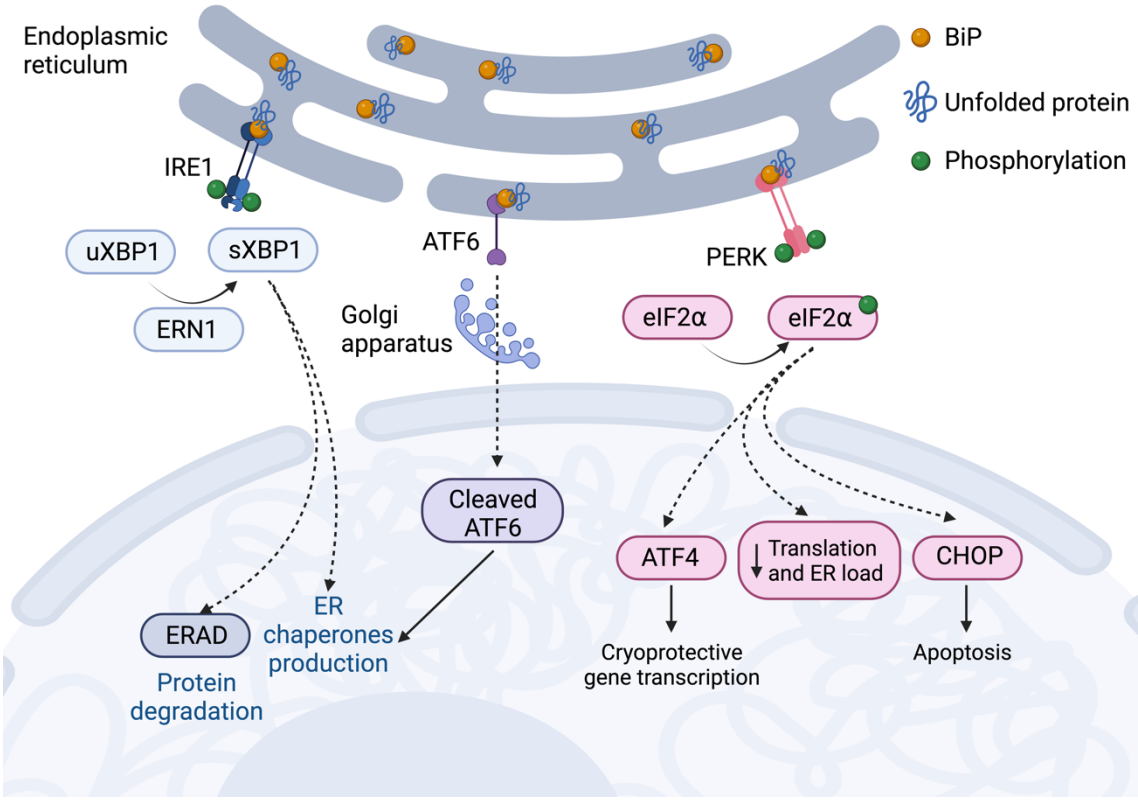


Figure 12 UPR mechanism of action.
IRE-1 senses the presence of unfolded proteins by its N-terminal luminal domain to which it responds by dimerization and autophosphorylation to activate. Its IRA1α isoform splices X-box binding protein 1 (XBP1) mRNA that, subsequently upregulated UPR target genes, including those acting in endoplasmic-reticulum-associated protein degradation (ERAD). ATF6, in its isoform ATF6α transfers to the Golgi apparatus to undergo cleavage and further translocates to the nucleus to trigger UPR genes involved in protein folding, processing, and degradation. Perk, similar to IRA1α, oligomerises, autophosphorylated and phosphorylates Ser51 on the α subunit of eukaryotic initiation factor 2 (eIF2α) upon sensing misfolded protein accumulation. Phosphorylated eIF2α reduces mRNA translation by halting the ribosome formation. This reduces the ER workload, protecting cells from exhaustion and ER-stress mediated apoptosis (Oslowski and Urano, 2011)

1.7 Skeletal manifestations in man and available mouse MPSIVA models

As previously mentioned, pathogenic variants of *GALNS* are the underlying cause of MPSIVA, causing abnormal protein activity, deleterious KS accumulation in tissues and severe clinical phenotypes, in humans. The correlation between GALNS deficiency and disease phenotype, however, is not as straightforward in animals. For this reason, developing animal models for MPSIVA has represented a challenging task, delaying the preclinical development of new treatment options too. For over 20 years, several groups have been working to develop innovative models to test novel treatments for this disease.

In 2003, a deletion was achieved between the intron 1 and exon 2 of the of the *Galns* gene by targeted homologous recombination. The region was selected because it contains C76, homologous to the human Cys79, a cysteine residue active in the catalytic domain for substrate binding in sulfatases, hence, an essential residue for correct EA (Schmidt et al., 1995; Tomatsu et al., 2003). The targeting vector employed for model generation contained the murine *Galns* gene cloned from the Strategene 129/Sv mouse genomic library, in which a 1.8 kb sequence spanning from intron 1 to exon 2 was replaced by *neo*^{r} cassette, containing the *neo*^{r} gene regulated by the mouse phosphoglycerate kinase (PGK) promoter (Tomatsu et al., 2003). A cassette containing thymidine kinase gene with a PGK promoter was also added upstream the *Galns*-encoding region. The LoxP sequences were placed at both ends of the *neo*^{r} *gene* (Tomatsu et al., 2003). Embryonic stem cells (ESCs) of 129SvJ mice were electroporated with the linearized targeting vector and selected in the presence of G418 and ganciclovir. Selected colonies were checked for homologous recombination by PCR and implanted into C57BL/6J mice blastocysts. The generated chimeric male mice were backcrossed for germline transmission to C57BL/6J females (F1). The F1 mice was further mated with mice expressing *Cre* to eliminate the *neo*^{r} gene and obtain a neo-excised heterozygous progeny that was crossed to generate the final homozygous *Galns*$^{-/-}$ strain (Tomatsu et al., 2003). The result strain showed no expression of *Galns* mRNA and enzyme activity, whilst lysosomal storage in tissues from soft organs was revealed on histological analysis (haematoxylin and eosin staining) (Tomatsu et al., 2003). Accumulation of GAGs was quantified using 1,9-dimethylmethylene blue staining and highlighted an increased level of GAGs detected in urine samples. An enzyme-linked immunosorbent assay (ELISA)-Sandwich method was used to measure KS in urine, serum and cornea, showing accumulation

in the cornea of *Galns*$^{-/-}$ mice, but undetectable levels of KS in urine samples (Tomatsu et al., 2003). Despite promising in terms of biochemical characteristics, this model did not show skeletal manifestations comparable to those observed in patients, making it a limited model to study the progression of the disease with primary skeletal involvement.

Using a similar method, a novel MPSIVA mouse model characterized by the C76S point mutation in the *Galns* gene and the presence of the human *GALNS* cDNA with a C79S pathogenic variant was generated in 2005 by the group of Tomatsu. In this case, the targeting vector contained the murine *Galns* gene cloned from the Stratagene 129/Sv mouse genomic library in which the C76 residue on exon 2 was mutated by mutagenic PCR (Tomatsu et al., 2005). A cassette composed of Thymidine kinase (TK), *neo*^{r} gene and human C79S mutated *GALNS* cDNA under the control of the actin-β chicken promoter was introduced in the intron 1 of murine mutated *Galns* gene (Tomatsu et al., 2005). The LoxP sequences were placed at both ends of the *neo*^{r} gene. The targeting vector was introduced into 129SvJ ES cells by electroporation. After G418 and ganciclovir selection, ES clones were checked for homologous recombination and injected into C57BL/6J blastocysts. Like the 2003 model, the generated chimeric male mice were backcrossed for germline transmission to C57BL/6J females (F1). The F1 mice was further mated with mice expressing *Cre* to eliminate the *neo*^{r} gene and obtain a neo-excised heterozygous progeny that was crossed to generate the final homozygous *Galns*$^{tm(hC79S:mC76S)slu}$ strain. This strategy generated mouse models, tolerant to the human GALNS, avoiding the development of antibody development as a result of repeated administration of ERT (Tomatsu et al., 2005). Produced mice showed evidence of lysosomal storage in bones, brains, cornea and visceral organs as early as 2 months of age. Urinary levels of excreted GAGs also appeared mildly increased (Tomatsu et al., 2005). In addition, levels of collagen X, a bioproduct of endochondral ossification associated with hypertrophic chondrocytes, appeared raised in MPSIVA tolerant mouse models compared to WT controls, with an increasing trend over time (Tomatsu et al., 2005). Although promising and improved compared to the model developed in 2003, this *Galns*$^{tm(hC79S \cdot mC76S)slu}$ mouse model still showed very mild phenotypes, particularly in terms of skeletal evidence.

Thus in 2007, a new MPSIVA mouse model was generated by introducing the C76S alteration in the exon 2 of the murine *Galns* gene, to examine the pathological phenotype in the absence of a human transgene (Tomatsu et al., 2007). In this case,

the targeting vector contained the 5' 4.2kb fragment and a 3' 4.5kb fragment of the *Galns* gene, cloned from the Stratagene SvJ129 mouse genomic DNA. This corresponded to the exon 1 and exons 2–4, respectively. The C76S pathogenic variant in the exon 2 was introduced by mutagenic PCR. In the complete targeting vector, the exon 1 fragment was introduced between the TK gene and *neo*^{r} gene, while the exons 2 (C76S)–4 of murine *Galns* was added to the end of *neo*^{r} gene (Tomatsu et al., 2007). The loxP sequences were positioned at both ends of the *neo*^{r} gene, for Cre recombinase-mediated removal. The targeting construct was linearized and electroporated into 129SvJ-derived ESCs (Tomatsu et al., 2007). Mutated ESCs were implanted into C57BL/6J mice blastocysts. Male chimeric mice were crossed with C57BL/6J females to generate the F1 heterozygous mice that were first crossed with mice expressing the Cre enzyme to excise the *neo*^{r}*.* Obtained *neo*^{r}-depleted heterozygous mice were mated to produce homozygous mice with a knock-in pathogenic variant to p.C76S (*Galns*$^{tm(C76S)slu}$) (Tomatsu et al., 2007). Despite showing very low EA, the novel mice were not distinguished from their heterozygous and WT littermates, in terms of skeletal phenotypes. Compared to the previously generated model (the *Galns*$^{tm(hC79S \cdot mC76S)slu}$ from 2005), *Galns*$^{tm(C76S)slu}$ mouse model presented a milder phenotype and a lower degree of storage (Tomatsu et al., 2007). It is believed that the 2005 *Galns*$^{tm(hC79S \cdot mC76S)slu}$ model show higher lysosomal storage due to the expression of a non-functional human mutant GALNS protein*.* Furthermore, 2007 *Galns*$^{tm(C76S)slu}$ mice show a missense pathogenic variant that can only affect GALNS activity, without interacting on other sulfatases, whereas 2005 *Galns*$^{tm(hC79S \cdot mC76S)slu}$ induced pathogenic mutation can impact on many other sulfatases in addition to causing severe GALNS deficiency (Tomatsu et al., 2007, 2003).

Thus, none of the three mouse models developed so far have achieved to effectively recapitulate human phenotype in terms of skeletal pathology. This may be due to the differences in terms of KS synthesis seen in mice compared to humans and to the absence of KSII in mice connective tissue, except for the cornea (Venn and Mason, 1985). Despite the fundamental contribution in understanding MPSIVA offered by these three models, none of them displays comparable evidence of bone phenotype to humans. This leaves an important gap in the field of MPSIVA research, leaving the disease still orphan of a representative murine model.

More recently, however, a rat model of MPSIVA was generated by CRISPR-Cas9 technology to reproduce the human Arg386Cys pathogenic variant and test the

efficacy of AAV9-based GT. The human Arg386Cys caused by C>T substitution in position 1156 of the human coding sequence corresponds to Arg388Cys in the rat protein, which was induced by C>T change in position 1162, in the rat's *Galns* coding sequence (Fukuda et al., 1996; Tomatsu et al., 2005). To produce the targeted pathogenic variant, two specific RNA guides, were designed to target exon 11 and drive the Cas9 double-strand break, close to the 1162 C genomic position. A single strand donor DNA sequence was designed to introduce both the 1162C>T missense pathogenic variant and a new MboII restriction site, required for genotyping analysis of the offspring (Bertolin et al., 2021). Two homology arms were also included in the donor DNA to enable homologous recombination with the rat *Galns* genomic sequence. The gRNA, donor DNA, and Cas9 mRNA were microinjected into the pronucleus of one-cell Sprague–Dawley (SD) rat embryos. Heterozygous knock-in male rats were backcrossed with WT rats for three generations (F1, F2, and F3) to segregate and eliminate possible CRISPR/Cas9-associated off-target events. Homozygous mutant rats were obtained by mating heterozygous littermates of the F3 generation (Bertolin et al., 2021). Homozygous mutant rats, obtained after 3 consecutive backcrosses, presented no GALNS activity in soft organ tissues and bones, elevated KS in the liver and serum and reduced body weight compared to WT counterparts. *Galns*$^{-/-}$ also showed naso-anal length reduced by about 20%, compared to WTs and shorter tibiae (Bertolin et al., 2021). Hypertrophic chondrocytes could be appreciated in the GP of the untreated *Galns*$^{-/-}$ rats and the models showed a reduction in terms of mineral density (BMD) and bone mineral content (BMC), tissue mass content and Bone volume/Tissue volume ratio (Bertolin et al., 2021). Such findings appear concordant with classical Morquio A manifestations, making the rat model a suitable option for the disease.

Until now, both rats and mice have been employed for *ex-vivo* bone culture investigations, with similar frequency (Abubakar et al., 2016). This may suggest that both species provide similar results when evaluating bone growth (Abubakar et al., 2016). However, the larger size of the rat model, positive in the case of bone dissection, appear limiting in terms of both animal housing and experimental protocols to be performed. Given the already established protocols available at Ospedale San Raffaele for both the analysis of the bone structure and HSCT procedures, the use of a rat model did not appear suitable for the current study (Biffi et al., 2006, 2004; Visigalli et al., 2010). At the same time, the limitations associated with the mouse models available (Figure 13) when this study began, led to consider

the development of a novel mouse model as the most appropriate route to study MPSIVA pathophysiology and test innovative therapies.

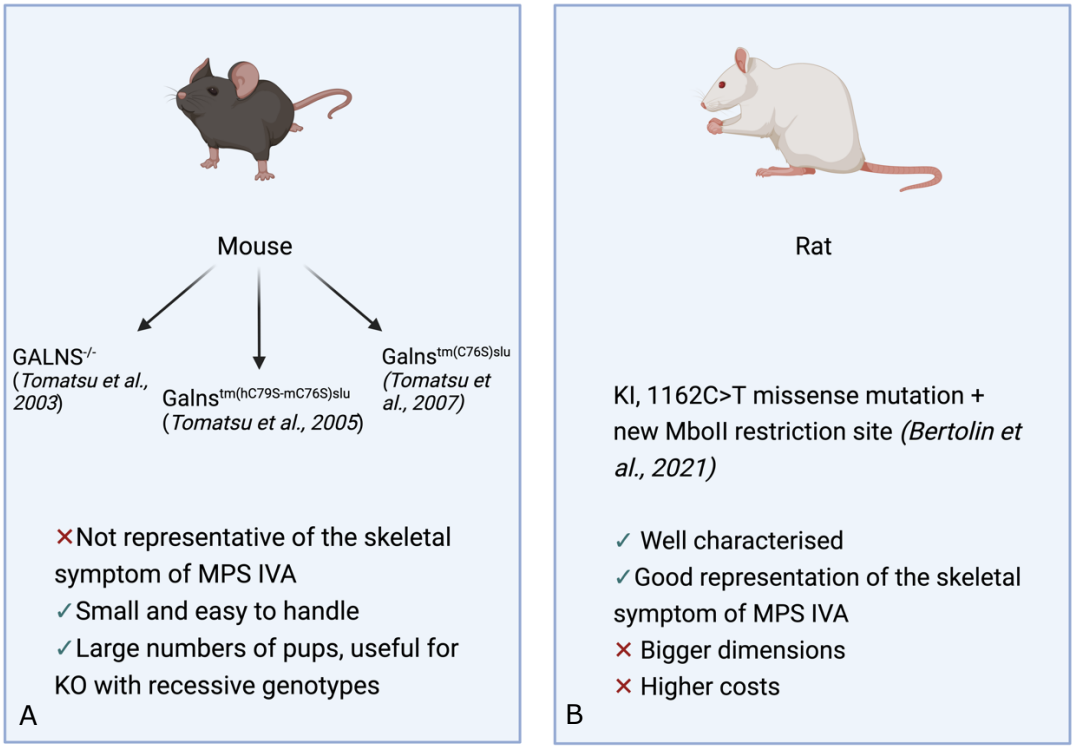


Figure 13 Summary of available mouse and rat models for MPSIVA.
Different techniques have been employed to develop these models, succeeding in generating models with no GALNS enzyme activity and various degrees of GAG accumulation. While the rat model (B) shows evidence of skeletal phenotype, none of the three mouse models developed (A) has achieved efficient representativeness of the skeletal symptom observed in humans.

1.8 Current therapeutic options

To date, available therapies against MPSIVA are mostly palliative or supportive, tackling the disease manifestations, rather than the root cause of the disease. The main therapeutic strategies include ERT, haematopoietic stem cell transplantation (HSCT), and corrective surgical interventions.

1.8.1 Enzyme Replacement Therapy

ERT aims at providing MPSIVA patients with recombinant GALNS (elosulfatase alpha, known with its commercial name as Vimizin). Administered enzymes bind to M6PRs on cell surface and are delivered to the lysosome (Taylor et al., 2019). The therapy was approved by both EMA and FDA in 2014 and currently represents a therapeutic option in both Europe and the U.S., showing persistence and stability (Sawamoto et al., 2020). Results from patients have shown good tolerance and

diminished urinary KS levels, though KS in blood appears to remain unaltered (Khan et al., 2018). Other than a good tolerability, a phase II study on patients younger than 5 years of age also highlighted considerable reduction of urinary KS and improved growth rate (Ficicioglu et al., 2020). Similarly, a randomised double blind phase III trial on patients older than 5 years of age further showed recovery of the pulmonary function, height and improved results on a 6-minute walking distance test (Hendriksz et al., 2014).

Results from a different phase III trial study showed the development of anti-drug antibodies and immunoglobulin E. However, an increase in anti-drug antibody did not correlate with decreased drug effect or with safety issues (Schweighardt et al., 2015). Similarly, although some MPSIVA patients treated with ERT has presented drug-specific antibodies, this aspect has not been correlated with anaphylactic events (Long et al., 2017). Still, several long-term studies have highlighted the limited effect of ERT on improving airways obstruction in patients. For example, despite the amelioration in forced vital capacity (FVC) and forced expiratory volume in 1s (FEV1), a general deterioration of static spirometry results has been registered in long-term follow up studies (Hendriksz et al., 2015, 2014; Kenth et al., 2019).Furthermore, a great limitation to the use of ERT is its intermittent effect with necessary repeated administration. This not only limits the treatment's effect, but also negatively impact on patients' QoL, requiring frequent injections of the drug.

Unfortunately, the most noteworthy limitation of ERT resides in its inability to correct skeletal lesions associated with MPSIVA, as highlighted by the analysis of chondrocytes and ECM from patients treated with the therapy up to 30 months (Tomatsu et al., 2015a, 2015b). Additionally, ERT has shown no effect on correcting short stature in severe MPSIVA patients, independently on the time of administration of the therapy (Do Cao et al., 2016; Doherty et al., 2019). Collectively, these drawbacks have drastically decreased the drug's cost-effectiveness, leading to several countries to halt reimbursement on this therapy (Sawamoto et al., 2016). In order to improve ERT efficacy, a modified version of the corrective enzyme has been developed to extend its clearance from the bloodstream after administration, to induce greater enzyme activity (Tomatsu et al., 2010).

Collecting evidence of the effect of ERT and all treatment options for MPSIVA has highlighted the importance of early diagnosis and prenatal screening (Ficicioglu et al., 2020). In light of the progressive nature of MPSIVA and, in general, of disease of

accumulation, early treatment can make a significant difference in terms of symptom progression or reduction. Hence, the better understanding of the skeletal symptom associated with the disease may enable early diagnosis and treatment, with positive effect on both morbidity and mortality (Ficicioglu et al., 2020).

1.8.2 Surgery

Though very supportive, especially if administered early in disease development, ERT remains ineffective to fully correct MPSIVA skeletal symptom, often making orthopaedic, cardiac or respiratory surgery necessary (Pizarro et al., 2016; Yasuda et al., 2016). One of the main complications associated with MPSIVA is the potential spinal compression due to cervical vertebrae instability, which arise from odontoid dysplasia, incomplete ossification process, and laxed ligaments. In particular, cervical anomalies involve mainly the C1-C2 vertebrae, predisposing to myelopathy, paralysis and increased mortality risk (Tomatsu et al., 2011). As a consequence, spinal cord compression can lead to numbness and hypotonia of the patients' extremities, hyperflexibility of the tendons, and generalised fatigue (Terai and Nakamura, 2020). In order to avoid such complications, routine Computed Tomography (CT) scan, X-rays and MRI are performed to monitor the progression of the lesions and prompt the surgical fusion from the occiput region to C2, if necessary (Sawamoto et al., 2020). However, such intervention is not definitive and additional surgeries to the cervico-thoracic vertebrae are often required to correct distal junction instability (Dede et al., 2013). Further areas that are likely required to undergo surgery include the ankle and knee joints, and hip, due to progressive worsening of genu valgum, ankle valgus, hip dysplasia and dislocation (Dhawale et al., 2012; Mikles and Stanton, 1997). As for ERT administration, the effectiveness of surgery is strongly dependent on the time of intervention, eventually not completely correcting the defects observed.

Another complication observed can be the obstruction of the airways, one of the most common causes of death recorded in MPSIVA patients (Lavery and Hendriksz, 2014; Tomatsu et al., 2016). The complication has been associated with deleterious accumulation of undegraded substrate in the tracheal tissues, abnormal development of the trachea, brachiocephalic artery (union of the ipsilateral internal jugular vein and subclavian vein), anomalies of the neck and chest (e.g. pectus carinatum, common feature of MPSIVA) (Do Cao et al., 2016, 2016). Tracheal involvement appears so severe that patients have shown evidence of storage material accumulation even after receiving ERT (Pizarro et al., 2016). In order to limit the

complications associated with abnormal growth, routine radiographic imaging should be performed to obtain an overview of the developing structures and the potential progression of the disease phenotypes, particularly those affecting the spine, chest, hips and limbs (Wood et al., 2013). Given the little effect ERT has shown on limiting the progression of skeletal symptom, surgery still appears the best option to free MPSIVA patients' airways. An example of standard intervention is tracheostomy, despite its severe impact on patients' QoL. Patients undergoing this type of surgery lose their speech ability, in addition to all potential complications of invasive surgery. Therefore, although surgical intervention is still necessary and highly helpful to ameliorate the skeletal and respiratory capacities of patients, its toll on the patients' QoL and the risks associated with it should not be underestimated. This makes surgery essential but, unfortunately, not resolutive of the disease.

1.8.3 HSCT

HSCT is a common method of treatment of patients with haematological and immunological diseases. In the case of MPSs, the method aims at exploiting the BM with all haematopoietic stem cells from a healthy donor to induce the production of a significant amount of healthy immune cells, such as leukocytes and macrophages, supplying the deficient enzymes (Figure 14). This allows an amelioration of the biochemical profiling of patients, although clinical improvements are highly dependent on the type and stage of MPS (Yabe et al., 2016).

The first successful attempt at treating a form of MPS with HSCT, dates back to the 1980s on MPSI-Hurler syndrome and since then, the method has been extended to patients suffering from MPS II, VI, and VII (Hobbs et al., 1981; Yabe et al., 2016). This treatment has shown remarkable amelioration of MPS symptoms such as hepatosplenomegaly and corneal clouding, raise in plasma enzyme levels particularly when administered very early in life (Hoogerbrugge et al., 1995; Yasuda et al., 2015). However, one of the potential complications associated with HSCT may be the development of graft-*versus*-host disease (GvHD). This was observed in a study from 1981, in which the recipient patient developed GvHD after receiving blood from his father first and his mother later, though amelioration of MPS symptom was also observed (Hobbs et al., 1981). At the time, HSCT was associated with elevated mortality risk, due to administration of the treatment to patients at late stages of the diseases and, hence, with poor prognosis (Taylor et al., 2019). Since then, HSCT has undergone significant technical advancements such as the employment of matched cord blood units as a source of haematopoietic stem progenitor cells (HSPCs) and

HLA-matching techniques to screen for candidate donors. Also, refinement of the chosen conditioning regimen for the patient has allowed engrafted survival rates to raise up to 90% (Bernardo and Aiuti, 2016; Boelens et al., 2014, 2013, 2007; Lum et al., 2017; Peters et al., 1998).

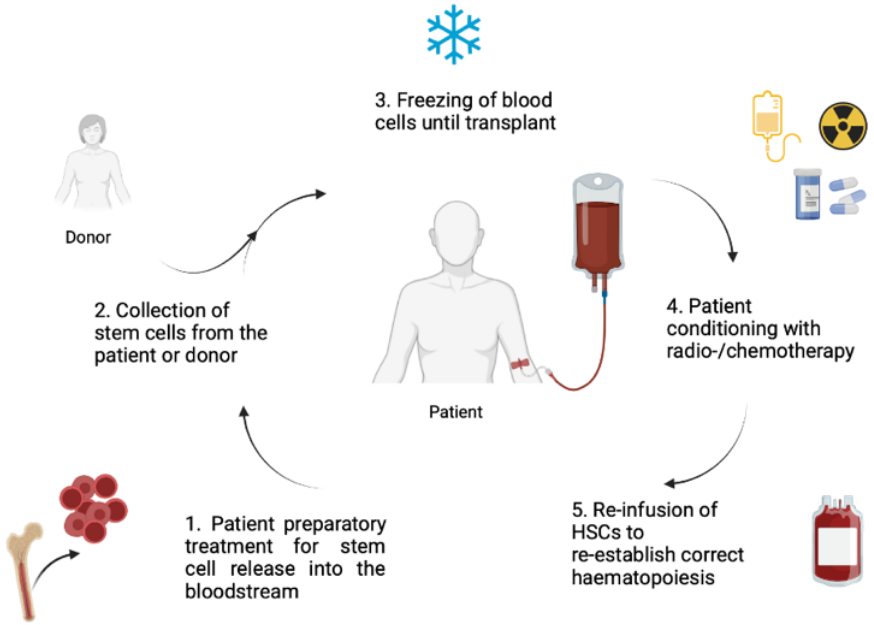


Figure 14 Schematic representation of standard HSCT procedure.
Patients or donors usually receive a preparatory regimen to make HSCs leave the BM and access the bloodstream, from which they can be collected and stored by cryopreservation until use. Patients are further administered a conditioning regimen to make space for the cells that will be re-infused. Thawed cells are then administered to patients by intravenous infusion.

In 2014, the treatment strategy was extended to MPSIVA, with one male patient undergoing allogeneic HSCT at 15 years of age (Chinen et al., 2014). At a 5-year follow-up, the patient showed GALNS activity matching that observed in the donor, improved pulmonary function and BMD, yet no improvement in height could be detected (Chinen et al., 2014). Four more patients were later successfully transplanted with no evidence of GvHD, while patients' clinical manifestations ameliorated (Chinen et al., 2014; Yabe et al., 2016). Further improvements could be observed in the activity of daily living (ADL) of treated patients, compared to untreated counterparts. Again, improvements appeared to be correlated with the time of treatment administration (Yabe et al., 2016). Between 2013 and 2020, 42 patients of different types of MPS received HSCT, of which 15 suffered from MPSIVA (Qu et al., 2022). The overall survival rate observed was >92%, with survival rate for patient varying according to the source material (i.e. 100% survival of patients receiving HSPCs from umbilical cord blood; 87.5% survival of patients receiving

HSPCs from peripheral blood) (Qu et al., 2022). All patients with MPSIVA reached a healthy enzyme level, improved respiratory and cardiac functions, and no severe complication (Qu et al., 2022). Similarly, in 2020, a study by Sawamoto *et al*., achieved the improvement of BMD, pulmonary function and scored of ADL, reducing the frequency of required surgical interventions (Sawamoto et al., 2020).

Overall, results from the last 20 years have provided evidence of the essential supportive role of HSCT, in several different types of MPSs. HSCT is normally a one-time treatment providing missing enzymes to patients, allowing for clearance of accumulated substrates (Noh and Lee, 2014). However, the treatment outcome seems to be highly dependent on several factors, like donor cell source, time of administration and conditioning regimen. In addition to these general limitations of the method, MPSIVA present airways obstruction and anomalies that can lead to complication in case of anaesthesia and difficult intubation procedures (Chinen et al., 2014). At the beginning of the current century, the method still presented 27% mortality risk, mainly associated with poor donor selection procedures, infections, late stage of disease at the time of transplant, GvHD and conditioning-associated complications (Kubaski et al., 2017; Vellodi et al., 1999). Nowadays, allogeneic HSCT with prior or concomitant ERT is the standard of treatment for MPSIH, providing high rates of survival, particularly in those cases where HSCT is administered early and transplanted HSPCs are sourced from cord-blood (Aldenhoven et al., 2015a, 2015b; de Ru et al., 2011; Parini et al., 2017). However, this combinatory strategy does not appear sufficient to ameliorate neither the skeletal nor the cognitive symptom of MPS patients (Aldenhoven et al., 2017). Moreover, the treatment still does not correct the genetic pathogenic mutation causing the diseases but relies on the chimerism induced by transplanted cells into recipient patients and on the crosstalk between transplanted and endogenous cells. Hence, though not exempt of limitations, HSCT has shown remarkable results and improvements in the context of MPS treatment. However, the technique may be further refined by combining it with genetic modification of HSPCs, as explained in the next chapter.

1.9 Proposed novel therapies and preliminary data.

To overcome the current limitations of MPS therapy, a novel therapeutic strategy has been recently developed in San Raffaele-Telethon Institute for Gene Therapy (Figure 15). The method based on genetic engineering of autologous HSPCs (HSPC-GT) has been developed to induce supra-physiological activity of the IDUA enzyme,

deficient in MPSIH. The therapy has been delivered to 8 patients affected by MPSIH so far, who have received gene-corrected HSPCs (Gentner et al., 2021). Gene-corrected cells, in turn, have provided the missing IDUA enzyme while relying on resident HSCs turnover for persistence of EA (Gentner et al., 2021). This, has so far demonstrated beneficial to reduce GAG accumulation levels across the organism, including the CNS. Importantly, the newly developed method offers two main advantages. Firstly, the employment of autologous cells for the correction and transplant drastically reduces the risk of rejection and GvHD, likely occurring with allogeneic transplant (Aldenhoven et al., 2015a; Boelens et al., 2013; Lum et al., 2017). Autologous HSCT also allows for a rapid reconstitution of the immune system together with a clearance of the system from antibodies that may develop with ERT (Gentner et al., 2021). Nevertheless, potential genotoxicity and insertional mutagenesis associated with the use of lentiviral vectors in GT remain a concern, requiring long-term monitoring of the recipient patients (Biffi et al., 2011; Gentner et al., 2021).

The second important advantage of HSPC-GT refers to its application to skeletal conditions. As previously observed, allo-HSCT's efficacy has proven very limited in terms of correction of skeletal phenotypes (Aldenhoven et al., 2015b; Gardner et al., 2011; Langereis et al., 2015). In the case of the LV-IDUA HSPC-GT strategy, supraphysiological activity of the enzyme has shown to increment penetration of the enzyme even in the less vascularized tissues, such as the bone and cartilage (Gentner et al., 2021). Furthermore, the differentiation of gene-corrected HSCs into OCs provides high levels of IDUA directly inside the bone microenvironment, which are aimed at cross-correcting the neighbouring osteocytes (OCts) (Gentner et al., 2021). Until now, results from the most recent follow-up have shown appropriate growth and stability of the typical skeletal manifestations in HSPC-GT patients, mirroring a positive effect of the therapy on their skeletal phenotypes. This was also observed in the MPSIH animal model (Visigalli et al., 2010).

Though long term follow ups are needed to draw definitive conclusions, results appear promising, suggesting potential application of a similar strategy to other skeletal MPSs, like MPSIVA. However, in order to develop and test innovative therapeutic strategies such as HSPC-GT, MPSIVA still lacks an appropriate mouse model, has highlighted previously. This leaves an unmet clinical need that this study aims at fulfilling.

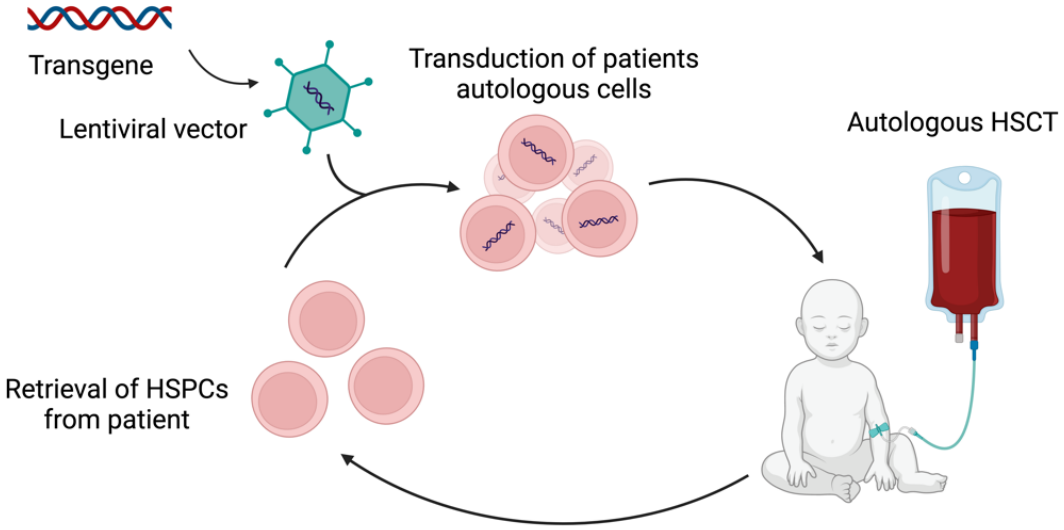


Figure 15 HSPC-GT strategy.
8 paediatric patients suffering from MPSIH have received autologous HSPCs previously transduced with a lentiviral vector containing the healthy sequence encoding for IDUA. The method has shown highly promising as sustained engraftment was observed in all patients, together with supraphysiological activity of IDUA enzyme. Though long-term monitoring is ongoing, the method appear a potential option for other similar diseases, including MPSIVA (Adapted from Gentner et al., 2021).

2 Aim of the work

Over the past century, the study of LSDs has experienced a significant expansion in our understanding of the underlying mechanisms driving disease progression. This, however, has involved the most severe and common diseases of this kind, thereby deferring the understanding of the rarest LSDs, as in case of MPSIVA. The limited availability of appropriate animal models has contributed to the slowing down of knowledge acquirement. Thus, the current study has focused on filling this gap by generating a novel mouse model for MPSIVA, by means of GE techniques. In addition, this study has focused on performing a complete characterisation of the newly developed mouse under several aspects, fundamental in MPSIVA patients.

Although other mouse models for the disease have been developed in the past, none of them has shown skeletal clinical features comparable to those observed in patients, therefore limiting their representativeness potential (Tomatsu et al., 2007, 2005, 2003). Hence, this project aims at comprehensively characterising the skeletal phenotype of the proposed gene-edited models. In addition, aspects of their inflammatory state, biochemical profile and behavioural and motor abilities will be all analysed to obtain a comprehensive description of the new model and significant parameters to be monitored in the case of therapy development.

A new MPSIVA mouse model not only will provide an alternative to the current rat model, easier to handle and manageable by the majority of animal facilities, but it may also provide novel insights on the disease pathophysiology, allowing the testing of innovative treatment strategies, at a preclinical stage (Bertolin et al., 2021).

3 Results

3.1 Generation of a murine model of MPSIVA by CRISPR-Cas9

To generate a novel mouse model for MPSIVA, we took advantage of CRISPR-Cas9 technology to delete a region between the intron 1 and exon 2 of the *Galns* genomic sequence of C57BL6/J mice. This region was selected due to the presence of the C76 residue, responsible for GALNS substrate recognition, and thus correct activity, as previously published (Schmidt et al., 1995; Tomatsu et al., 2003). A *Galns*$^{-/-}$ mouse model was generated in 2003 by the group of Tomatsu by homologous recombination in 129SvJ background mice (Tomatsu et al., 2003). Contrarily as to the previously described model, we induced the pathogenic variant to the target site directly into ESCs of C57BL6/J mice, a strain that is believed to exacerbate skeletal symptoms. Details of pathogenic variant generation can be found in section 6.1 of the Materials and Methods section. Six variants of the desired mutation were obtained with deletions of variable base-pair (bp) length, as shown in Figure 16. Of these, two of the obtained variants (named 14C and 22D) were excluded from further characterisation experiments, as they did not produce any viable offspring. Obtained pathogenic mutation 3, appear resemblant of the one carried by the mouse model developed in 2003 by the group of Tomatsu, previously discussed (Tomatsu et al., 2003).

	Deletion length (bp)	Start	End
KO3	278	122605192	122605469
KO6	140	123332210	123332349
KO7	70	122605467	122605536
KO9	58	122605189	122605246

Figure 16 Obtained variants of the pathogenic mutation induced by CRISPR-Cas9. Description and location of the obtained pathogenic variants. All pathogenic variants span from intron 1 and exon 2 of the *Galns* genomic sequence, though variants differ for bp length. Mice with pathogenic variants 14C and 22D have been excluded from characterisation experiments.

The remaining four variants were all employed for a multi-step characterisation that would define the biochemical, morphological, inflammatory, histopathological, and behavioural profile of our *Galns*$^{-/-}$ (knockouts, KOs) mice (Figure 17), with the aim of selecting the most representative model for MPSIVA. Data obtained from analysis of our mice at the earliest timepoints of 2 and 4 months were used to select

the model with the most evident symptom of MPSIVA, on which we performed the same analysis at a later timepoint of 8 months and further confirmatory genetic analyses and inflammatory profiling. Though our main experiments were performed at 2, 4 and 8 months of age on our models, the required time for acclimatization of mice between experiments led to some tests to be performed at a 3, 5 and 9 months of age. For all experiments C56BL6/J wild-type (WT) mice were used as control.

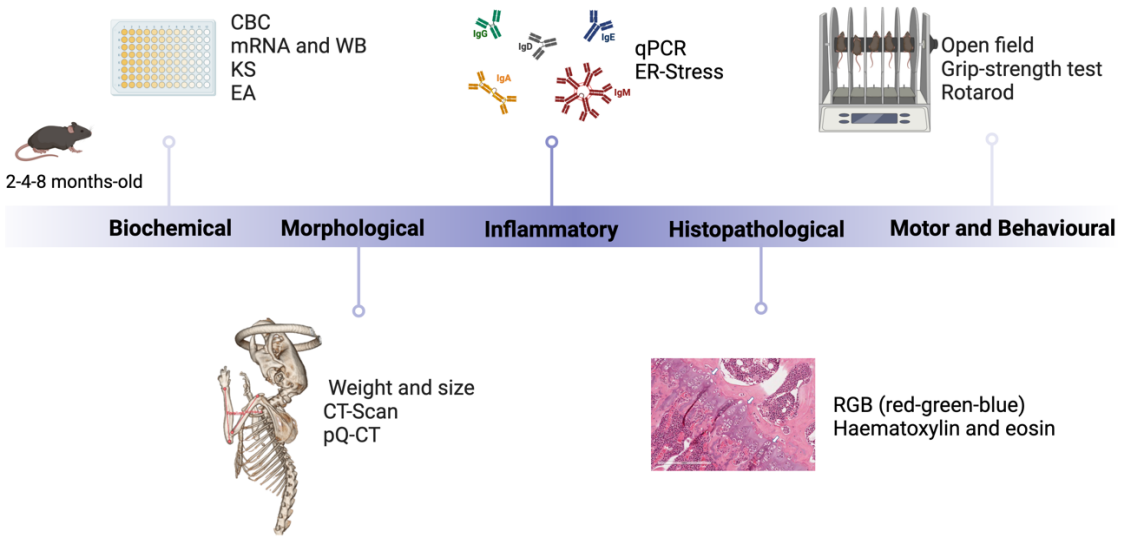


Figure 17 Characterisation experimental plan of MPSIVA mouse model.
Summary of the experimental plan to carry out a comprehensive characterisation of the newly generated mouse models. Characterisation of our models aims at comprehensively analyse the organisms under a biochemical, morphological (skeletal), inflammatory, histopathological, and behavioural point of view, to determine the most representative model.

3.1.1 Whole Blood composition

An initial evaluation of the gross composition of the mice blood was performed on all 4 viable strains by means of a complete blood count (CBC) on haemocytometer. C57BL6/J WTs were used as control samples. Statistically significant differences were observed among the males of different strains in terms of platelets (PLTs), monocytes (MONs), NEUTs, lymphocytes (LYMPHs) and white blood cells (WBC) count. More specifically, KO6 mice showed a decreased in the LYMPH count at 4 months of age while KO7 mice showed a clear drop in the number of PLTs, WBCs, LYMPHs, MONOs and NEUTs (Figure 18). No difference was highlighted in terms of haemoglobin (HGB) in any of the strain variants. Alterations in the blood composition appeared clearer in males of the same strains, though could not be observed in female counterparts (data shown in section of the Appendix 7.1). To confirm these differences, further analyses will be performed to reach an equal minimum n=12 of mice per group, at each timepoint.

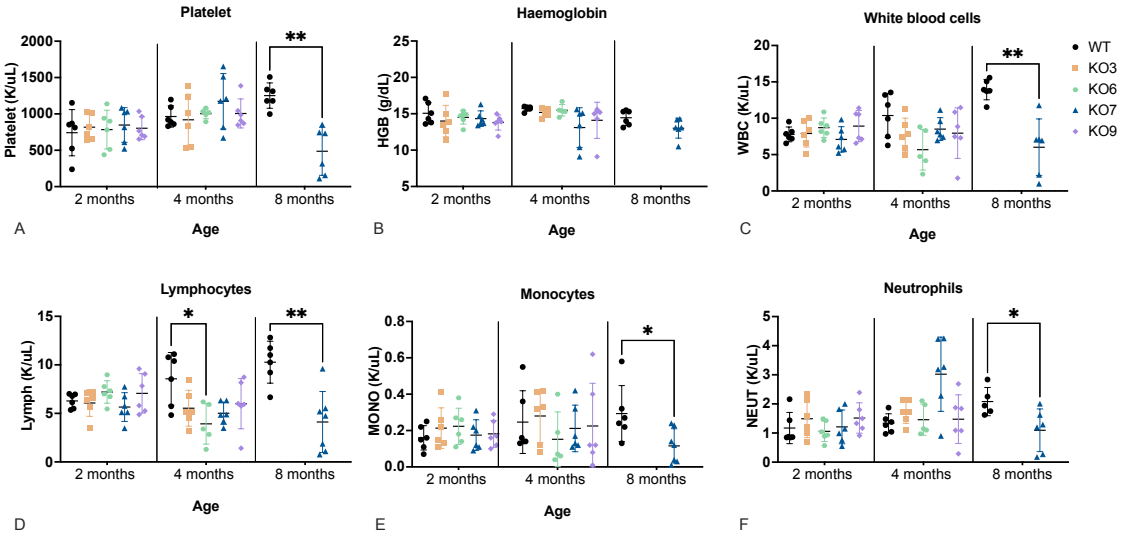


Figure 18 Complete Blood Count analysis of whole blood of male mice.
Analysis performed on samples retrieved from WT and KO male mice at 2 (n=6) and 4 months of age (n≥5). Only WT (n=6) and KO7 (n=6) mice were evaluated at 8 months timepoint. Data are represented as single values with means +/-StD. Filled symbols represent the males; empty symbols represent the females. Two-Way ANOVA (non-parametric; *p-value<0.03; **p-value<0.0021; Bonferroni test for correction).

3.1.2 GALNS *protein detection and activity in KO mice*

In order to monitor whether the different genomic variants led to the absence of GALNS protein, we performed a Western Blot (WB) analysis on liver protein extracts collected from WT and KO mice at 4 months of age (n=3 males and 3 females, per variant). Results were normalised by Actin-β, as seen in Figure 19A. Despite presenting different in terms of base-pair length, we confirmed the 4 variants created by CRISPR-Cas9 excision all targeted the region comprised between the intron 1 and exon 2 of the *Galns* sequence, as expected. Regardless of the specific pathogenic variant, all KO mice presented a protein of similar molecular weight to GALNS. However, the amount and the molecular weight of the detected protein were lower compared to the protein expressed in WT livers. We hypothesised the activation of an alternative open reading frame (Alt-ORF) that could trigger the synthesis of an aberrant protein with a lower molecular weight (51kDa) that we intend to investigate in the future.

Next, we evaluated whether the enzyme expressed in the KO mice was functional. For this reason, we measured GALNS activity in peripheral blood mononuclear cells (PBMCs) collected from 2-months-old mice (see section 6.2.1) using a protocol previously established at SR-TIGET by the Good Laboratory Practice (GLP) group and

described in section 6.2.2 (Filocamo et al., 2018; Filocamo and Morrone, 2011). To avoid assay variability due to the different HGB content, we decided to load 10μl of PBMCs protein extract obtained from the same whole blood volume and normalised the enzyme activity on the volume (ml) of loaded extract. While WT mice showed highly variable but detectable EA (Mean= 98.87; Max value=191.8; Min value=0.35; SD 52,85), all KO mice presented undetectable EA (<0), regardless of the genetic strain variant (Figure 19B). No difference was observed between females and males. We concluded that the pathogenic variants induced by CRISPR-Cas9 led to the production of a non-functional protein with a lower molecular weight to WT GALNS.

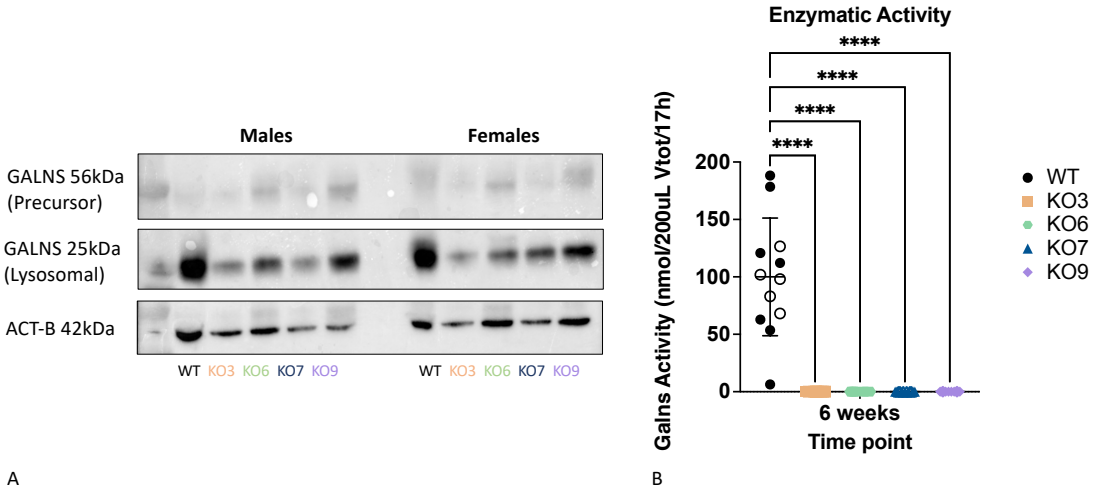


Figure 19 Evaluation of Galns expression and activity in KO and WT.
A) WB analysis of liver tissues from one representative WT and and one KO per strain. Three males and three females were analysed in total (three different gels). 30ug proteins loaded for each sample. Both the precursor and lysosomal forms of GALNS appear evident from the WB. B) EA at 2 months of age measured on PBMCs isolated from 200uL blood. All measures from KOs appeared undetectable (<0), thus, they have been normalised to 0. Non-parametric One-way ANOVA (Kruskal-Wallis; Dunn's test for multiple comparison; ****p-value<0.001). Filled symbols represent males; empty symbols represent females. Data are represented as single values with means +/-StD WT (n=6 males; 6 females), KO3 (n=6 males; 6 females), KO6 (n=6 males; 6 females), KO7 (n=6 males; 6 females), KO9 (n=6 males; 4 females). See Appendix 7.2 for full picture of the gel.

The lower expression of GALNS on WB in KO mice compared to WTs suggested an involvement of an enhancer site in the region affected by our induced mutations. This hypothesis was confirmed by analysis of the mice genomic DNA and lower mRNA expression in liver tissues analysed (Figure20).

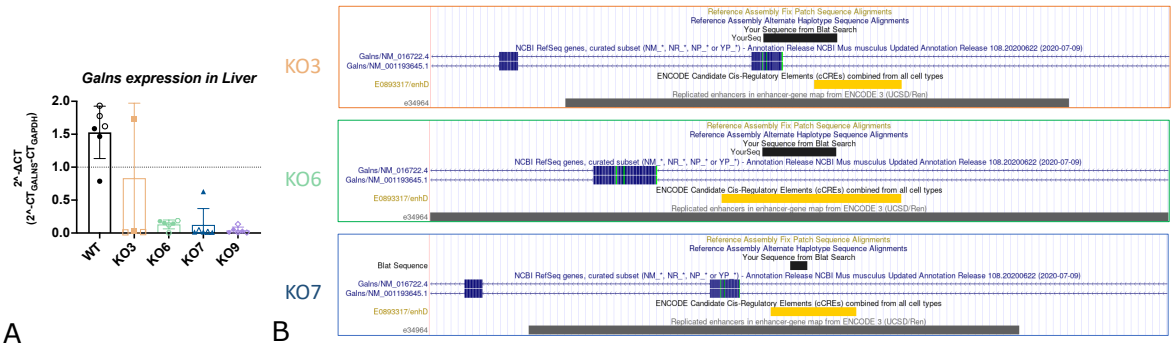


Figure 20 Genetic analysis of KO mice.

A) Levels of *Galns* mRNA in KOs liver samples compared to WT controls. *(liver). Results are expressed as* $2^{-\Delta CT}$ *and normalised on the housekeeping gene Gapdh. All KO mice show a reduced expression of Galns compared to WT controls. B) mRNA expression prompted the analysis on a DNA level, which revealed the involvement of an enhancer site within the frame of our induced pathogenic variants.*

3.1.3 KS in plasma and urine samples at different timepoints

To investigate the effect of inactive GALNS in our mice, an Enzyme-linked immunosorbent assay (ELISA) assay was performed to assess potential systemic accumulation of KS in plasma and urine samples of our models. Though mild accumulation was detected in KO6 mice at 4 months of age, we did not detect any statistically significant difference between WTs and KOs (Figure 21).

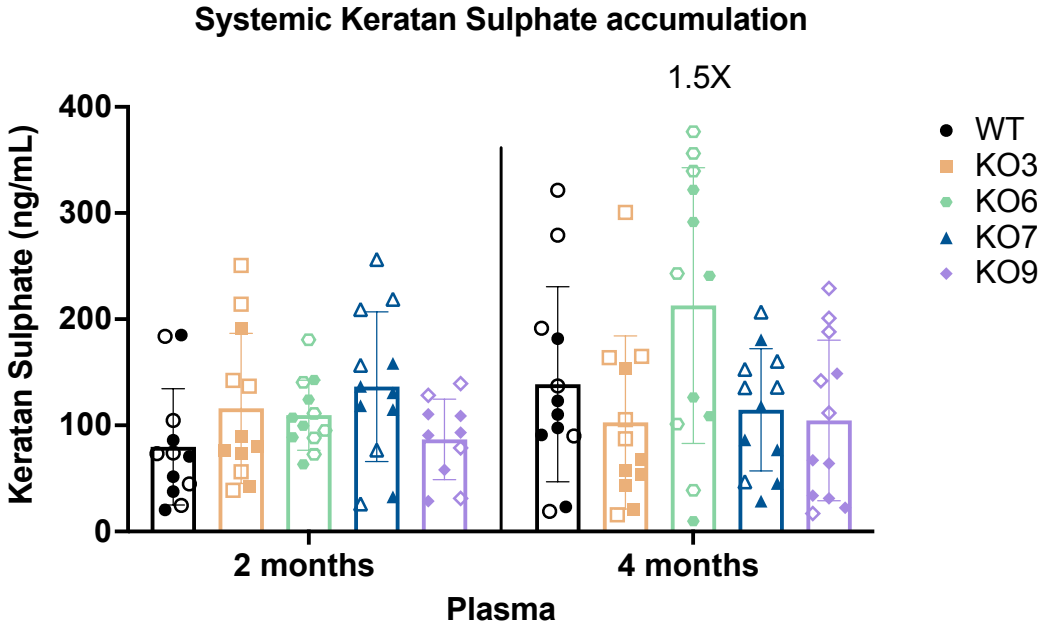


Figure 21 ELISA Assay to detect KS accumulation in plasma.

Plasma samples form WT (n=6 males; 6 females), KO3 (n=6 males; 6 females), KO6 (n=6 males; 6 females), KO7 (n=6 males; 6 females) and KO9 (n=6 males; n≥4 females) were tested at 2 and 4 months of age. Data are represented as single values with means +/- StD. Two-Way ANOVA (non-parametric; Bonferroni test for correction). Fold increase calculated over the mean of WT KS measure.

Next, we performed the same ELISA assay on mice's urine samples, which are routinely screened in MPSIVA patients and hence to obtain comparable results to those obtained in clinical practice. Again, no statistically significant difference could be appreciated. However, though ELISA can be employed for KS detection in fluids, its limited specificity has been previously highlighted, leading to the employment of MS as the preferred method for KS detection (Hintze *et al.*, 2011).

Hence, in collaboration with the University of Modena, we performed high-performance liquid chromatography MS with selected ion recording (HPLC-MS(SIR)) on urine samples of mice at 2, 4 and 8 months timepoints (Figure 22). In this case, an increasing trend of KS accumulation is suggested in KO7 mice at 2 and 4 months of age, though data shown are preliminary and a larger cohort will be necessary to confirm such trend. Also, preliminary data at the latest timepoint of 8 months suggest the difference to be lost with age. However, since data are still preliminary, we could not confirm these speculations.

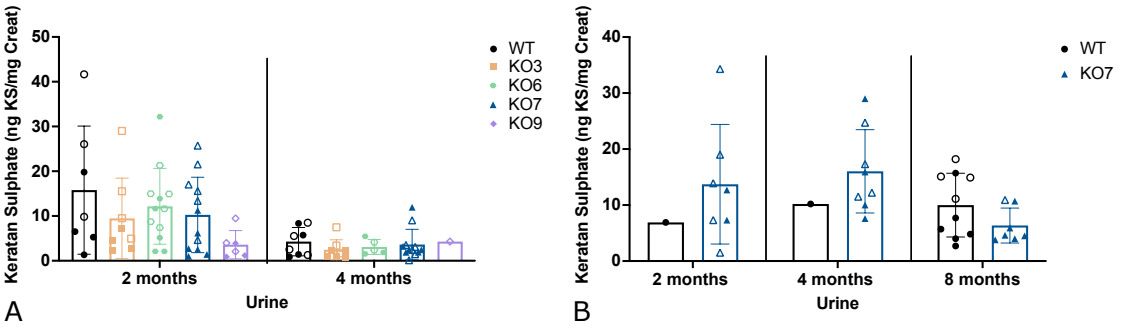


Figure 22 Comparison between KS detection on ELISA Assay vs. HPLC-MS(SIR).
Analysis by ELISA assay (A) and HPLC-MS(SIR) (B) of urine samples retrieved from mice at different timepoints. Preliminary ELISA assay was performed on all KO strains, while HPLC-MS(SIR) was performed following model selection on WT and KO7 mice only. Both males and females are reported in the graphs. Data are represented as single values with means +/-StD.

3.2 Morphological characterisation of MPSIVA mouse models

3.2.1 KO7 appear smaller in weights than all other groups.

After examining the biochemical alterations induced by our induced pathogenic alterations, we investigated their effect on the correct growth and skeletal development of our mice models. Starting from 2 months, our mice were weighed once a month (within the same week of reference) to monitor the weight gain and general growth over time. All strains were weighed from 2 to 5 months timepoint, highlighting a decrease by 7% in total body weight of KO7 males compared to the males of other strains. The difference in weight gaining appears evident from 4

months and persists over time. No difference was observed in females (Figure 23). After the model selection, the weight of KO7 mice was monitored up until 8 months of age, as the selected model strain. Despite variability, differences in weight recorded appear to persist in males up to the latest timepoint. This represented the first suggestion that at least one of our newly generated models presented alterations in growth, that could potentially be a result of skeletal system anomaly.

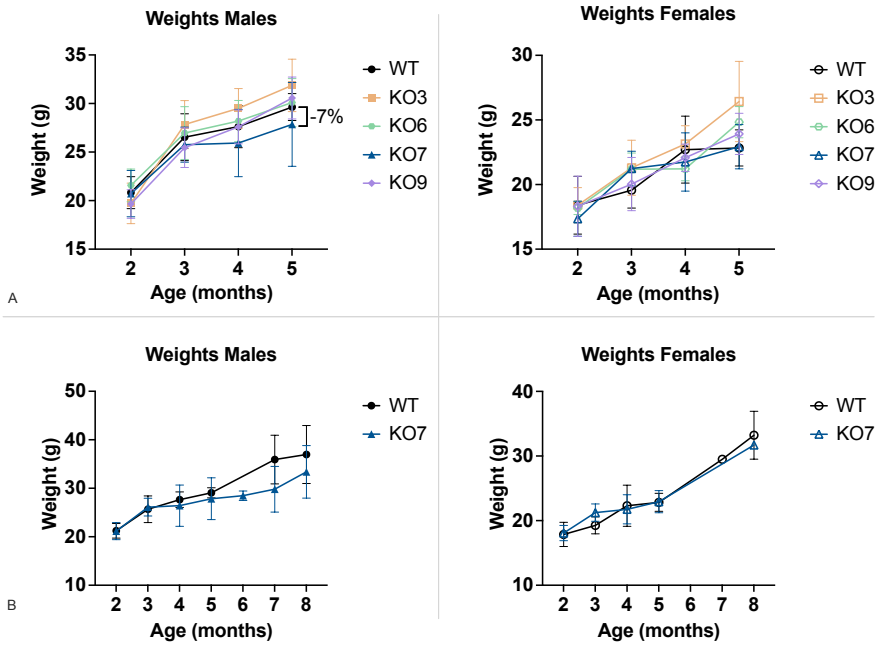


Figure 23 Weight growth over time.
A) Mice weight recorded at 2, 3, 4 and 5 months of age (n≥10, per group). KO7 male mice show reduced weight from 3 months of age and maintain this difference up to 5 months. B) WT and KO7 mice were weighed up to 8 months of age. Male mice from the KO7 group appear to maintain a lower weight compared to controls. Data presented as means +/-SD. Two-Way ANOVA (non-parametric; **p*-value<0.03; ***p*-value<0.0021; ****p*-value<0.0002; Bonferroni test for correction).

3.2.1 Reduced length of femurs and tibiae of KO7 mice.

To evaluate possible skeletal involvement in our potential mouse models, *in-vivo* total body computed tomography scan (CT-Scan) was performed. In collaboration with the Preclinical Imaging Facility at Ospedale San Raffaele, we measured selected bones at 2 and 4 months of age in all strains. On the basis of preliminary results at early timepoints, only KO7 mice were selected for characterisation at 8 months (n=6 males and 6 females per strain). The length of the humerus, upper forepaws (radius and ulna structure), femur, and tibia, as well as the cranium diameter and cheekbone area were measured using 3D Slicer Software (5.0.3 r30893 / 7ea0f43) and compared, as described in section 6.4.1 of the Materials and Methods section. Results showed KO7 male mice to have consistently shorter femurs compared to WTs (an average of the measures taken from both sides was used for comparison).

Specifically, the femurs of KO7 mice appeared shorter from 2 months of age. Female KO7 mice, instead, show differences in the tibia length from 4 months of age (Figure 24). No difference was observed for the other KO mice.

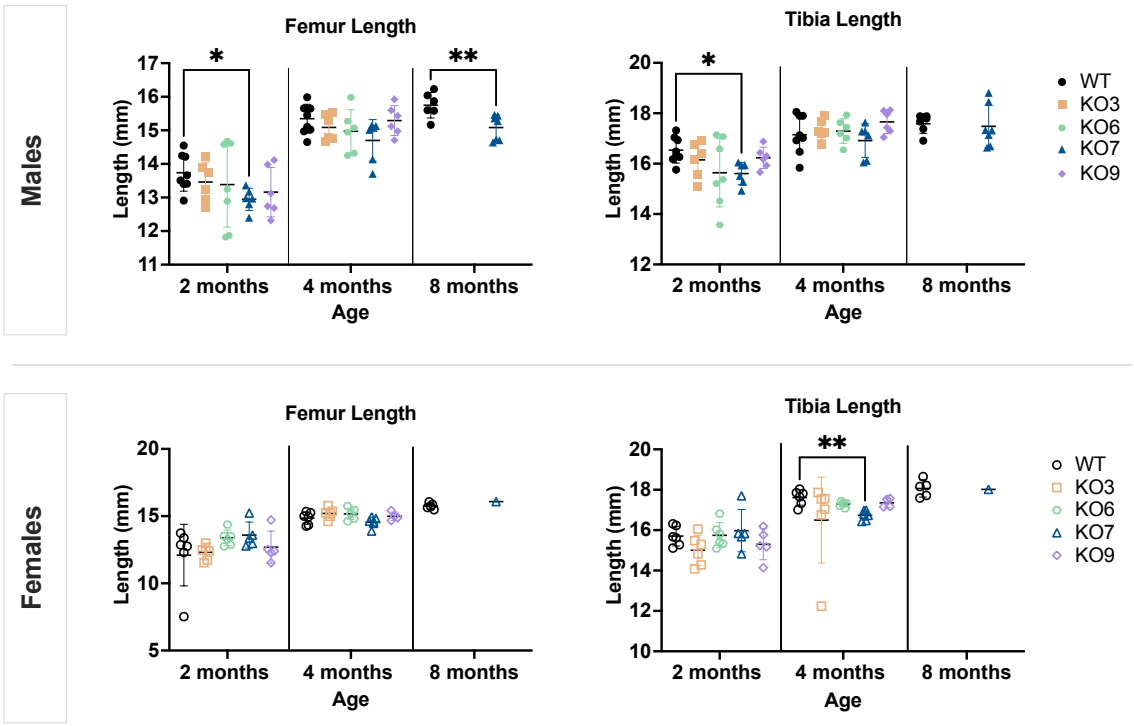


Figure 24 Measures of the tibiae and femurs' length on CT-scan.
Decreased Femur and tibia length measured in males and females of KO7 strain at different timepoints. Two-Way ANOVA (non-parametric; *p-value<0.03; **p-value<0.0021; Bonferroni test for correction). WT (n=9 males; 6 females); KO7 (n= 6 males; 6 females) analysed. Data are represented as single values with means +/-StD.

3.2.2 Reduction in Cortical Area and SSI of KO7s compared to WTs.

To corroborate the results obtained from *in-vivo* CT-scan analyses, we performed *post-mortem* peripheral quantitative computed tomography (pQCT) on the right tibiae of all mice at the endpoints of 3 and 5 months (Figure 25), in collaboration with the Osteoporosis and Bone and Mineral Metabolism Unit at Ospedale San Raffaele. Though not statistically significant, the trabecular BMD and area, the cortical area and stress-strain index (SSI) of KO7 male mice appeared reduced compared to that of other groups evaluated. A reduction by 18-22% in the SSI mirrors the ratio of the stress acting over a body to the strain or deformation that it has gone through. The parameter acts as a marker of bone strength, determined from a cross-sectional scan. Thus, the greater SSI, the more fragile the bone appears. At 9 months of age, differences in the trabecular area, SSI and cortical area appear clearer. Differences cannot be observed in female counterparts (see Appendix 7.7 for results on female mice).

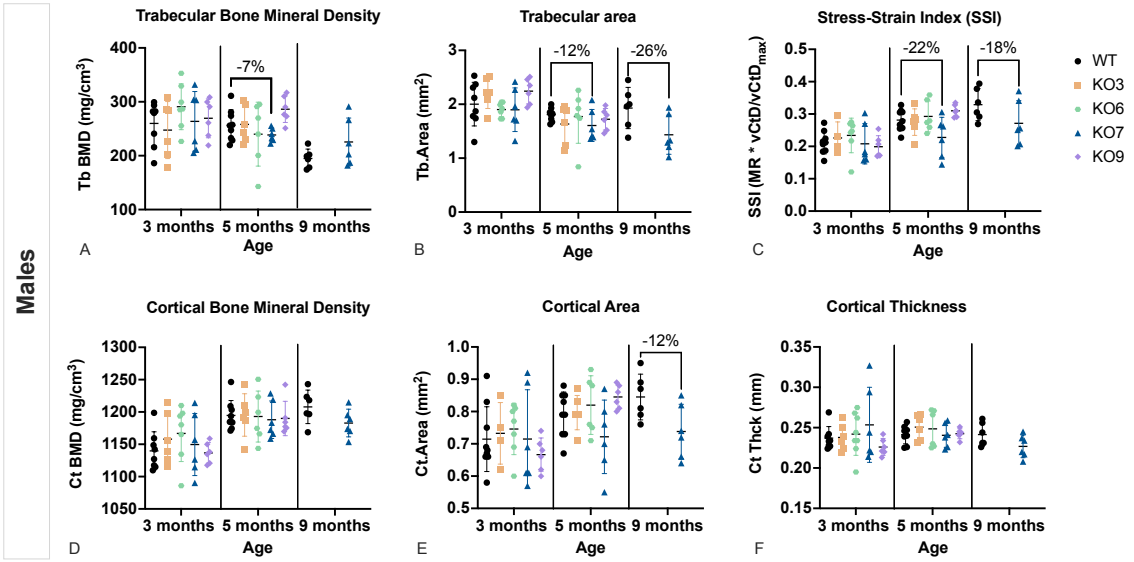


Figure 25 pQCT results at 5 months endpoint.

Analysis of the right tibia of male mice was performed at 3-, 5- and 9-months endpoints. Analysis by pQCT showed reduced Trabecular Area, Cortical Area and SSI in KO7 male mice compared to the other groups. Reduction appears to persist or worsen over time. Two-Way ANOVA (non-parametric; Bonferroni test for correction). Percentage calculated over the means of WT's.

3.3 Histopathological findings

To evaluate in depth the extent to which the skeletal system was affected by the induced pathogenic variants, the whole left lower paw of our mice was collected at the endpoint of 3, 5 and 9 months of age. The region of the knee joint and GP comprised between the tibia and femur was evaluated, after haematoxylin and eosin staining (Figure 26A). The analysis was performed on KO3, KO6, KO7 and WT controls. KO7 mice were shown to have a generalised disorganisation of the GP, with evidence of chondrocyte swelling. Mineral deposits were also detected in the epiphysis region. Additionally, inflammatory cells infiltrates were noted in the meniscus region, as shown in Figure 26B. No major alteration of the tendon was observed. Overall, all KOs analysed presented minimal to moderate skeletal alterations (Figure 26C), though KO6 and KO7 mice appeared the most compromised.

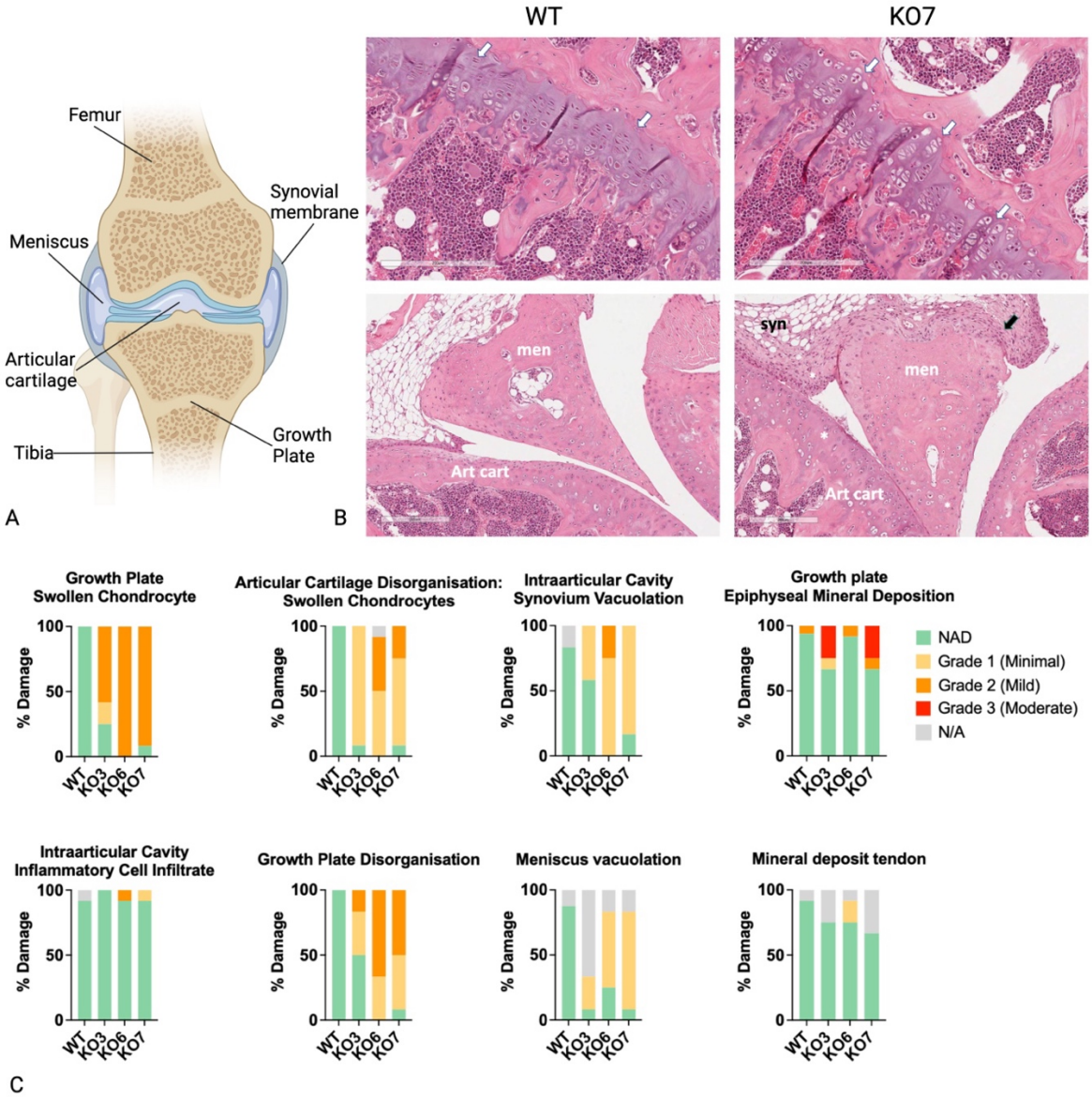


Figure 26 Haematoxylin and Eosin staining of the knee joint.
Articular cartilage (Art Cart); Meniscus (Men): fibrocartilage collagen and small proportion of proteoglycans; Synovial membrane (Syn). A) Analysed region of the knee joint. In the upper two pictures, analysis of the GP with evidence of disorganisation and swollen chondrocytes (white arrows). In the lower two pictures, analysis of the Me with evidence of chondrocytes' swelling, inflammatory cell infiltrates and vacuolation of the synovial region (*). C) Summarised histopathological data in bar-charts with stacked data. Legend on the right show the degree of severity of the measured lesion. Analysis performed on lower left paws of 4-months-old WT (n=8 males; n=7 females), KO3, KO6 and KO7 (n=6 males; n=6 females) mice.

3.4 Motor and behavioural functions

After observing skeletal involvement at the microscopic level, we evaluated the impact of the skeletal pathology on the correct exploratory behaviour, balance, coordination, and strength of our models. Our mice behavioural and motor functions were evaluated at 3 and 5 months of age, to investigate the impact of our pathogenic

variants on the correct functioning of the musculo-skeletal system. First, an open-field test was performed as described in section 6.6.1 of the Materials and Methods section. No significant difference was appreciated in either male or female mouse models (Figure 27). However, we observed great variability among our mice, particularly in the case of WTs, which may have limited our observations.

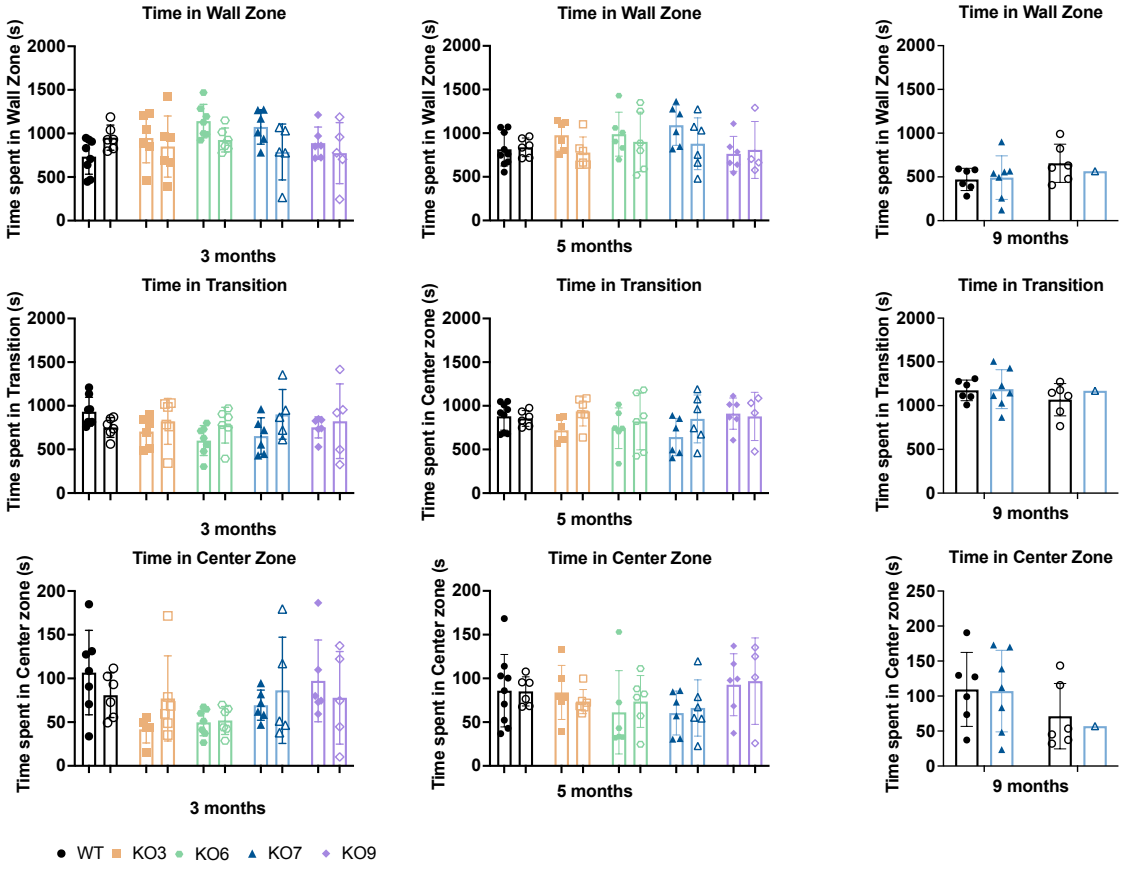


Figure 27 Open field test results.
Evaluation of behaviours abilities of our mice models on Open-Field. No difference was appreciated among any of the groups evaluated. Two-Way ANOVA (non-parametric; *p-value<0.03; **p-value<0.0021; Bonferroni test for correction).

Next, our models underwent a rotarod test to evaluate their balance and motor coordination. The test, however, did not highlight any significant differences among the strains. Finally, the strength of our models' anterior paws was tested by Grip strength test. This showed a markedly lower force detected in KO7 mice at 5 months of age, compared to the WT groups. For the other strains we observed a trend of reduced force. However, in KO7 both the maximum force (GMax) and the average force detected during the test appeared significantly decreased compared to the WT controls (Figure 28). Moreover, a reduced force compared to KO3 was observed.

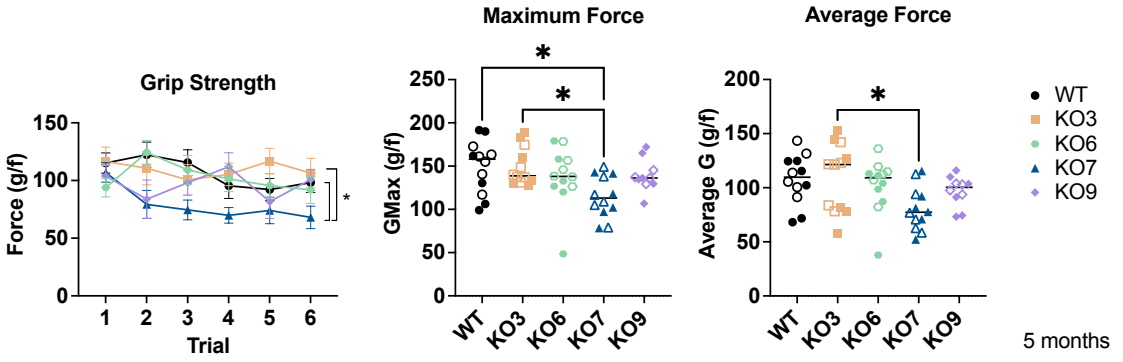


Figure 28 Grip strength test results at 5 months of age.
Analysis of the grip strength of the anterior paws of all mouse strain variants at 5 months of age. Reduction in the Maximum and Average Force measured in KO7 mice at 5 months of age, compared to all other group. Two-Way ANOVA (non-parametric; *p-value<0.03; **p-value<0.0021; Bonferroni test for correction).

Therefore, in light of the obtained biochemical, histological and behavioural results, we selected KO7 mice for additional confirmatory analysis, given their clearer skeletal phenotype, compared to the other KO groups. A summary of the abovementioned results can be found in Figure 29. In addition to the initial characterization, we performed further genetic analyses as well as a preliminary investigation of the strain inflammatory profile.

Results at 3- and 5-months timepoint for selection					
Assays	**WT**	**KO3**	**KO6**	**KO7**	**KO9**
EA in PBMCs	+	Absent	Absent	Absent	Absent
KS accumulation (plasma)	-	-	✓ 4 months	-	-
Growth	-	No difference	No difference	✓Reduced weight	No difference
CT-Scan	-	-	-	✓ Reduced Femurs/Tibiae	-
pqCT	-	-	-	✓ Trabecular Area ✓ Cortical Area ✓ SSI	-
Histopathological analyses	-	✓✓ Mild to moderate	✓Mild	✓✓Mild to moderate	N/A
Motor and Behavioural Tests	-	-	-	✓ Reduced Grip strength	-

Figure 29 Summary of results from models' characterisation
Summary of results at the earliest timepoints for selection of MPSIVA mouse model. Results were used to narrow our investigation to one selected model *Biochemical characteristics of MPSIVA mouse model.*

3.5 Confirmatory analysis on selected model

3.5.1 Genetic mechanisms

Following the model selection, the DNA of KO7 mice was screened for off-target mutations by Sanger sequencing to exclude that the skeletal pathology could be associated with alterations to off-target regions. Details on the inclusion criteria and methodology employed can be found in section 6.1.2 of the Materials and Methods chapter. None of the potential off-target pathogenic variants selected among those flagged by CRISPOR Software were observed in the DNA of one representative KO7 mouse (see Figure 30 for example). Further confirmation of the association between our induced pathogenic alterations and the observed phenotype will be evaluated after 3 consecutive backcrosses (ongoing). This way, transmission of the required pathogenic variant and phenotypes across generations will be monitored. Full list of potentially altered genes can be found in Appendix 7.3.

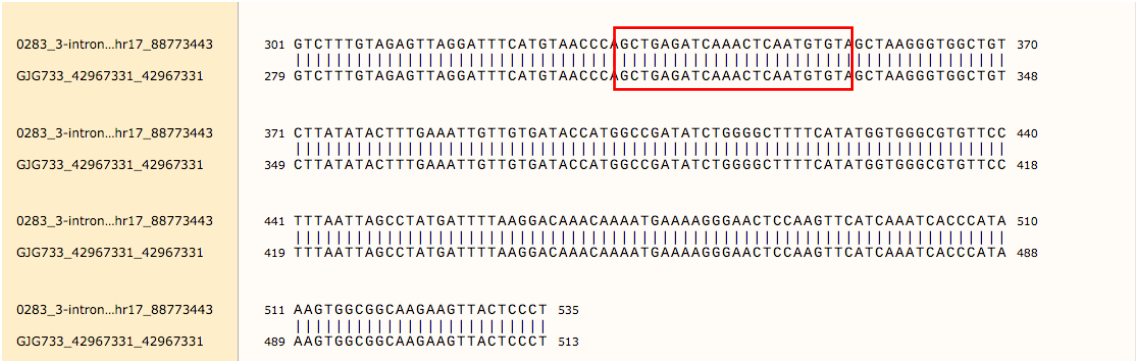


Figure 30 Example of potentially mutated region sequence, aligned with the genome of a representative KO7 mouse.
Result from Sanger sequencing of KO7 mouse genomic DNA with primers targeting an off-target mutation. The red frame highlights the region of potential off-target pathogenic variant on the intronic region of the Foxn2 gene. No mismatch was observed on alignment. The same analysis was carried out on a total of 27 genes.

3.5.2 Histo-morphometry analyses of tibiae

To obtain a deeper understanding of the bone composition that may have determined a reduced length, Cortical Area and SSI, histo-morphometrical analysis of the tibiae of WT and KO7 mice have also been performed. Tissues from 3- and 5-months old mice were analysed. Results showed a reduction in the number of OBs of KO7 mice, compared to WT counterparts, with a persistent reduction of 20-27%, over time (Figure 31).

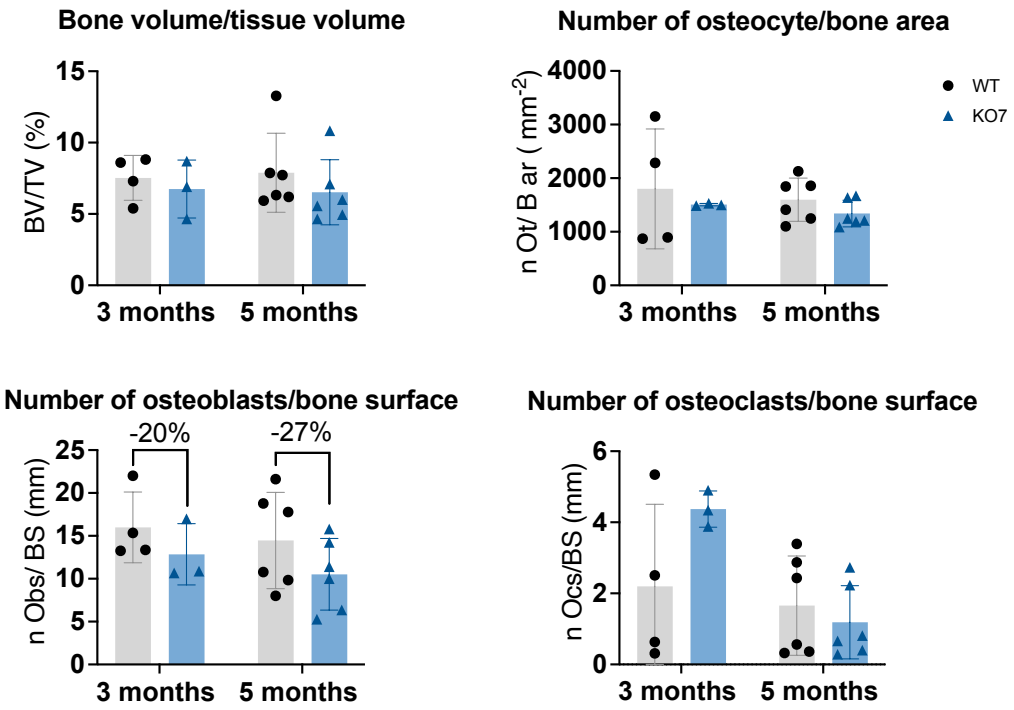


Figure 31 Histomorphometry results of males at 3 and 5 months.
WT vs. KO7 mice tibiae were evaluated by histo-morphometrical techniques. Male KO7 mice showed a reduction in terms of OBs counts from 3 months of age, persistent over time. Two-Way ANOVA (non-parametric; Bonferroni test for correction)

3.5.3 Pro-inflammatory markers appear upregulated in KO7 mouse organs .

In light of the known pro-inflammatory effect exerted by accumulation of undigested substrates in LSDs, we decided to investigate the expression of pro-inflammatory markers by quantitative reverse transcription polymerase chain reaction (RT-qPCR) in representative tissues of WT and KO7 mice. We directed our analysis to markers that had been previously observed to upregulate in several types of MPSs, as specified in paragraph 6.3.1. of the Materials and Methods chapter (van den Broek et al., 2021). We decided to employ liver, kidney, and spleen biopsies, which express high levels of *Galns* and could be more impacted by the deficit of the functional protein. Analysis of the liver tissue revealed IL-1β and HGF increase in KO7 mice compared to WT counterparts, though in a gender-dependent manner (Figure 32). In addition, the spleen samples from our mice showed overexpression of Axin, C-C Motif Chemokine Ligand 4 (Ccl4), CD40, Interleukin-18 (IL-18), interleukin-1α (IL-1α), TNF, vascular endothelial growth factor-A (VEGF-A), Interleukin-7 (IL-7), CXC-motif chemokine ligand 5 (Cxcl5), Tweak, CD224 and TRAIL. Complete data can be found in the Appendix section 7.5 (Figures 40 and 41). Although not statistically

significant, an increasing trend was also observed in the expression of IL-1α, TRAIL, Cxcl5, and TLR4, measured in the kidney tissue.

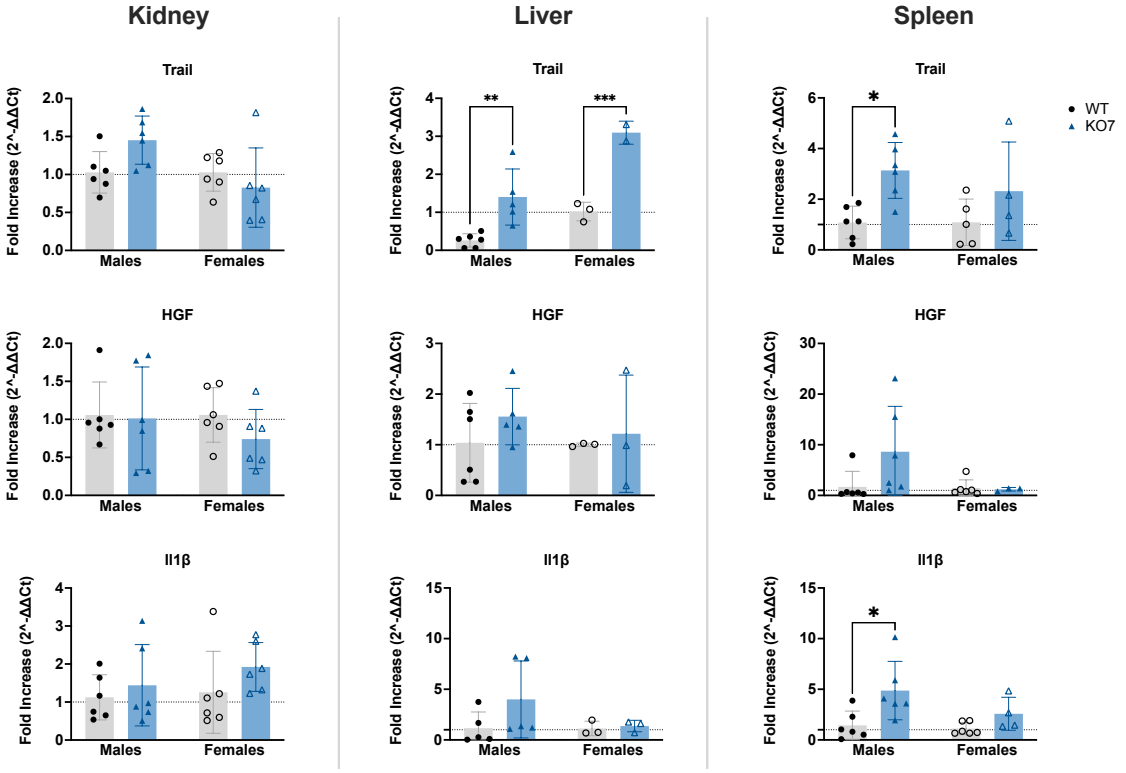


Figure 32 Representative results of inflammatory markers in kidney, liver, and spleen tissues from our mouse models.
RT-qPCR expression analysis of inflammatory and skeletal-tissue remodelling associated gene in WT (n=6 males; 6 females) and KO7 (n=6 males; 6 females). Data presented as single values with Mean +/-SD. Two-Way ANOVA (non-parametric; *p-value<0.03; **p-value<0.0021; ***p-value<0.0002; Bonferroni test for correction).

3.5.4 ER-Stress evaluation.

In addition to the regulation of pro-inflammatory markers, the expression of UPR-associated genes was also measured by RT-qPCR analysis on kidney and spleen of our mouse models. Since in our models an aberrant form of GALNS was expressed, we aimed to excluding that the pathological alterations could eventually be associated to the presence of an unfolded aberrant protein. No statistically significant difference was observed between WT and KO mice in any of the evaluated markers, linked with ATF6- and PERK-associated pathways of UPR. However, the relative ratio between spliced, un-spliced and total X-box binding protein 1 (sXBP1, uXBP1 and tXBP1) has highlighted a statistically significant difference between WT and KO7 mice, in both the kidney and spleen tissues analysed at 4 months of age (Figure 33). This suggests the activation of the IRE1-mediated signalling pathway of UPR, although difference appears minimal. We proposed, however, that the activation of such pathway could

be a result of GAGs accumulation, rather than that of an unfolded aberrant protein, as discussed later.

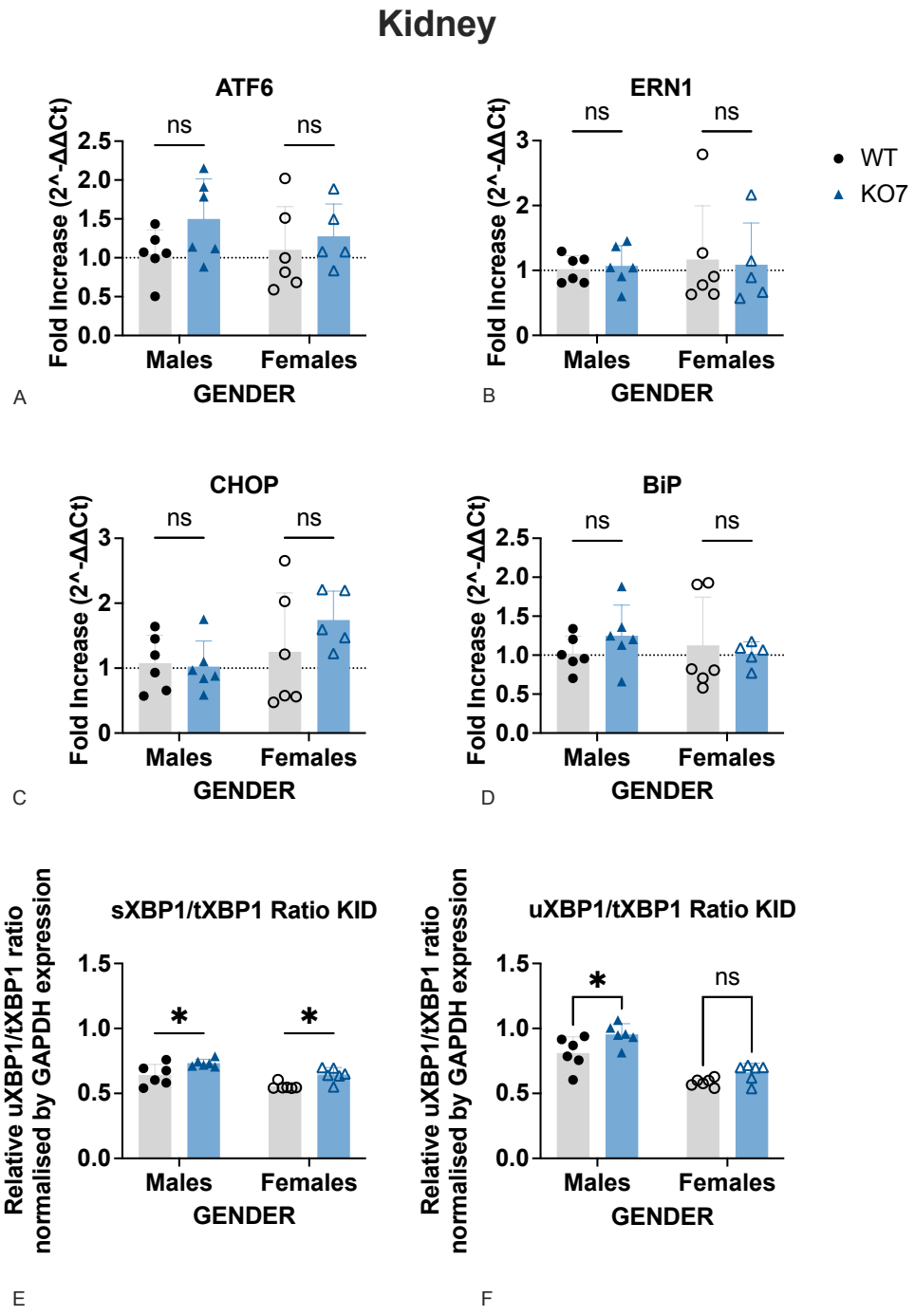


Figure 33 RT-qPCR analysis of the expression of biomarkers of ER-stress in samples of kidney retrieved from WT and KO7 mice.
A-D) Fold increase expression (2-ΔΔCT, normalised on GAPDH expression and average expression in relative WT controls) of ER-associated markers. E, F) Relative abundance of u/s/tXBP1 in the kidney tissue of WT (n=6 males; 6 females) and KO7 (n=6 males; 6 females) mice of 4 months of age. GAPDH used as housekeeping gene. Data presented as single values with Mean +/-SD. Two-Way ANOVA (non-parametric; *p-value<0.03; **p-value<0.0021; ***p-value<0.0002; Bonferroni test for correction).

4 Discussion

MPSIVA is a rare, yet dreadful condition that severely impacts on the correct development of affected children across the world, every year. It is estimated that the birth prevalence for this disease ranges from 1 in 71,000 to 1 in 179,000, across multiple countries (Leadley et al., 2014). *GALNS* pathogenic variants and consequential uncontrolled accumulation of undegraded KS and C6S causes very premature, severe skeletal symptoms in children, without, however, damaging their cognitive abilities (Chen et al., 2021). This makes MPSIVA patients unable to reach the usual milestones in growth, experience rapid deterioration of their skeletal development, severe pain and to require frequent surgical interventions. Nevertheless, therapeutic strategies for MPSIVA predominantly address the clinical manifestations of the condition rather than the underlying aetiology, without correcting the skeletal defects of the disease. Most importantly, both ERT and canonical HSCT fail to significantly ameliorate the skeletal manifestations associated with the disease (Mynarek et al., 2012; Taylor et al., 2019). All these limitations make current therapies insufficient to tackle MPSIVA, leaving a significant unmet clinical need in terms of disease management.

On the basis of previous clinical experience in MPSIH treatment with *ex-vivo* HSPC-GT development and common pathogenic mechanisms of LSDs, one of the main aims of our group is to apply a similar strategy to treat diseases with primary skeletal symptom, such as MPSIVA. This way, the risk of complications generally associated with HSCT may be reduced by the use of autologous HSPCs that avoid the risk of GvHD and transplant rejection. Further advantages of HSPC-GT include the single administration of the cure and permanent correction of cells that would provide persistent supra-physiological activity of the enzyme required. At the same time, HSPC-GT favours treatment of cartilage, which appears highly vascularised during endochondral ossification, early in life, but becomes poorly vascularised with age. Considering that the main complications of these LSDs alter the correct bone formation process, treating cartilage at early stages of the disease could support correct bone turnover, endochondral ossification, and patients' growth. However, a great burden to the development of innovative therapies against MPSIVA is the lack of preclinical models fully replicating the skeletal disease to test their safety and efficacy, prior to clinical use. As previously mentioned, a rat model of MPSIVA is available and efficient in mirroring the disease characteristics (Bertolin et al., 2021). However, given the previous set up of procedures for HSCT and HSPC-GT in mouse

models and considering the translational potential of our approach, we decided to invest in the generation of a novel mouse model for MPSIVA, using CRISPR-Cas9 technology. Despite targeting a previously published pathogenic variant (Tomatsu et al., 2003), we obtained a *Galns*$^{-/-}$ mouse model (named KO7 in this study) with a more exacerbated skeletal phenotype. We hypothesised that the more evident disease phenotype could be associated with the targeting of an active enhancer site located on the intron 1 region, targeted by our CRISPR-Cas9 system. This theory was confirmed by the lower detection of GALNS protein on WB, in the liver tissue of our KO mice. Furthermore, the employment of direct GE in C57BL6/J mice is believed to be determinant to obtain models with a more evident phenotype. Though both gene targeting and GE aim at modifying specific regions, the precise and coordinated mechanisms determining GE, make the method superior to the standard recombinant approach. Besides, the time between correctly edited ESCs cell clones' production and model generation, is prolonged by the generation the construct, targeting and validation of clones. In the case of CRISPR-Cas9, gRNAs and repair templates can be swiftly designed and synthetized. Also, mutated ESCs injection into blastocysts generates chimeric mice that need further breeding to transmit the targeted allele, with highly variable transmission rate efficacy and potential attenuation of the required disease phenotype. Contrarily, injection of CRISPR reagents into one-cell embryos can directly yield heterozygotes animals, readily available for breeding and with a transmission rates often higher than in the case of chimeras from traditional methods (Liu et al., 2017). Another hypothesis for the clearer phenotype observed in our newly developed KO7 mouse model may lie in the production of a substitute protein, translated from an Alt-ORF, which we will discuss in detail later in this chapter.

In the current project, in addition to successfully generating 4 potential mouse models of MPSIVA by GE, we have completed their all-round biochemical, morphological, immunological, histopathological, and behavioural characterisation. Such analyses led to the selection of the most efficient model in terms of symptom representativeness. The generation of a new mouse model may embody a valid alternative to current models and provide a useful means to test innovative treatments like *ex-vivo* gene therapy.

Despite the absence of GALNS EA in all our KO mice, no significant accumulation of KS was observed, neither in the plasma nor in the urine samples retrieved. At first, different methods for KS detection were tested to evaluate whether low sensitivity or

specificity could have altered the correct detection of substrate accumulation. A previous comparative study had highlighted the suitability of both sandwich ELISA and MS to detect KS in fluid specimens, though MS had proven more sensitive (Hintze et al., 2011). In our study, both methods appear to detect KS correctly and within the same range, without however emphasising any significant difference among the groups. The limited detection of KS in mice body fluids may lie in the differences in the GAG's biosynthesis and distribution between mice and humans, particularly in the case of KSII, prevalent in the bone and cartilage tissues (Tomatsu et al., 2003). Of importance, previous studies have proven mice aggrecan, a large aggregating protein component of PGs and abundant in cartilage, to be made up of a truncated core protein and to be devoid of a KS-rich region, otherwise present in mammals including humans, cats and dogs (Anthony J Hayes and Melrose, 2020). Such difference is evident in all murine tissues, except for the cornea (Venn and Mason, 1985). Hence, poor detection of KS in mice plasma and urine appears not surprising but rather explanatory of the difficulties encountered in generating an MPSIVA mouse model with severe symptomatology. Further investigation on our selected KO model may involve the analysis of the corneas to evaluate KS content in the organ most closely resembling the human equivalent. At the same time, alternative pathways of GAG degradation should be investigated, in order to shed a light over potential compensatory mechanisms retained by rodents. Considering the absence of KSII in mice, future investigation should be shifted towards C6S accumulation, another substrate left undegraded by GALNS inactivity. This may reveal noteworthy differences in the pathophysiological mechanisms of MPSIVA in mouse models and pave the way for alternative routes for research.

Furthermore, the functional importance of different types of KS in aggrecan structure remains unclear. For example, while KSI shows interactive properties with other proteins, the higher resistance of KSII to depolymerization is believed to hinder KSII interactions with different ligands (Caterson and Melrose, 2018; Conrad et al., 2010; Weyers et al., 2013). Hence, understanding the interacting mechanisms of KS with other proteins may provide useful insights on the behaviour of this GAG and highlight important differences between mice and their human counterparts.

Despite limitations to KS detection, all KO mice were evaluated in terms of growth and skeletal phenotype, from which KO7 mice emerged with moderate, yet clear alterations of their skeletal system from the earliest timepoint (Figure 21 and 22 from the results section). More specifically, KO7 mice showed shorter femurs and tibiae

than all other groups, on CT-scan analyses. Shortened posterior paws in our KO7 models appear comparable to the skeletal dysplasia suffered from children with MPSIVA, presenting with shortened limbs (Sawamoto et al., 2020). A deeper analysis of the tissues of the knee joint with immunohistochemistry (IHC) also unveiled mild to moderate evidence of structural disorganisation with hypertrophic chondrocytes, vacuoles in the synovial region and inflammatory infiltrates in the meniscus area (Figure 24). The joints wellbeing is highly dependent on the integrity of cartilaginous tissues, which may be significantly altered by aggregation and unfolding of cartilage matrix proteins, driven by metabolic disease (Goldring, 2012; Hardin et al., 2015). Abnormal protein behaviours and loss of matrix proteins damage cartilage ability to resist to mechanical stress, increasing bone fragility (Buckwalter et al., 2005; Martel-Pelletier et al., 2006; Wen et al., 2012). Similar characteristics have been previously observed in MPSVI, in which pathogenic variants to *ARSB* gene leads to accumulation of undegraded DS and results in swollen chondrocytes filled with vacuoles and deformed nuclei (Simonaro et al., 2001). Such distortion impacts on the appropriate columnar structure normally observed in cartilage and is suggested to compromise the normal bone development. Similarly, patients of MPSIVA have also shown distorted bone geometric shape, collagen deposits in ECM and abnormal bone remodelling on histopathological analysis (Kecskemethy et al., 2016; McClure et al., 1986). Thus, our findings also suggest an alteration of the connective tissue and a defect in the correct bone mineralisation process of KO7 mice, with a perturbation of the regular microarchitecture of the bones.

Corroborating these findings, pQCT analysis highlighted a reduction in Trabecular and Cortical Areas as well as a decreased SSI (Figure 23). In healthy subjects, trabecular bone is responsible for distributing mechanical pressure from the articular surface to the cortical bone (Ott, 2018). Thus, both tissue types contribute to long bones' strength and a decrease in their areas may flag an imbalance in bone formation and yield more fragile structures to mechanical stressors. pQCT findings were also supported by histo-morphometry. Analysis of the tibia of KO7 mice at different timepoints suggested an alteration of the bone structure with a reduction in the OBs count (Figure 29). Given the necessary coordination of both chondrocytes and OBs for correct endochondral ossification, a reduction in the number of OBs with no variation in bone volume reflects an imbalance in bone formation. Uncoupling of bone formation and resorption processes leads to bone disease, as previously suggested. In the bone formation process, OBs are responsible for the secretion of ECM proteins including osteocalcin, and osteopontin (Berendsen and Olsen, 2015).

Hence, an analysis of the abovementioned markers, as well as bone-specific alkaline phosphatase (BSAP) and amino-terminal pro-peptide of type I procollagen (PINP), may clarify the impact of OBs reduction on bone formation process, in our newly developed models (Hannon et al., 1998; Nakamura-Utsunomiya, 2021).

The functional effect of bone alterations could be assessed when the motor abilities of our mice were tested. The aforementioned defects in bone structure were reflected by KO7 mice performance on the Grip Strength Test. Whilst all other groups appeared relatively homogeneous and similar in their scores, KO7 mice demonstrated consistently and significantly weaker, both in terms of maximum and average force exercised during the trials (Figure 26). Though strength appeared reduced, no compromission of their cognitive abilities or behavioural anomaly was observed in behavioural tests. This is concordant with the results of analysed ADL in Morquio A patients, that have shown a marked decrease in movement-based assessments and only occasional compromission of the cognition-based test (Chen et al., 2021). However, in those cases, it was hypothesised that the severe limitations in terms of movement could also compromise the normal social and cognitive learning abilities of participants (Chen et al., 2021). Therefore, we confirmed our pathogenic variants to provoke no alteration to our mice behavioural abilities, as expected in MPSIVA, though their musculo-skeletal system appeared compromised until 5 months of age. Differently from MPSIVA patients, none of our KO mouse models show anomalies in their coordination and walking abilities, with similar results on the rotarod assay. This differs from MPSIVA patients, given the common inability to complete walking tests (Quijada-Fraile et al., 2021). Further investigations at 9 months of age will clarify whether the trend is also maintained over time. In addition, performing different motor tests, such as the inverted grid test, may be complementary to our current results. The test consists in measuring the time spent by a mouse hanging to an inverted grid and could provide information on the strength distribution among the four paws, as well as the animal's coordination (Tillerson and Miller, 2003). Overall, these results confirmed KO7 mouse skeletal phenotype to be detectable, though it appeared milder than that observed in patients. Final analysis at the latest timepoint of 9 months will clarify the trends over time.

As previously explained, several inflammatory pathways are believed to contribute to the exacerbation of MPSIVA phenotype in patients. GAGs accumulation has been linked to inflammatory reactions in multiple cell types, as demonstrated by the higher production of NO in rat chondrocytes, altered by DS accumulation or by the

inflammatory state induced by HS and CS in connective tissue (Simonaro et al., 2001; Wang and Roehrl, 2002). In MPSIIIB, mice brain present with overexpression of pro-inflammatory markers, whereas MPSVI human fibroblasts display an overproduction of reactive oxygen species (ROS) due to GAG-associated imbalance of homeostasis, autophagy, mitochondrial function and accumulation of polyubiquitinated proteins (DiRosario et al., 2009; Killedar et al., 2010; Simonaro et al., 2010; Tessitore et al., 2009). GAGs accumulation and release can alter the immune system, leading to clonal expansion of several immune cell populations, such as macrophages, T- and B-cells (Wang and Roehrl, 2002).

In the current study, newly developed KO mice appeared undistinguishable from WTs, with the exception of KO7 mice, which displayed lymphopenia, neutropoenia, leucopoenia and lowered platelets and monocytes, at 8 months of age. In patients, though CBC usually appears normal, it is not uncommon to observe Alder Reilly syndrome associated with MPSIVA. The condition presents with inclusion bodies of incompletely degraded protein-carbohydrate aggregates within the lysosomes of WBCs (Biswas et al., 2017). Though we did not test for inclusion bodies, our mice WBCs appeared significantly reduced in number in KO7 male mice, at 8 months of age. In addition, cells of both myeloid (PLTs, MONs, and NEUTs), and lymphoid (LYMPHs) origin appeared decreased in the same mouse strain. These data triggered an investigation of the inflammatory profile of this strain of mice, which revealed an upregulation of several proinflammatory markers across different organ tissues, on qPCR. From this analysis, three biomarkers stood out as persistently upregulated in all three organs examined: TRAIL, HGF and IL-1β.

By interacting with TRAIL-receptor 2 (TRAILR2), TRAIL is believed to perturb the balance between bone formation and resorption, by increasing OCs destruction (Zhang et al., 2011). This effect is concordant with our findings on CBC and the reduction of OBs count on histo-morphometric analysis, confirming skeletal damage and inflammation.

On the other hand, HGF is a paracrine and morphogenic factor secreted by mesenchymal stromal cells (MSCs). It is responsible for the regulation of IL-11 from OCs-like cells and for the inhibition of OBs differentiation (van den Broek et al., 2021). In addition, higher concentration of HGF has been observed in patients with OA and RA cartilage, particularly in the deep zone of calcified cartilaginous tissue (Bau et al., 2004; Feuerherm A.J. et al., 2001; Tonomura et al., 2020). Thus, we

hypothesised that structural damage to MPSIVA cartilage due to chondrocytes swelling and GP disorganization could trigger HGF release from MSCs in the attempt to supply to damage. To better understand HGF pathogenic mechanisms in MPSIVA, we could investigate HGF secretion from MPSIVA patient derived-MSCs. Additionally, our lab's expertise in murine MSCs isolation, could also be used to investigate HGF behaviour in MSCs isolated from our selected model.

Finally, IL-1β overexpression in our mice tissues, is believed to be the result of the skeletal evidence observed in KO7 mice knee joint. As previously discussed, IL-1β release contributes to a detrimental imbalance between resorption and formation of the bone, by stimulating OCs production and inhibiting OBs activities. Thus, it's overexpression represents a marker of sustained inflammation with damaging effects to the bone structure, making IL-1β, together with HGF and TRAIL, good markers to monitor the bone pathological state in our MPSIVA mouse models. This could be used to evaluate the efficacy of potential new therapies on the immunological state of our mice.

The fine balance between bone resorption and formation is essential to maintain bone homeostasis. In pathogenic conditions involving bone loss, the altered activation of OCs appear a common denominator (Mundy, 2007; Romas et al., 2002). When OCs' resorptive activity exceeds OBs' replenishing action, an acceleration in the bone remodelling mechanism is observed, resulting in bone loss and increased structural fragility (Eriksen, 2010; Raisz and Rodan, 2003). Hence, the upregulation of inflammatory factors that over-stimulate OCs activity can be correlated with the evidence of reduced OBs, bone structure and SSI observed in our models. Through the monitoring of these inflammatory markers, we could confirm the abnormal bone development process in our mice.

In addition to systemic inflammation, pathological stimuli can alter the ER homeostasis, leading to a condition known as ER-stress and the activation of the unfolded-protein response (UPR). Studies on LSD-derived fibroblasts have highlighted UPR activation to be a mediator of apoptosis, also seen in other LSDs (Wei et al., 2008). As an example, UPR activation has been previously detected in the neutrospheres from GM1 gangliosidosis models and in the brain cultures from infantile neuronal ceroid lipofuscinosis (Kim et al., 2006; Tessitore et al., 2004). In the case of our MPSIVA mouse models, there was no evidence of activation of the ATF6 and PERK signalling pathways, though a variation in the spliced/unspliced XBP1

ratio was observed by RT-qPCR analysis, hinting at the activation of the IRE1 pathway. Previous studies on MPSs have underlined the retaining of correct UPR activation mechanism in fibroblasts derived from patients with different types of MPS. By means of an XBP-1 splicing assay, however, MPS fibroblasts (of type I, II, IIIA, IIIB and IVA) appeared to behave like healthy cells, both at steady state and after stimulation with UPR-inducing tunicamycin (Villani et al., 2012). On the other hand, activation of the TLR2 and 4 signalling pathways in macrophages has been associated with IRE1 activation and increased XBP1 splicing (Martinon et al., 2010). This has been proven in RA patients' synovial fluids, suggesting that persistent inflammation triggers TLR pathway, which, in turn, can upregulate XBP1 splicing. As previously mentioned, accumulated GAGs have been linked with activation of TLR4-dependent inflammatory response (Termeer et al., 2002). This leads us to believe that persistent GAG accumulation in MPSIVA could induce TLR-mediated inflammatory response, and indirectly, the UPR process. Thus, further investigation on the secondary initiation of the UPR pathway by means of specific assays may clarify the upregulation of markers associated with IRE1 signalling pathway, detected in our KO7 mice. This may help understand the relation and triggering mechanisms between KS/C6S accumulation and UPR activation.

Overall, the analyses we performed have revealed mice gender to be a discriminant. Most of the differences observed between KO7 and WTs appear more prominent in male mice than in females. Gender related differences in C6S concentration have previously been highlighted in humans, with women normally showing lower concentration of C6S than men, as for C4S and C6S/C4S ratio (Uesaka et al., 2004). In addition, female animals have shown a poorer PGs content in their cartilage tissue (Nakayama et al., 2002; Wei et al., 1996).This may be the case also in mice, though, to our knowledge, no study on the specific characterisation of murine C6S exists. Hence, further analysis on the prevalence of C6S between male and female mice may be advisable to understand the gender-specific discrepancies observed in our MPIVA models. Regardless of the pathological or physiological state, gender factors have long been identified as determinant for the musculo-skeletal system. As a matter of fact, gonadal hormones are known to affect the bone compartments, with testosterone supporting periosteal bone growth and oestrogen preventing cortical bone loss in both sexes (Ott, 2018). On the other hand, oestrogen and testosterone prevent trabecular bone loss in women and men, respectively. Prior studies have underlined significant dissimilarities in the BMD of different bones between the two genders, with men generally showing higher BMD than women (Ho-

Pham et al., 2018). Interestingly, gender-associated discrepancies in trabecular BMD originate during growth, whereas differences in cortical BMD are significantly affected by age (Ho-Pham et al., 2018). In this study, the newly developed mouse models showed a higher degree of skeletal compromission in the case of male animals. Considering the importance of sex hormones in supporting a healthy bone formation, evaluating the mice hormonal levels may help clarify why MPSIVA symptomatology is more severe in males and help designing accurate experimental strategies to test future therapies.

Importantly, we excluded any off-target mutation being responsible for the skeletal disease in KO mice. KO mice produced in this study have been generated by CRISPR-Cas9, which, though extremely accurate, previous studies have shown to potentially induce excisions on off-target genes (Hsu et al., 2013). For this reason, we have completed the screening for potential off-target pathogenic alteration, as explained in section 6.1.2 of the Materials and Methods chapter. We could confirm that none of the off-target mutations we have been screening for was detected in the genomic DNA retrieved from KO7 mice. This confirmed the phenotypes observed in our mice to be a direct consequence of our pathogenic variant of choice, without any genetic confounding factor involved.

In addition, we are currently in the process of backcrossing our KO7 mice models in order to monitor the transfer of the desired pathogenic variant and associated phenotypes, across generations. This requires a two-generations breeding protocol. First, a hybrid F1 generation is developed from two inbred strains to produce a colony of heterozygous mice, polymorphic for the genetic markers inherited by the parents. From these, two heterozygous mice are further inbred to generate an F2 progeny with mixed genotype. The same process is repeated three times, after which the obtained KOs from the final progeny will be employed for a biochemical and histopathological characterisation to confirm the inheritance of the desired pathogenic mutation.

Our results showed the expression of an aberrant enzyme in KO7 mice, with a lower molecular weight compared to WTs, which may cause a gain of function pathogenic variant exacerbating the skeletal disease compared to previous animal models. We are currently investigating this hypothesis in the KO7 selected strain. In the presence of the KO7 genomic alteration, we predicted the activation of a second ORF at +65 nucleotides from the starting WT ATG codon. The activation of this Alt-

ORF could induce the synthesis of an abnormal protein with a lower molecular weight. In order to prove our hypothesis, we have synthesised the sequence encoding for the WT and mutated murine protein (using the predicted Alt-ORF) and cloned into a lentiviral vector for protein overexpression. We plan to transduce GALNS deficient cells to confirm a lower molecular weight corresponding to the enzyme detected in KO7 mice and the absence of EA (Figure 34). This experiment should help unveil the mechanism of action of the mutated sequence of *Galns*, containing our pathogenic variant of interest.

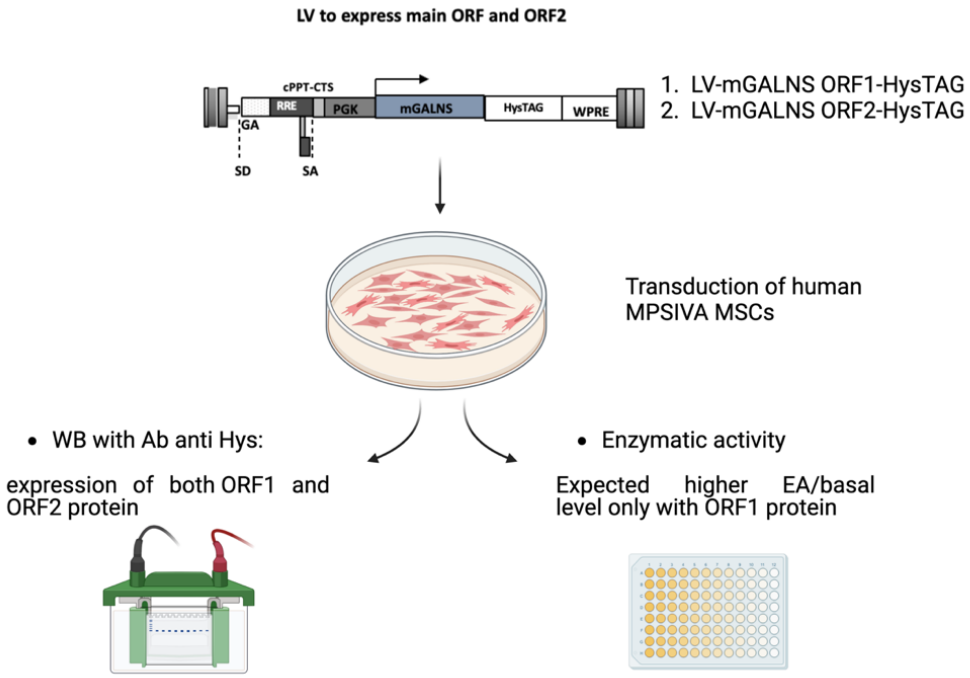


***Figure 34 Experimental plan of transduction of hMSCs with mutated or* WT GALNS.**
In-vitro cultured hMSCs will be transduced with LV containing wither the WT (ORF1) or mutated (ORF2) version of the *GALNS* encoding sequence. The cells will be collected and evaluated for protein expression and EA. The expected results should prove both proteins to be correctly translated but activity on in the case of transduction with the *GALNS* WT form. hMSCs from MPSIVA donor appear a highly representative model as they are completely devoid of GALNS background activity.

In conclusion, we have generated a novel mouse model for MPSIVA displaying a set of moderate, yet evident phenotypic characteristics. We have completed a comprehensive characterisation of the model under different aspects, which has revealed alterations at the biochemical, inflammatory, and skeletal level. We plan to perform additional functional experiments to clarify further unanswered questions on the mechanism of action of the mutated GALNS protein produced by our mouse models. Collectively, the results discussed above provide evidence of the suitability of this newly generated model for future testing of innovative therapies, including

HSPC-GT, together with a set of characteristics that can be used to monitor therapy efficacy over time.

5 Limitations of the study

Results discussed in this study present few limitations. First, the use of KS as the marker of reference for MPSIVA in patients has led us to consider the substrate appropriate for potential mouse models too. Review of the literature has highlighted, however, how measuring the content of C6S might be more appropriate to monitor disease progression in mouse models. Hence, future MS analysis of plasma and urine samples of our selected model should focus on investigating C6S content. Furthermore, availability of patients-derived cells has been significantly limited by the infrequency of the disease, which makes the development of alternative models necessary to be employed to test our hypotheses. Thus, future studies should further clarify the unclear molecular mechanisms involved in disease pathogenesis. Also, selection of our mouse model should be employed for pre-clinical testing of HSPC-GT as well as other potential innovative treatments.

6 Material and Methods

6.1 Model generation by sgRNA CRISPR-Cas9

Clustered regularly interspaced short palindromic repeats (CRISPR) are genomic sequences originally discovered in prokaryotes and archaea organisms aimed at detecting and excising the DNA from bacteriophages, recognized from previous infections. These DNA sequences are key players in antiviral defence mechanisms of prokaryotes. In recent years, such sequences have been employed in combination with the bacterial protein Cas9 to induce site-specific genetic modifications (i.e. GE). In the context of mouse model generation, this innovative system has emerged as a highly versatile and cost-effective approach to engineer the genome of specific mouse strains to produce deletions of different kinds.

In order to generate a precise pathogenic variant comprised between intron 1 and exon 2 of *Galns,* two single-guide RNAs (sgRNAs) have been designed (mGalns-ex2_0054F: ACAGAGGUUGAUCUCAGCU; mGalns-in_0283F: AGACCGGAUGGCUGCAGAA), as schematised in Figure 35. Independent lyophilised gRNAs were centrifuged for 2 minutes at 13,000rpm at room temperature and maintained at -20°C until use. Later, gRNAs were resuspended in 15uL IDTE buffer to obtain a concentration of 200uM (=6.4ug/uL). Resuspended gRNAs were centrifuged again for 2 minutes at 13,000rpm and 5uL of each sample retrieved. Each 5µl aliquote was diluted 1:2 in 5µl IDTE buffer to reach a final concentration of 100uM (=3.2ug/µl) in 10µl of final volume and stored at -80°C prior to use.

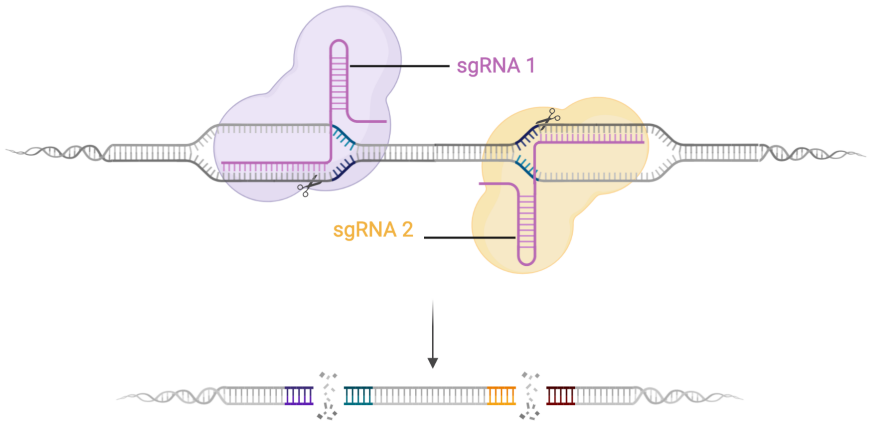


Figure 35 Schematic representation of CRISPR-Cas9 strategy employed to generate a KO pathogenic variant on the Galns-encoding sequence of C57BL/6J mice.
Two sgRNA were designed to induce the excision of the region comprised between the intron 1 and exon 2 of the *Galns* sequence and C76 residue, responsible for GALNS enzymatic activity.

In order to generate mice with mutated *Galns*, the gRNAs were injected directly into C57BL/6J mice embryos. The mice born from such embryos were genotyped and six alternative pathogenic variants were obtained; four of which appeared viable for further characterization and selection of the model, whilst the remaining two were excluded from characterisation due to inability to produce a viable progeny.

All *in-vivo* experiments were submitted to the approval of IRCCS San Raffaele Scientific Institute and Institutional Animal Care and Use Committee, following the Italian Ministry of Health guidelines for experimental animals' use and care. The procedures were optimized to minimize the number, pain, and discomfort of the animals, during and after experimental procedures, in accordance with the 3Rs principles.

6.1.1 Genotype

To discriminate between the 5 strains obtained, a sample of tissue (tail clip/phalange) was retrieved from pups and the DNA was extracted using the Prepare Extraction Mix from Kit (REDExtract-N-Amp™ Tissue PCR Kit, Sigma-Aldrich, Cat. R4775-1.2ML Foster City, California, US). A Forward (ACTCATGTAGTCAGGGAAC) and a Reverse Primer (GAGTCTTCTGGCTGCCAT) were designed to confirm the pathogenic variant by PCR (Table 2). PCR product was run on a 2.5% agarose gel with 0.1% Atlas ClearSight DNA Stain (Bioatlas, Cat. BH40501, Tartu, Estonia) to confirm the mice genotype. While homozygous mice for the pathogenic variant KOs and WTs were maintained for characterization experiments, heterozygous mice were excluded from the analyses. In order to confirm the obtained deletions, a sample of extracted DNA was purified using the Wizard® SV Gel and PCR Clean-Up System (Promega, Cat. A9281, Madison, WI, USA) and sent for sanger sequencing.

Table 2 PCR protocol for MPSIVA mouse models' genotyping

Step	Temperature	Time	Note
1	95°C	5 min	
2	95°C	30 sec	x35 cycles
3	54°C	30 sec	
4	72°C	1min	
5	72°C	7min	
6	4°C	∞	

6.1.2 Off-target pathogenic variants evaluation on selected model

Though very precise, previous studies have shown how sgRNAs could induce excisions both to on- and off-target genes (Hsu et al., 2013). Thus, in order to screen for potential off-target mutations induced by the CRISPR-Cas9 system, the two sgRNA sequences were uploaded onto CRISPOR Software (Haeussler et al., 2016). The software provided potential genome variants, predicted off-target and on-target scores. Potential off-target pathogenic alterations were selected according to the following inclusion criteria: we screened for potential mutations that would target the exon with up to 4 mismatch and inter-genic mutations up to 3 mismatches by designing associated primers. Primers were tested using proofreading Pfu DNA Polymerase (Promega) protocol (see tables 3 and 4). PCR products with optimal annealing temperature (T_a) were sequenced to check for possible mismatch. The full list of potential off-target pathogenic variants we screened for can be found in the Appendix Section 7.3

Table 3 PCR Protocol for off-target pathogenic variants.
Pfu owns a 3´→5´ exonuclease (proofreading) activity that ensures swift excision of possible base misincorporations that may take place during polymerization. Ideal annealing temperature was tested by a gradient and selected for each primer couple.

	Amount
DNA (300ng/µl)	1µl
Pfu Taq Polymerase Buffer (Promega M776A)	5µl
dNTPs (10uM)	1µl
FP (*Galns* int1- 10uM)	2.5µl
RP (*Galns* ex2- 10uM)	2.5µl
Pfu Taq Polymerase (Promega M774B)	0.5µl
H_2O	V_{final}=50µl

Table 4 Pfu Taq Polymerase PCR protocol to screen for off-target pathogenic variants.

Step	**Temperature**	**Time**	**Note**
1	95°C	2 min	
2	95°C	30 sec	x35 cycles
3	54.6-55°C	30 sec	
4	72°C	2min	
5	72°C	5min	
6	4°C	∞	

6.1.3 Back-crossing

In addition to checking for potential off-target pathogenic variants, we performed three consecutive backcrosses. Knock-out mice (*Galns*$^{-/-}$) have been backcrossed with WT littermates for three consecutive generations (F1, F2, and F3) to segregate and eliminate possible CRISPR/Cas9-associated off-target events. Back-crossing also ensures the observed phenotype to be maintained over generations and to not be attenuated or 'lost'.

6.1.4 RNA extraction

RNA extraction has been performed on both cells and mouse organ tissues, following two protocols. Initially, RNA was isolated using Invitrogen™ PureLink™ RNA Mini Kit (Invitrogen™, Cat 12183018A, Carlsbad, CA, US). At experiment endpoint of 4 months, samples of liver, kidney, spleen and heart tissues were obtained from mouse models and homogenized in Trizol (Invitrogen™, Cat. 15596026). Trizol was added to each tissue sample, in a ratio of 1ml every 100mg of tissue and processed by means of a tissue homogeniser. The machine was cleaned with consequential washes in nuclease-free H_2O, 70% ethanol and nuclease-free H_2O between each sample, to avoid contamination between samples. Once homogenised, 200µl chloroform were added per 1ml Trizol and samples were centrifuged at 12,000 x g for 5 minutes to pellet the cellular debris and separate the Trizol phase from the clear phase containing the RNA, to be collected. The clear liquid was transferred to a clean Eppendorf tube and an equal volume of 70% ethanol was added to each sample. The mixture was loaded onto a column, provided with the kit. The sample was centrifuged for 15-30 seconds, and the liquid discarded. A DNase step has been added to the protocol for additional RNA purification and incubated for 15 minutes at RT. After incubation with the DNase mix, a first wash was performed loading 700µl of Wash Buffer I onto the column filter and the sample was centrifuged for 15-30 seconds at 12,000 x g and the liquid discarded. The column was washed with 500uL Wash Buffer II and centrifuged 15-30sec at 12,000 x g, twice. After the second wash with Wash Buffer II, the column was centrifuged for 1 min at 12,000 x g to make any residual ethanol evaporate. ~100uL nuclease-free H_2O was then added to the filter and incubated for 1 minute, before being eluted by centrifugation for 1 min at 12,000 x g. Samples were quantified and stored at -80°C until use.

RNA extraction from organ tissue has been later optimised using the Maxwell® RSC simplyRNA Cells and Tissue Kits (Promega, Cat. AS1340). The use of this kits

allowed for greater purification of the samples and reduced the amount of tissue required for extraction.

After extraction, the samples were quantified using NanoDrop 2000 (Thermo Scientific). Total RNA (1µg) was reverse-transcribed with the High-Capacity cDNA Reverse Transcription Kit (Applied Biosystems, Cat. 4368814).

6.1.5 RT-qPCR pre-amplification (pre-Amp)

In order to measure the expression of *Galns* mRNA in WT and KO mice, samples of RNA isolated from liver tissue of our mice were pre-amplified. 30ng of RNA samples were retrotranscribed into cDNA, as per usual. A primer mix was prepared with 1uM primers diluted in nuclease-free H_2O. At the same time, a MasteMix containing 12.5µl DNA, 5µL of TaqMan™ Pre-Amp mix (2X) (Applied Biosystems, Cat. 4488593) and 12,5µl of Primers Mix was prepared for each sample. A PCR reaction was performed with the protocol of Table 5 to pre-amplify the sequence of interest. Obtained pre-amplified samples were diluted into 950µL H_2O (1:20 dilution). A forward (TGCTCATGGACGATATGGGG) and a reverse primer (AGCTTGGGAAAAGCATCCCT) were designed for expression quantification by RT-qPCR (Table 6).

Table 5 RT-qPCR protocol for pre-amplification of Galns

Step	Temperature	Time	Note
1	95°C	10 min	
2	95°C	15 sec	X14 cycles
3	60°C	4 min	
4	95°C	10 min	
6	12°C	∞	

Table 6 RT-qPCR protocol for gene expression quantification, after pre-Amp.

	Amount
SYBR Green Mix	5µl
FP (7uM)	0.5µl
RP (7uM)	0.5µl
cDNA	2.5µl
H_2O	1.5µl
	V_{final}=10µl

6.1.6 Protein extraction

To monitor the effect of the CRISPR-Cas9 induced pathogenic variants, Western blot was performed to detect the presence of GALNS in cell lysate obtained from liver samples of our mice or from cultured cells. Tissue samples were processed by tissue homogeniser, while maintained in RIPA buffer containing protease inhibitor cocktail. Samples were incubated on ice for 30min and then centrifuged for 10min at 10,000 rpm at 4°C. The supernatant was retrieved. Using the solutions provided by the *DC* Protein Assay kit (Biorad, Cat.5000111, USA), an A1 mix with 20µl S in 1ml A was prepared. 25µl of A1 mix were added to each well, to which 5µl of the sample or standard point were added. 200µl of solution B were added to each well and incubated at 37°C for 30min. Samples were read at 655 nm on the FLUOstar® Omega (BMG Labtech, Ortenberg, Germany) and concentration of proteins was calculated. An equal amount of proteins was resuspended in Pierce® RIPA buffer (ThermoFischer Scientific, Cat. 89900, Rockford, IL, USA) containing laemmli buffer 4X (Biorad, Cat. 1610747) and β-mercaptoethanol (1:100 dilution).

In the case of cell cultures, cell supernatant was also collected, and protein content was precipitated by adding 4X volume of iced-cold acetone. The mix was incubated at -20°C overnight. Samples were centrifuged for 15min at 4000rpm and the supernatant was discarded. The obtained pellet was left to dry for 2-4 hours and then resuspended in 1X laemli buffer with β-mercaptoethanol (1:100 dilution).

6.1.7 Western Blot

Samples were boiled at 99°C for 5min and then loaded on a Mini-PROTEAN® TGX™ Precast Protein Gels (Biorad) and run at 100V. Once the running process was completed, the gel content was transferred on a Trans-Blot® Turbo™ Transfer membrane (BioRad) (25V for 3 minutes using Trans-Blot® Turbo™ Transfer System). The membrane was washed five times in 1xTBS-Tween before being incubated for a minimum of 1 hour at room temperature in 5% milk solution in 1xTBS. After blocking, the membrane was incubated with primary antibody overnight at 4°C. The following day, the primary antibody was discarded, and the membrane washed again five times in 1xTBS-Tween. A secondary antibody consisting in horseradish peroxidase was added to the membrane and incubated for 1 hour at room temperature, before the membrane was washed again five times in 1x TBS-tween. A 1:1 solution of Immobilon® Classico Western HRP Substrate mix (Merck Millipore Cat. WBKLS0500 Burlington, MA, USA) was employed for chemiluminescent detection of the target proteins. The same procedure was repeated to detect our housekeeping protein of

choice (actin-beta). Western Blot results were analysed using the iBright Analysis Software 5.2.1.

6.2 Biochemical analysis

6.2.1 Complete Blood Count

A first line evaluation of the mice blood composition was performed. A sample of PB was retrieved by lateral tail vein bleeding at 2, 4 and 8 months of age, for a maximum volume of 250µl/mouse. The samples were collected into capillary blood collection tubes pre-treated with EDTA to prevent blood coagulation and blood clots formation.

50uL of total PB were employed for a hemogram using the Hemocytometer ProCyte Dx (IDEXX). The remaining 200µl were centrifuged at 13,000rpm for 10 minutes to separate the plasma from the cell fraction. Plasma samples were aliquoted and stored at -80°C until use. The extracted volume of plasma was replaced with 1XPBS. The cell fraction in PBS was incubated for 15 minutes in 1ml of ACK to lyse haemoglobin and further washed in 1X PBS. The sample was centrifuged at 2000rpm for 5 minutes and the supernatant aspirated. The same process was repeated a second time before final aspiration and collection of the PBMCs. Cells were stored at -80°C before being employed to monitor GALNS EA.

6.2.2 Enzymatic Activity Assay

Frozen pellets of PBMCs were diluted into 100uL 1XPBS and sonicated for 25 seconds on 0.5 amplitude, using the 28 ADV-00654PTEP Sonoreaktor UTR200 (Hielscher, Teltow, Germany) to obtain a protein extract. 10µl of each sample was diluted in 10µl of PBS and loaded onto a 96-well plate with flat bottom. 20µl of 4-Methylumbelliferyl β-D-Galactopyranoside-6-sulphate (4MU-Gal-6S) substrate was added to the 20µl of diluted sample and incubated at 37°C for 17 hours. On the following day, the reaction was stopped by adding 5µl of Stopping buffer 1. 10µl β-Gal working solution (10U/ml) was added and samples were incubated for 2 hours at 37°C. After the second incubation, the samples were loaded onto a 96-well Spectra Plate (Perkin Elmer, Milan, Italy) together with a 5-point standard curve, a healthy donor DNA as positive control, 0.2%BSA solution as a negative control and a blank sample of 250µL of Stopping Buffer 2 alone. 200µl of Stopping Buffer 2 were added to each well and the plate was read immediately at 450nm Multiskan SkyHigh Microplate Spectrophotometer (ThermoFisher Scientific, Cat. A51119500C).

6.2.3 KS accumulation detection by ELISA

Accumulated KS in the blood plasma of mice was measured by ELISA, using the Mouse KS ELISA kit provided by Assay Genie (Assay Genie, Cat. MOEB2495 Dublin, Ireland). A single aliquot of 50µl of plasma was diluted in 50µl sample diluent included in the ELISA kit. 50µl of diluted samples, blank (sample diluent alone) and standard were loaded in duplicates on a pre-coated 96-well micro-ELISA plate with a flat bottom, avoiding foaming. 50µl of Detection reagent A working solution were added to each well immediately and incubated at 37°C for 1 hour, after sealing the plate with an adhesive plate sealer, provided with the kit. After incubation, the wells were washed three consecutive times with 200µl 1X Wash Buffer using a multi-well pipette. After the last wash, the plate was vigorously tapped onto absorbent paper to ensure complete removal of Wash Buffer. 100µl of Detection Buffer B working solution were then added to each well. Once the plate was sealed with an adhesive plate sealer, it was incubated at 37°C for 45 minutes. After incubation, the plate was washed 5 times with 200uL 1X Wash buffer and again vigorously tapped onto absorbent paper for complete removal of Wash Buffer. 90µl of Substrate Solution were directly added to each well and incubated at 37°C for 10-15 minutes, after sealing and covering the plate with tin foil, to protect the wells from light. The reaction was stopped by adding 50uL of Stop Solution to each well, once the standard wells showed a clear colour gradient. Addition of the Stop Solution generated a colour change from blue to yellow. The plate's light emission was measured at 450nm on Multiskan SkyHigh Microplate Spectrophotometer (Thermo Scientific). An optical density (OD) value was obtained for each well. OD results have been averaged, adjusted for the blank sample OD value and KS concentration has been obtained from the standard curve equation. Results were normalised by the loaded volume per well of 0.025ml. The same assay was also performed on samples of urine collected from our mice, following 24 hours of in metabolic cages.

6.2.1 KS accumulation detection by HPLC-MS(SIR)

In order to improve the assay sensitivity to KS detection in plasma and urine of our mice, we established a collaboration with Prof Volpi and his team, at University of Modena. 60µl of sample, plasma or urine, were centrifuged at 10,000rpm for 10 minutes. 50µl of obtained supernatant were loaded onto a YM10 filter (Centriprep® Ultrafiltration Centrifugal Filters, Millipore, Cat. 430-10, Burlington, US), after washing of filter. Add 450µl MilliQ water and centrifuge at 14000 x g for 60 minutes.

Discard the flowthrough. Add 49µl of Buffer (100mM ammonium acetate, pH 7.0) and 1µl of EKR II (0.2mU) and incubate at 37°C, for a minimum of 4 hours. Add 450µl MilliQ water and centrifuge at 14000 x g for 60 minutes. Obtained solution (V_{final}=500µl) is analysed though HPLC-MS(SIR) on a HPLC Discovery® C18 column (Sigma-Aldrich, Cat. 504955, California, US). An MS detector with single ion monitoring (SIM) mode was employed. Both urine and plasma can be analysed with the same protocol.

6.2.2 Creatinine measurement

In order to normalise the measured KS, the creatinine content in the urine samples was measured using the Mouse Creatinine Assay Kit (CrystalChem, Cat. 80350 Zaandam, Netherlands). We optimised the protocol provided in accordance with the maximum capacity of our plates. 4µl of each sample was loaded in duplicates onto a 96-well plate with flat bottom. 135µl of sarcosine oxidase solution were added to each well and incubated for 5 min at 37°C. The samples were read a first time at 550nm wavelength on the Multiskan SkyHigh Microplate Spectrophotometer. 45µl of peroxidase solution were added to the samples and incubated again for 5 min at 37°C. The samples were read again at 550nm wavelength on the Multiskan SkyHigh Microplate Spectrophotometer and a difference in the measured OD_{550} was calculated.

6.3 Inflammatory profiling

6.3.1 Quantification of inflammatory markers by RT-qPCR

In addition to a broad biochemical evaluation of our newly developed models, the inflammatory profile of WT and KO7 mice (n=6 males; n=6 females) has been evaluated. A sample of 18 markers of pro-inflammatory and anti-inflammatory nature (Table 7) has been selected in light of a prior analysis of human patients with different types of MPS, available in literature (van den Broek et al., 2021). Additional common markers of inflammation like IL-1α, IL-1β and TNF-α have been added to the list. A portion of spleen, liver and kidney from our mice was collected at endpoint and processed to extract RNA using the Invitrogen™ PureLink™ RNA Mini Kit (Invitrogen™, Cat. 12183018A, Carlsbad, CA, US). cDNA was obtained by reverse transcription using High-Capacity cDNA Reverse Transcription Kit with RNase Inhibitor (ThermoFisher Scientific, Cat. 4368813). A SYBR-Green RT-qPCR was performed to quantify the biomarkers' expression in samples of Kidney and Spleen

of 4 months old mice. Biomarkers' expression by RT-qPCR analysis were presented as $\Delta\Delta_{CT}$.

Table 7 Panel of Biomarkers for inflammatory profiling.
Biomarkers of inflammation evaluated by SYBR-Green RT-qPCR on tissue samples from our mice (Adapted from van den Broek et al., 2021).

Marker	Forward Primer	Reverse Primer
CD244	CAGTTGCCACAGCAGACTTTCC	CTTCCTGGAAGGCTGGACTACT
AXIN	GTCCAGTGATGCTGACACGCTA	GCCCATTGACTTGGATACTCTCC
CXCL9	CCTAGTGATAAGGAATGCACGATG	CTAGGCAGGTTTGATCTCCGTTC
HGF	GTCCTGAAGGCTCAGACTTGGT	CCAGCCGTAAATACTGCAAGTGG
IL-7	CAGGAACTGATAGTAATTGCCCG	CTTCAACTTGCGAGCAGCACGA
MPP.1-	CTACAGAAGCGTAACCGACCTG	ATGAGACGAACTCTCCGAGCCT
TWEAK	CTGCGCTACGACCGCCAGATT	ACACCGTTCACCAGCAAGTCCA
CCL4	ACCCTCCCACTTCCTGCTGTTT	CTGTCTGCCTCTTTTGGTCAGG
CD40	ACCAGCAAGGATTGCGAGGCAT	GGATGACAGACGGTATCAGTGG
IL-18	AGAGCTGATCCAGGACACATGG	TGGTGGACAGAAAACACGCAGG
IL-1α	CCAGAAGAAAATGAGGTCGG	AGCGCTCAAGGAGAAGACC
IL-1B	TGCCACCTTTTGACAGTGATG	TGATGTGCTGCTGCGAGATT
TNF	ATAGCAAATCGGCTGACGGT	AGCCGATGGGTTGTACCTTG
TRAIL	GGAAGACCTCAGAAAGTGGCAG	TTTCCGAGAGGACTCCCAGGAT
CD274	TGCGGACTACAAGCGAATCACG	CTCAGCTTCTGGATAACCCTCG
CXCL5	CCGCTGGCATTTCTGTTGCTGT	CAGGGATCACCTCCAAATTAGCG
VEGF-α	GCAGCGACAAGGCAGACTAT	AACCTCCTCAAACCGTTGGC
TLR4	AATCCCTGCATAGAGGTAGTTCC	ATCCAGCCACTGAAGTTCTGA

In addition to this broader analysis of expression of inflammatory markers, we screened for ER-stress associated biomarkers (Table 8) on the liver and kidneys of our mice, to evaluate the impact of the induced pathogenic variants on the ER and monitor a potential association of the phenotype observed with ER-stress.

Table 8 List of ER-stress associated biomarkers evaluated in two representative organs of WT and KO7 mice.

Marker	Forward Primer	Reverse Primer
ATF6	CACCCATCCGAGTTGTGAGG	GCAAACAACGTCGACTCCCA
BiP	GGACCACCTATTCCTGCGTC	CAATCAGACGCTCCCCTTCA
CHOP	TTGAAGATGAGCGGGTGGCAG	CACGTGGACCAGGTTCTCTCTC
ERN1	CTGGCTTCTCATAGGACACCAT	TCTCGATGTTTGGGCAGGTT
ERN2	AGAGCTCCGCTATTGCCTGA	CCTGACAGACTGGACCTGTG
sXBP1	GCTGAGTCCGCAGCAGGT	CAGGGTCCAACTTGTCCAGAAT
uXBP1	CAGACTATGTGCACCTCTGC	CAGGGTCCAACTTGTCCAGAAT
tXBP1	TGAAAAACAGAGTAGCAGCGCAGA	CCCAAGCGTGTTCTTAACTC

6.4 Morphological analysis

6.4.1 Computed tomography scan

Mice from each variant (n=6 males and n=6 females) originated by our CRISPR-Cas9 approach were monitored in terms of weight gain over time at selected timepoints of 2, 3, 4, and 5 months of age. Once selected, the mouse model of choice was also measured at 6, 7 and 8 months of age. Representative pictures of our mice teeth and gross dimensions (body and tail length) were taken at 3 and 5 months of age, while our models were under sedation. These parameters were used to evaluate potential skeletal involvement prior to complete the analysis of computed tomography scan (CT-Scan). Cone beam CT (CBCT) was performed using the X-RAD225Cx, SmART equipped with a flat panel detector. Mice were anesthetised with gaseous anaesthesia (2–3% isoflurane and 1 l/min oxygen) during the entire imaging workflow. The correct positioning of our mice in the machine was determined by an initial "scout scan". CBCT images were acquired using the following settings: tube voltage=60 kVp, current= 5 mA, voxel size=0.1 mm^3. Obtained images were used to measure selected long bones' length, the mandibular area Figure 36E), the cranium diameter between the joints of squamosal body to zygomatic process of squamosal (Figure 36D) and spinal curve angle (Figure 36C) by 3D Slicer Software (5.0.3 r30893 / 7ea0f43).

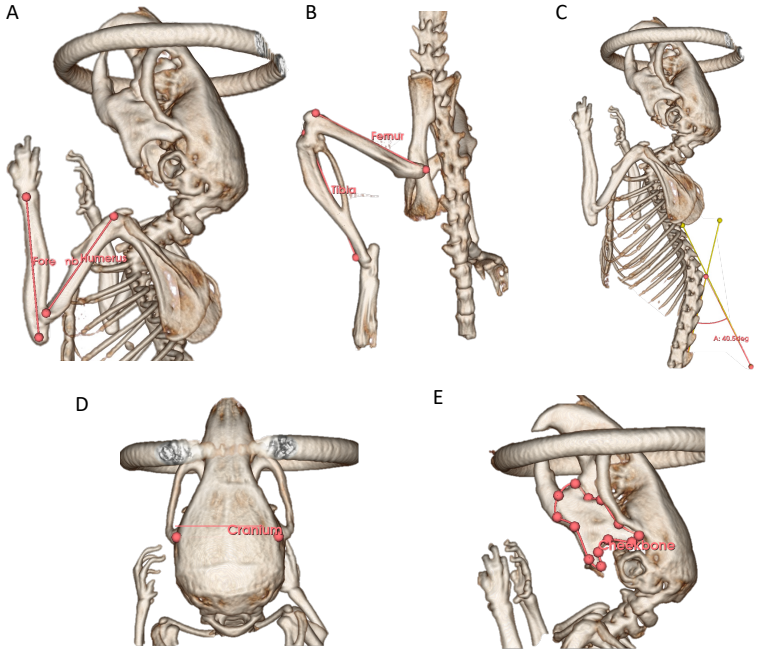
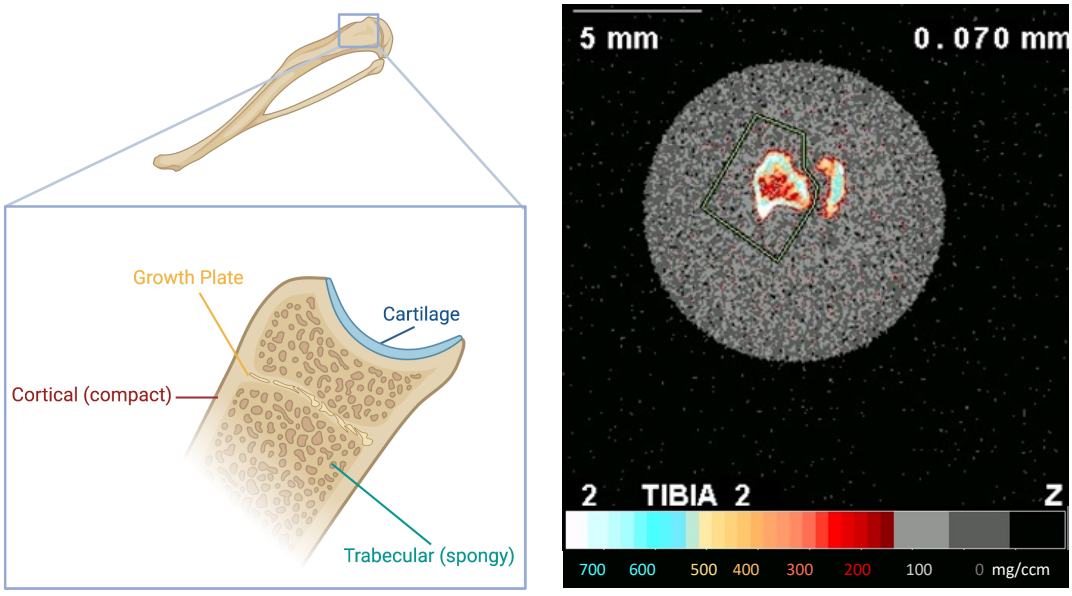


Figure 36 Measurements retrieved from total body CT-Scans of mice models. CBCT images were used to measure the femur, tibia, humerus, and radius' length (Figure_), the mandibular area excluding the superior rim point on lower incisor alveolus (Figure_) and the cranium diameter measured coronally from one zygomatic root connecting squamosal body to the other (Figure_).

6.4.2 Histo-morphometry

pQCT measurements were performed on the tibiae of our models, using a Stratec Research SA+ pQCT scanner (Stratec Medizintechnik GmbH, Pforzheim, Germany) with a voxel size of 70 µm and a scan speed of 3 mm/s. To orientate the long axes of the bones parallel to the image planes, the excised bone specimens were fixed with manufacturer-made plastic holders. The correct longitudinal positioning was determined by means of an initial "scout scan". The scans were performed at the proximal metaphysis and at the diaphysis of the tibiae. The scans were analysed with pQCT software 6.00B using contour mode 2 and peel mode 2 with a threshold of 500 mg/cm³ for the calculation of trabecular and total bone parameters and with a threshold of 710mg/cm^3 for cortical bone parameters (see Figure 37 for reference).



A B

Figure 37 Representative picture of pQCT scan on tibia.

A) Schematic representation of the bone layers and structures evaluated by pQCT scan. B) Representative image obtained by measurement.

In addition, the bones' composition in terms of OBs, OCs and OCts has been determined via histomorphometry. The tibiae were incubated overnight in 0.5M EDTA after fixation. Bones were embedded in 8% gelatine 20% sucrose 2% PVP 40 in PBS. Using a Leica cryostat, samples were partitioned into 5µm sagittal sections. A Toluidine blue staining was performed to quantify nOBs, nOt, BV/TV in the secondary spongiosa, whilst the nOcs was measured by TRAP staining (Merck) (Dempster et al., 2013). All images were acquired at a 20x magnification on a Nikon Eclipse 50i and quantified with Fiji software. Employed methods followed the standards provided by the ASBMR Histomorphometry Nomenclature Committee.

6.5 Histopathological analyses

In order to select the genomic pathogenic variant causing the pathological phenotype most similar to the human disease, the skeletal defects and GAG accumulation in the long bones of all KO mice have been evaluated and compared to wild-type counterparts at different times points. The morphological alterations and GAG vacuolization were evaluated in bone and cartilage tissue from one posterior paw collected in 6 male and 6 female mice at 3 and 5 months of age (range 8-10, 16-18 weeks). After selection of the most representative model, the same histopathological stainings have been performed on samples from 9 months-old mice (range 32-35 weeks) and WT counterparts. In addition to the previously mentioned measurements, analysis of the spinal column was performed at the latest timepoint.

At the selected endpoints of 3, 5 and 9 months, the left posterior paw of our models was surgically collected and fixed in 10% buffered formalin. After 24h the samples were transferred into a 4% EDTA solution for two weeks to decalcify. For the purpose of histopathological examination, the samples were embedded in paraffin wax to be sectioned, mounted on glass slides and stained with haematoxylin and eosin. The histopathological stainings and analyses were performed by registered pathologists Dr Francesca Sanvito, Dr Martina Rocchi and Dr Rossana Norata of the SR-Tiget GLP Test Facility. Pictures were provided.

6.6 Motor and Behavioural tests

After undergoing CT-Scans, our models were moved to the Animal Behaviour Facility at San Raffaele Hospital, where they were maintained on an inverted 12 h light/dark cycle, at a stable temperature of 22–24 °C. After two weeks of acclimatisation, the mice underwent an open-field test, two rotarod tests and a grip-strength test to evaluate either their behavioural, motor and strength abilities. All behavioural procedures were approved by the Animal Care of the San Raffaele Scientific Institute, and by the National Ministry of Health.

6.6.1 Open field test.

Exploratory behaviour of independent groups of littermate mice was tested at 3 and 5 months of age by means of an open field test. Lighting in the room was indirectly diffused and maintained to the minimum to avoid interference (4x40W bulbs, 12lx). The mice were introduced into an empty arena and recorded for 30 minutes. For time course analysis, the total observation time has been portioned into three periods of 10min (t1-t3). For quantification of exploration activity, the area ì recorded was distinguished in three different zones: exploration, home, and intermediate zone (Madani et al., 2003). The exploration zone corresponds to the more aversive area of the arena, such as the central zone in the open field. The home zone is the preferred part of the arena, corresponding to the wall zone. The remaining areas are defined as intermediate zone. Exploration activity such as the total path length and number of visits in different zones of the arena were measured and scored.

6.6.2 Rotarod

The rotarod test has been developed to evaluate motor coordination in mice and rats (Dunham and Miya, 1957). A mouse must keep its balance on a horizontal rotating rod (diameter approx. 3 cm, rotating at either constant or accelerating

speed. The latency to fall off the rod was taken as the dependent measure. GALNS KO models have been tested using a Rotarod apparatus by Ugo-Basile 47650 Rota-Rod NG. On the first day, five mice were placed on the rotarod with the rod rotating at 5 rpm (rotations per minute). Initial speed was maintained stable for one minute, after which it was gradually increased every 30 sec by 5rpm until reaching 37 rpm as final speed in 300 sec. Each trial ended when the tested mouse fell from the rod or when 5 min were completed. Each mouse underwent 5 trials on day 1 with an intertrial interval (ITI) of 30 min. On the second day of rotarod test all mice were tested again for 5 min at a constant speed (average of maximum speeds reached from all mice on day 1). Again, each mouse underwent 5 trials with an ITI of 30 min.

6.6.3 Grip-Strength test

A grip strength test was performed on all mice at 3 and 5 months of age. The mice were tested one at the time. Each animal was placed in a horizontal position and lowered towards the grip bar until the animal grasped it. Both paws had to grasp the opposite side of grip bar in order to consider it held correctly. The tested mouse was then gently pulled backward until it released the grid. An arrow on the machine's screen indicated that the mouse was being held as centrally as possible, confirming that the experimenter was pulling the animal correctly (nor too strongly neither too gently). The maximum force strength parameter set on the machine was 500g/f.

6.7 Statistical analysis

Two-way ANOVA with a mixed effects model and a Bonferroni test for correction of multiple comparisons were selected for statistical analysis. Results were analysed using GraphPad Prism 10 and presented as mean values ± standard deviation (StD) or mean values ± standard error. Differences were considered significant at * $p<0.0332$; ** $p<0.0021$; *** $p<0.00021$, **** $p<0.0001$.

Images were created with BioRender.com website.

7 Appendix

7.1 CBC analysis of whole blood samples from female mice models at different time points

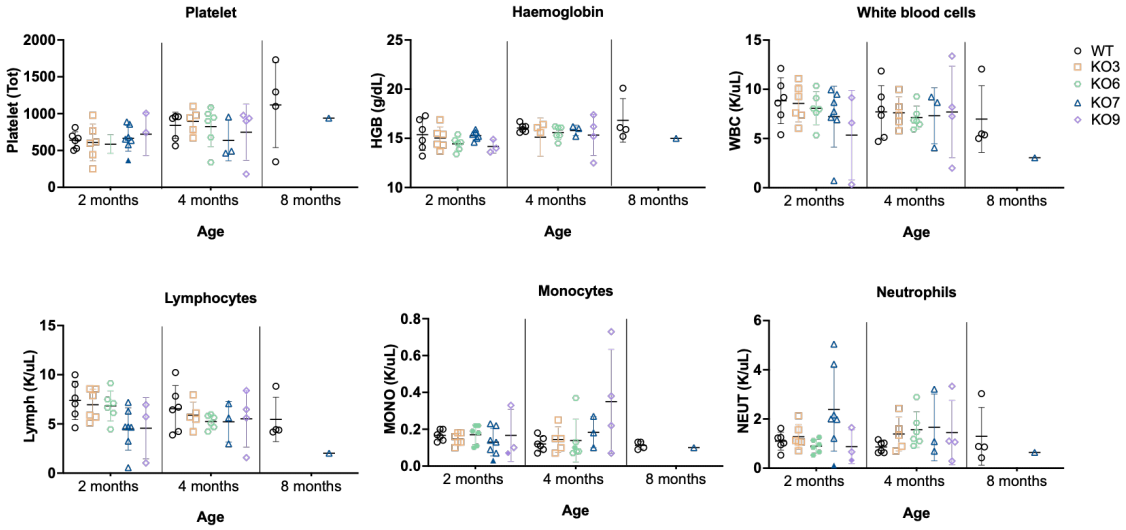


Figure 38 Results from CBC in female mice at time points of 2, 4 and 8 months of age. Analysis performed on samples retrieved from WT and KO female mice at 2 (n=6) and 4 months of age (n≥5). Only WT (n=6) and KO7 (n=6) mice were evaluated at 8 months timepoint. Data are represented as single values with means +/-StD. Empty symbols represent the females. Two-Way ANOVA (non-parametric; *p-value<0.03; **p-value<0.0021; Bonferroni test for correction).

7.2 WB of GALNS expression in liver samples from 5-months-old mouse models, full picture of analysed membranes.

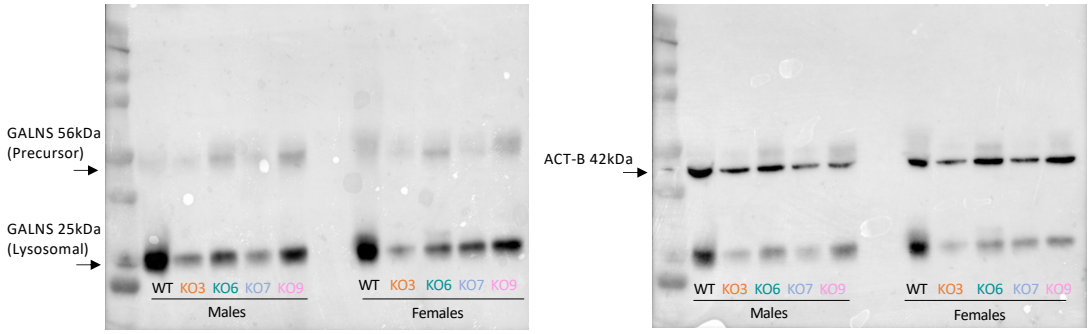


Figure 39 Results from 5-months-old liver samples evaluated by WB.
On the left side, expression of GALNS can be detected in both its precursor and lysosomal forms. On the right side, expression of Actin-β (considered the housekeeping gene)indicated by arrow.

7.3 Off-target pathogenic variants screening

Table 9 Panel of genes potentially affected by off-target mutations.

Gene interested	Mismatch Count	Chromosome location	Locus
Olig1-Ifnar2	4	chr16	Intergenic
Fbn2	4	chr18	Intron
Foxn2	4	chr17	Intron
Gm19689-Pkdcc	4	chr17	Intergenic
Akr1e1	4	chr13	Exon
Mill1	4	chr7	Exon
Dll4-Chac1	2	chr2	Intergenic
Slc12a8	4	chr16	Intron
Pde11a	4	chr2	Intron
D630003M21Rik-1700060C20Rik	4	chr2	Intergenic
Adgrv1	4	chr13	Intron
Ttll7-Adgrl2	3	chr3	Intergenic
Gm20757-Nedd1	2	chr10	Intergenic
Ccdc88a	3	chr11	Exon
Pcdh10	4	chr3	Exon
Speer9	4	chr7	Exon
Dapl1-Tanc1	2	chr2	Intergenic
Slc16a1	2	chr10	Intron
Xpa-Gm12446	3	chr4	Intron
Olfm4-Gm32455	4	chr14	Intergenic
Kif4	4	chrX	Intron
Fam3b-Mx2	2	chr16	Intergenic
Fbxl7	4	chr15	Intron
Gm2164	4	chr4	Exon
Tbc1d9b	4	chr11	Intron
Ampd2	4	chr3	Intron
Zfp618	4	chr4	Intron

7.4 Alternative Open Reading Frame sequences

7.4.1 Murine Galns ORF1 (WT) plasmid sequence:

EcoRV (gatatc)+ Kozak + CDS + linker+ HA TAG + stop codon + SalI (gtcgac)

GATATCGCCGCCACCATGGGGTGGGGTGACTTGGGTGTGAATGGAGAACCTTCCAGAGAGACCCCAAA
TTTAGACCGGATGGCTGCAGAAGGGATGCTTTTCCCAAGCTTCTATTCTGCCAACCCTTTGTGCTCACCA
TCTAGGGCAGCCCTGCTCACAGGACGGCTGCCCATCCGCAATGGCTTCTACACAACCAACGCTCATGCAA
GGAATGCTTACACACCTCAGGAGATCATGGGTGGGATCCCTAACTCAGAGCACCTCCTGCCCGAGCTCCT
GAAGAAGGCAGGCTATACCAACAAGATCGTGGGCAAGTGGCATCTGGGTCATAGGCCCCAGTTCCACCCC
CTGAAGCATGGATTTGACGAGTGGTTTGGATCTCCCAACTGTCACTTTGGACCGTATGACAACAAGGCCA
AGCCCAACATCCCTGTGTACAGGGACTGGGAGATGGTCGGCAGATTTTATGAAGAGTTCCCAATTAACCG
GAAGACTGGGGAAGCTAACCTCACCCAGCTCTACACACAAGAAGCGCTGGACTTCATCCAGACACAACAT
GCAAGGCAGAGCCCCTTCTTCCTCTACTGGGCCATCGACGCCACTCATGCACCAGTTTACGCCTCAAGAC
AGTTCTTGGGCACCAGCCTTCGAGGGCGGTATGGCGATGCTGTTCGGGAAATAGATGACAGTGTTGGGAA
GATCTTGAGCCTTCTGCAGAACTTGGGCATCAGTAAGAACACATTTGTCTTCTTCACGTCTGATAATGGT
GCGGCCCTCATTTCTGCTCCCAACGAAGGTGGCAGCAACGGTCCCTTCCTGTGTGGGAAGCAGACGACAT
TTGAAGGCGGGATGAGGGAGCCTGCGATCGCATGGTGGCCAGGACACATTGCTGCAGGCCAGGTCAGCCA
CCAGCTGGGAAGCATCATGGATCTCTTCACCACCAGCCTGTCCCTTGCAGGCCTGAAGCCCCCCAGTGAC
AGGGTGATTGATGGACTTGACCTCCTCCCCACCATGCTCAAGGGCCAGATGATGGACAGGCCCATATTTT
ATTACCGTGGCAACACTCTGATGGCTGTCACTCTTGGCCAGTACAAAGCACACCTCTGGACTTGGACCAA
CTCCTGGGAGGAGTTCACACAGGGCACTGACTTCTGCCCCGGGCAGAACGTCTCAGGAGTTACAACCCAC
ACCCAGGAAGAACACACGGAGCTACCCCTGATCTTCCACCTGGGACGGGACCCAGGGGAGAGATTCCCAC
TCAGCTTCCACAGTGACGAATACCAGGACGCCCTCAGCAGGACCACCCAGGTTGTCCAGGAGCACCAAAA
GTCCTTGGTCCCCGGACAGCCCCAGCTCAATGTGTGTAACCAGGCTGTCATGAATTGGGCACCCCCAGGC
TGTGAAAAACTAGGGAAGTGTCTGACACCTCCTGAGTCTGTCCCTGAGAAGTGTTTCTGGGCCCATGGAG
GATCAGGATACCCATACGATGTTCCAGATTACGCTTAAGTCGAC

7.4.2 Murine Galns ORF2 plasmid sequence:

EcoRV (gatatc)+ Kozak + CDS + linker+ HA TAG + stop codon + SalI (gtcgac)

GATATCGCCGCCACCATGCTTTTCCCAAGCTTCTATTCTGCCAACCCTTTGTGCTCACCATCTAGGGCAG
CCCTGCTCACAGGACGGCTGCCCATCCGCAATGGCTTCTACACAACCAACGCTCATGCAAGGAATGCTTA
CACACCTCAGGAGATCATGGGTGGGATCCCTAACTCAGAGCACCTCCTGCCCGAGCTCCTGAAGAAGGCA
GGCTATACCAACAAGATCGTGGGCAAGTGGCATCTGGGTCATAGGCCCCAGTTCCACCCCCTGAAGCATG
GATTTGACGAGTGGTTTGGATCTCCCAACTGTCACTTTGGACCGTATGACAACAAGGCCAAGCCCAACAT
CCCTGTGTACAGGGACTGGGAGATGGTCGGCAGATTTTATGAAGAGTTCCCAATTAACCGGAAGACTGGG
GAAGCTAACCTCACCCAGCTCTACACACAAGAAGCGCTGGACTTCATCCAGACACAACATGCAAGGCAGA
GCCCCTTCTTCCTCTACTGGGCCATCGACGCCACTCATGCACCAGTTTACGCCTCAAGACAGTTCTTGGG
CACCAGCCTTCGAGGGCGGTATGGCGATGCTGTTCGGGAAATAGATGACAGTGTTGGGAAGATCTTGAGC
CTTCTGCAGAACTTGGGCATCAGTAAGAACACATTTGTCTTCTTCACGTCTGATAATGGTGCGGCCCTCA
TTTCTGCTCCCAACGAAGGTGGCAGCAACGGTCCCTTCCTGTGTGGGAAGCAGACGACATTTGAAGGCGG
GATGAGGGAGCCTGCGATCGCATGGTGGCCAGGACACATTGCTGCAGGCCAGGTCAGCCACCAGCTGGGA
AGCATCATGGATCTCTTCACCACCAGCCTGTCCCTTGCAGGCCTGAAGCCCCCCAGTGACAGGGTGATTG
ATGGACTTGACCTCCTCCCCACCATGCTCAAGGGCCAGATGATGGACAGGCCCATATTTTATTACCGTGG
CAACACTCTGATGGCTGTCACTCTTGGCCAGTACAAAGCACACCTCTGGACTTGGACCAACTCCTGGGAG
GAGTTCACACAGGGCACTGACTTCTGCCCCGGGCAGAACGTCTCAGGAGTTACAACCCACACCCAGGAAG
AACACACGGAGCTACCCCTGATCTTCCACCTGGGACGGGACCCAGGGGAGAGATTCCCACTCAGCTTCCA
CAGTGACGAATACCAGGACGCCCTCAGCAGGACCACCCAGGTTGTCCAGGAGCACCAAAAGTCCTTGGTC
CCCGGACAGCCCCAGCTCAATGTGTGTAACCAGGCTGTCATGAATTGGGCACCCCCAGGCTGTGAAAAAC
TAGGGAAGTGTCTGACACCTCCTGAGTCTGTCCCTGAGAAGTGTTTCTGGGCCCATGGAGGATCAGGATA
CCCATACGATGTTCCAGATTACGCTTAAGTCGAC

7.5 Complete results of Inflammatory profiling of mice.

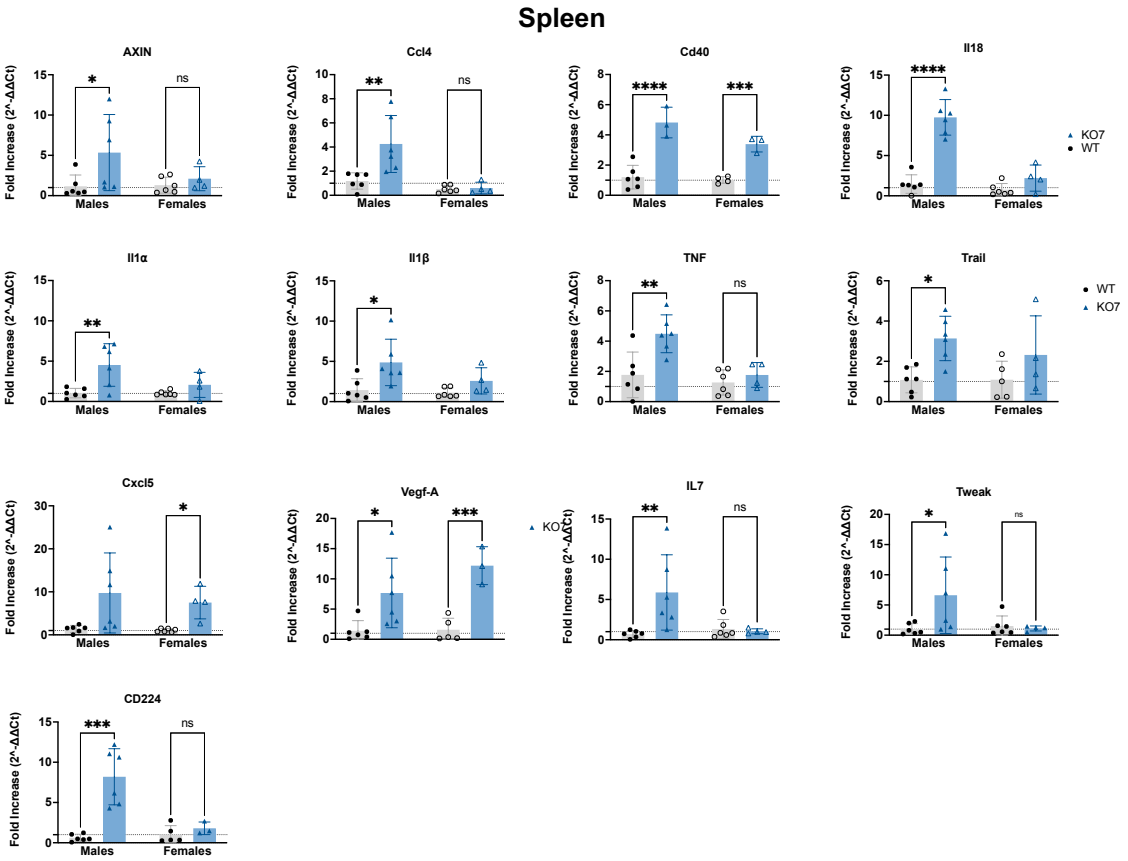


Figure 40 RT-qPCR results of inflammatory markers screening on spleen samples of WTs and KOs mice.

Despite showing variability, KO7 male mice overexpress several markers of inflammation of pro-inflammatory and pro-apoptotic nature. In addition, Axin increase reflects alteration in bone homeostasis, expected in MPSIVA. Two-Way ANOVA (non-parametric; *p-value<0.03; **p-value<0.0021; Bonferroni test for correction).

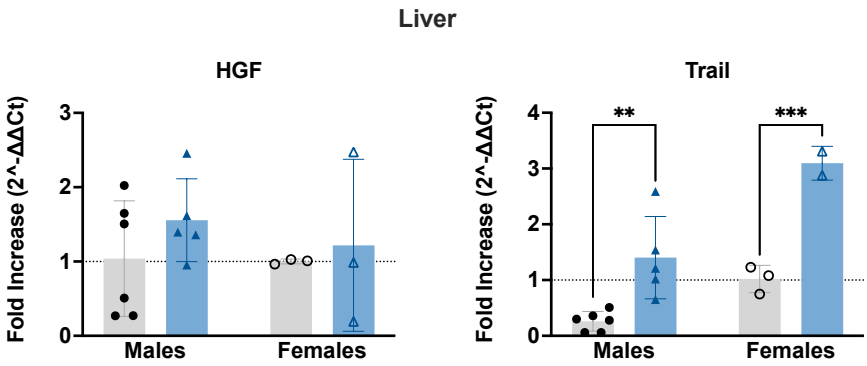


Figure 41 RT-qPCR results of inflammatory markers screening on Liver samples of WTs and KOs mice.

As for the spleen samples, Trail, a pro-apoptotic marker appears upregulated in both males (n=5) and females KO7 mice (n≥2), evaluated at 5 months of age. Two-Way ANOVA (non-parametric; *p-value<0.03; **p-value<0.0021; Bonferroni test for correction).

7.6 CT scan measurements

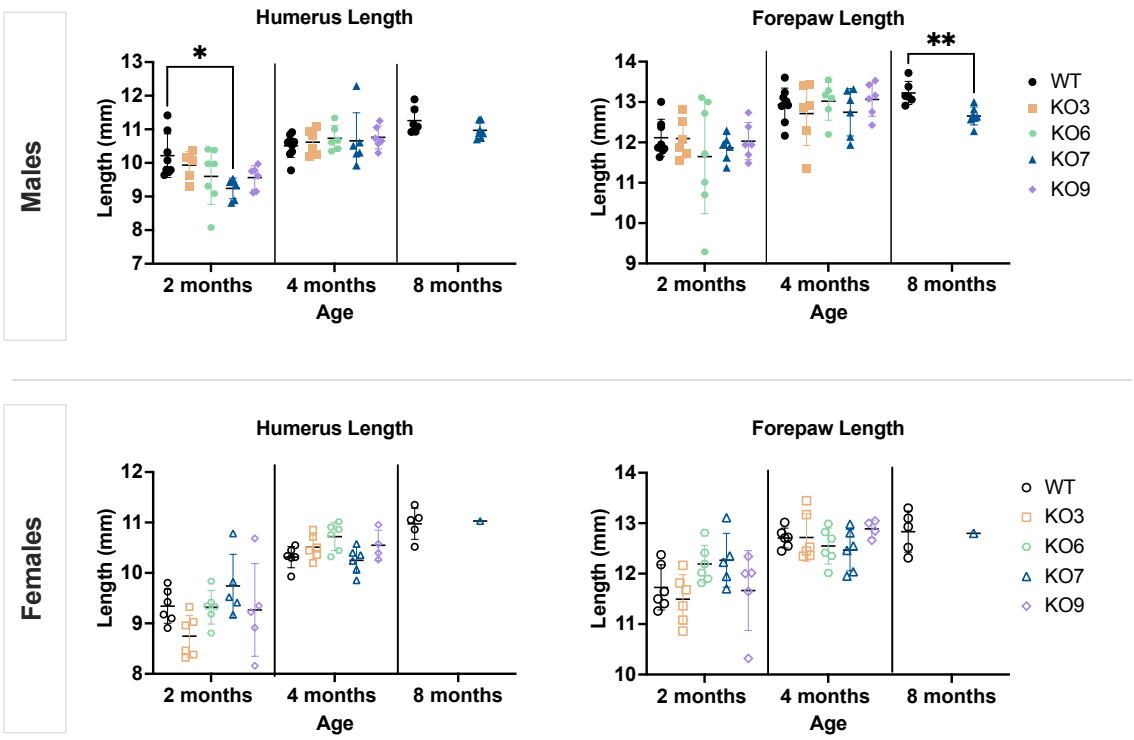


Figure 42 Gender-matched results from CT-scan analysis of the anterior paws. Male KO7 mice show a significant reduction in the length of the forepaw *(the radio and ulna structure)* at 8 months of age, compared to WT controls. The difference appears evident only at the latest timepoint in males and is not detected in females. Two-Way ANOVA (non-parametric; *p-value<0.03; **p-value<0.0021; Bonferroni test for correction).

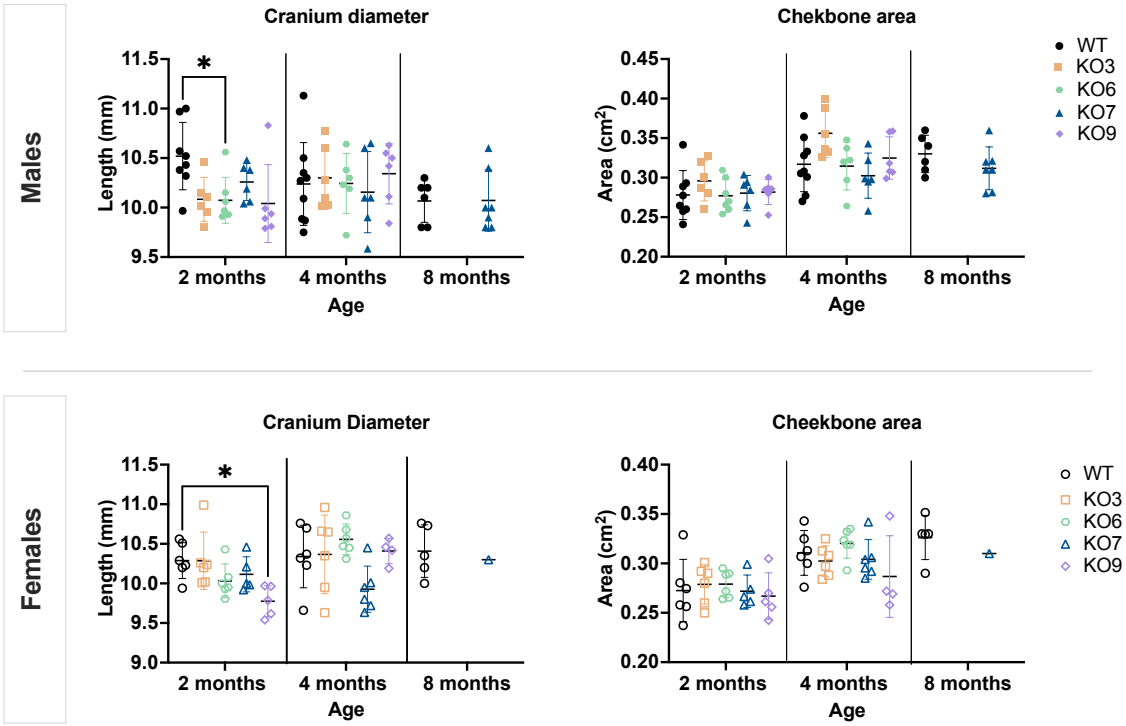


Figure 43 Gender-matched measurements of the craniofacial bones on CT scan.

Analysis on CT-scan of the cranium diameter and cheekbone area show mild and transient differences in KO6 and KO9 mice, compared to WTs. Reduction in those measures, however, appears to be compensated as the mice grow. Two-Way ANOVA (non-parametric; *p-value<0.03; Bonferroni test for correction).

7.7 pQCT complete analysis

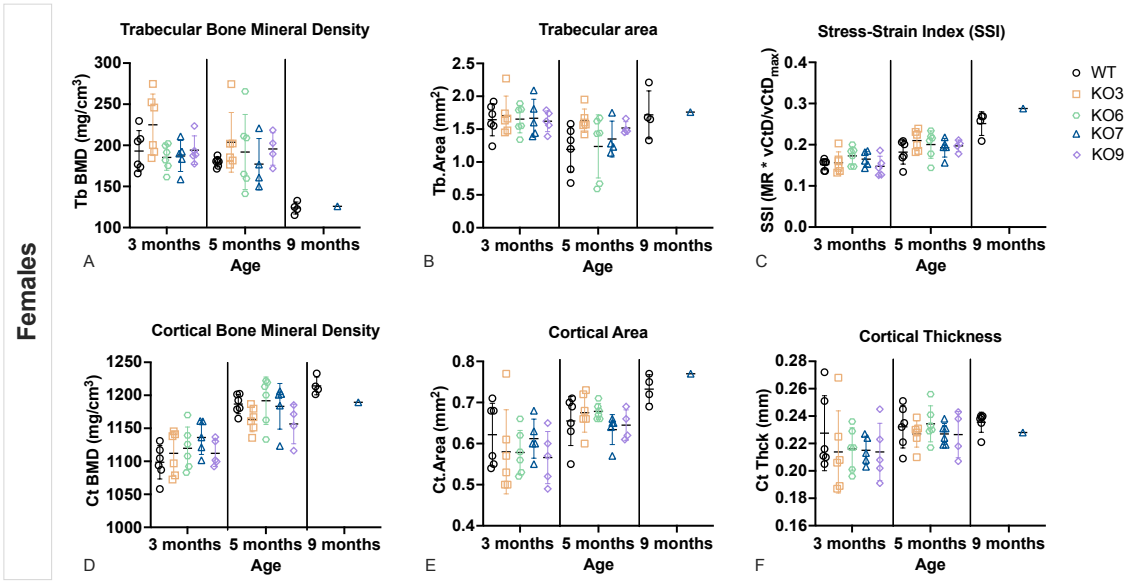


Figure 44 Analysis on pQCT of the bone structure of the tibia of our female mouse models.

Analysis at 3 and 5 months timepoint of the right tibia of the female mice of each strain (n≥4). At 9 months timepoint, only WT and KO7 mice have been analysed. No statistically significant alteration was observed. Two-Way ANOVA (non-parametric; Bonferroni test for correction).

7.8 Histo-morphometry on female WT and KO7 models

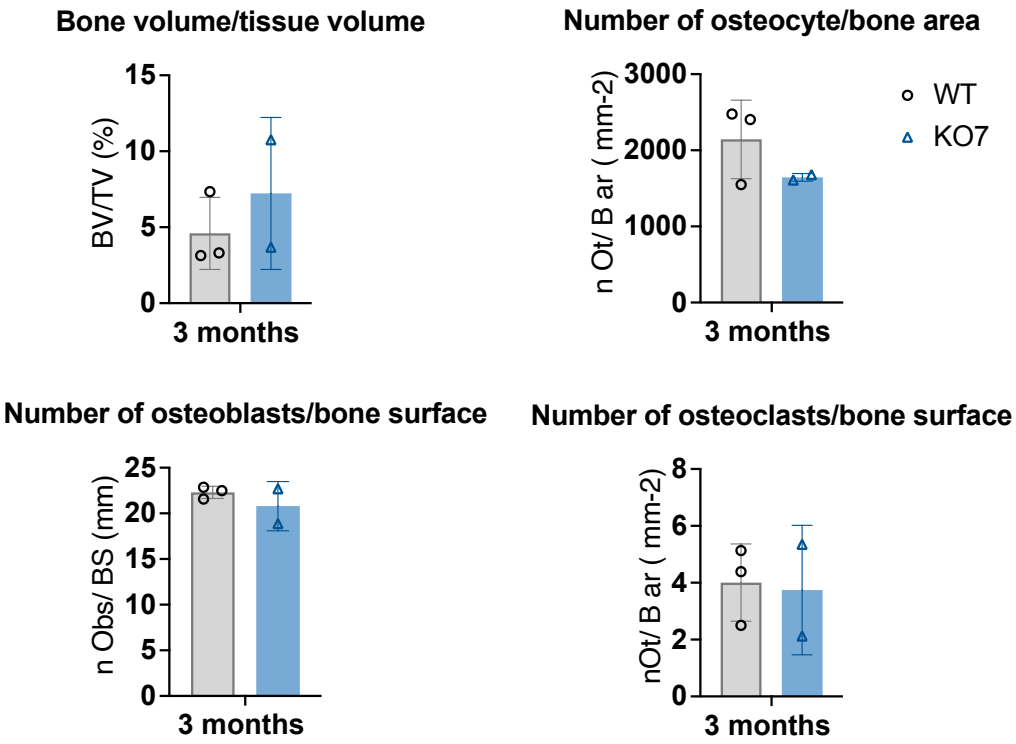


Figure 45 Histo-morphometrical analysis on the tibia of WT and KO7 female mice. Two-Way ANOVA (non-parametric; *p-value<0.03; **p-value<0.0021; Bonferroni test for correction).

7.9 Motor and Behavioural tests complete

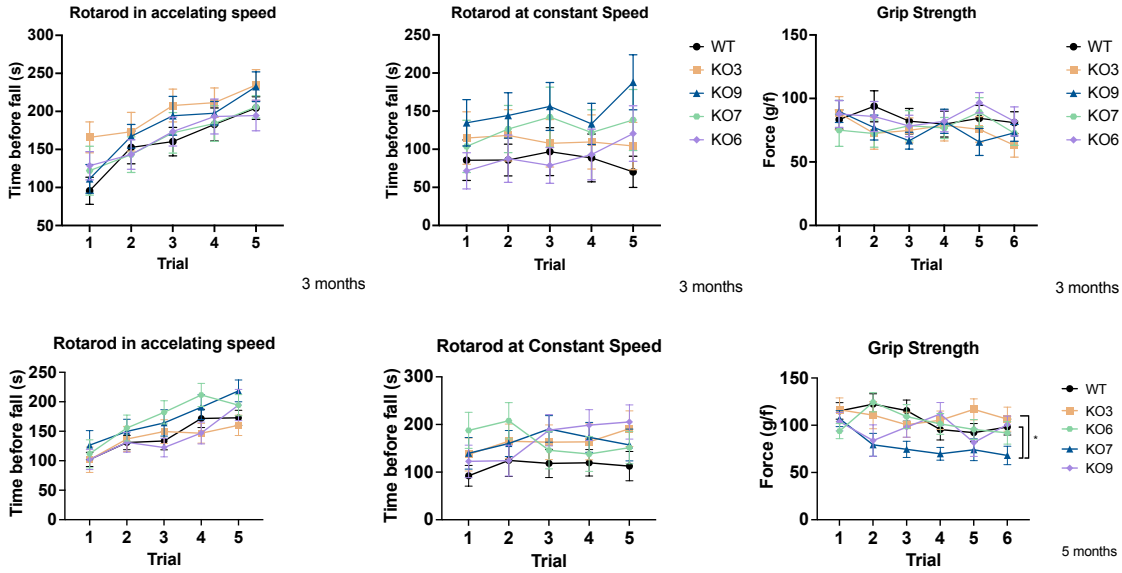


Figure 46 Complete analysis of Rotarod and Grip Strength test at 3 and 5 months timepoint.

8 References

Abdulkhaleq, L.A., Assi, M.A., Abdullah, R., Zamri-Saad, M., Taufiq-Yap, Y.H., Hezmee, M.N.M., 2018. The crucial roles of inflammatory mediators in inflammation: A review. Vet. World 11, 627–635. https://doi.org/10.14202/vetworld.2018.627-635

Abubakar, A.A., Noordin, M.M., Azmi, T.I., Kaka, U., Loqman, M.Y., 2016. The use of rats and mice as animal models in ex vivo bone growth and development studies. Bone Jt. Res. 5, 610. https://doi.org/10.1302/2046-3758.512.BJR-2016-0102.R2

Adamopoulos, I.E., Xia, Z., Lau, Y.S., Athanasou, N.A., 2006. Hepatocyte growth factor can substitute for M-CSF to support osteoclastogenesis. Biochem. Biophys. Res. Commun. 350, 478–483. https://doi.org/10.1016/j.bbrc.2006.09.076

Aflaki, E., Moaven, N., Borger, D.K., Lopez, G., Westbroek, W., Chae, J.J., Marugan, J., Patnaik, S., Maniwang, E., Gonzalez, A.N., Sidransky, E., 2016. Lysosomal storage and impaired autophagy lead to inflammasome activation in Gaucher macrophages. Aging Cell 15, 77–88. https://doi.org/10.1111/acel.12409

Aguilar Delgado, C., Hammerschmidt, T., Faverzini, J.L., Lopes, F., Giugliani, R., Baldo, G., Vargas, C.R., 2023. Inflammatory process and oxidative/nitrative stress: in vivo study in mucopolysaccharidosis type IV A patients under long-term enzyme replacement therapy. Arch. Biochem. Biophys. 737, 109541. https://doi.org/10.1016/j.abb.2023.109541

Aldenhoven, M., Jones, S.A., Bonney, D., Borrill, R.E., Coussons, M., Mercer, J., Bierings, M.B., Versluys, B., van Hasselt, P.M., Wijburg, F.A., van der Ploeg, A.T., Wynn, R.F., Boelens, J.J., 2015a. Hematopoietic Cell Transplantation for Mucopolysaccharidosis Patients Is Safe and Effective: Results after Implementation of International Guidelines. Biol. Blood Marrow Transplant. 21, 1106–1109. https://doi.org/10.1016/j.bbmt.2015.02.011

Aldenhoven, M., van den Broek, B.T.A., Wynn, R.F., O'Meara, A., Veys, P., Rovelli, A., Jones, S.A., Parini, R., van Hasselt, P.M., Renard, M., Bordon, V., de Koning, T.J., Boelens, J.J., 2017. Quality of life of Hurler syndrome patients after successful hematopoietic stem cell transplantation. Blood Adv. 1, 2236–2242. https://doi.org/10.1182/bloodadvances.2017011387

Aldenhoven, M., Wynn, R.F., Orchard, P.J., O'Meara, A., Veys, P., Fischer, A., Valayannopoulos, V., Neven, B., Rovelli, A., Prasad, V.K., Tolar, J., Allewelt, H., Jones, S.A., Parini, R., Renard, M., Bordon, V., Wulffraat, N.M., de Koning, T.J., Shapiro, E.G., Kurtzberg, J., Boelens, J.J., 2015b. Long-term outcome of

Hurler syndrome patients after hematopoietic cell transplantation: an international multicenter study. Blood 125, 2164–2172. https://doi.org/10.1182/blood-2014-11-608075

Alliston, T., 2010. Chondroitin sulfate and growth factor signaling in the skeleton: Possible links to MPS VI. J. Pediatr. Rehabil. Med. 3, 129–138. https://doi.org/10.3233/PRM-2010-0117

Amaral, O., Martins, M., Oliveira, A.R., Duarte, A.J., Mondragão-Rodrigues, I., Macedo, M.F., 2023. The Biology of Lysosomes: From Order to Disorder. Biomedicines 11, 213. https://doi.org/10.3390/biomedicines11010213

Arfi, A., Richard, M., Gandolphe, C., Bonnefont-Rousselot, D., Thérond, P., Scherman, D., 2011. Neuroinflammatory and oxidative stress phenomena in MPS IIIA mouse model: the positive effect of long-term aspirin treatment. Mol. Genet. Metab. 103, 18–25. https://doi.org/10.1016/j.ymgme.2011.01.015

Ausseil, J., Desmaris, N., Bigou, S., Attali, R., Corbineau, S., Vitry, S., Parent, M., Cheillan, D., Fuller, M., Maire, I., Vanier, M.-T., Heard, J.-M., 2008. Early neurodegeneration progresses independently of microglial activation by heparan sulfate in the brain of mucopolysaccharidosis IIIB mice. PloS One 3, e2296. https://doi.org/10.1371/journal.pone.0002296

Azevedo, A.C.M., Artigalás, O., Vedolin, L., Komlós, M., Pires, A., Giugliani, R., Schwartz, I.V.D., 2013. Brain magnetic resonance imaging findings in patients with mucopolysaccharidosis VI. J. Inherit. Metab. Dis. 36, 357–362. https://doi.org/10.1007/s10545-012-9559-x

Baehner, F., Schmiedeskamp, C., Krummenauer, F., Miebach, E., Bajbouj, M., Whybra, C., Kohlschütter, A., Kampmann, C., Beck, M., 2005. Cumulative incidence rates of the mucopolysaccharidoses in Germany. J. Inherit. Metab. Dis. 28, 1011–1017. https://doi.org/10.1007/s10545-005-0112-z

Baker, E., Guo, X.H., Orsborn, A.M., Sutherland, G.R., Callen, D.F., Hopwood, J.J., Morris, C.P., 1993. The morquio A syndrome (mucopolysaccharidosis IVA) gene maps to 16q24.3. Am. J. Hum. Genet. 52, 96–98.

Ballabio, A., Bonifacino, J.S., 2020. Lysosomes as dynamic regulators of cell and organismal homeostasis. Nat. Rev. Mol. Cell Biol. 21, 101–118. https://doi.org/10.1038/s41580-019-0185-4

Barton, N.W., Brady, R.O., Dambrosia, J.M., Di Bisceglie, A.M., Doppelt, S.H., Hill, S.C., Mankin, H.J., Murray, G.J., Parker, R.I., Argoff, C.E., 1991. Replacement therapy for inherited enzyme deficiency--macrophage-targeted

glucocerebrosidase for Gaucher's disease. N. Engl. J. Med. 324, 1464–1470. https://doi.org/10.1056/NEJM199105233242104

Barton, N.W., Furbish, F.S., Murray, G.J., Garfield, M., Brady, R.O., 1990. Therapeutic response to intravenous infusions of glucocerebrosidase in a patient with Gaucher disease. Proc. Natl. Acad. Sci. U. S. A. 87, 1913–1916. https://doi.org/10.1073/pnas.87.5.1913

Bau, B., McKenna, L.A., Soeder, S., Fan, Z., Pecht, A., Aigner, T., 2004. Hepatocyte growth factor/scatter factor is not a potent regulator of anabolic and catabolic gene expression in adult human articular chondrocytes. Biochem. Biophys. Res. Commun. 316, 984–990. https://doi.org/10.1016/j.bbrc.2004.03.001

Beck, M., 2001. Variable clinical presentation in lysosomal storage disorders. J. Inherit. Metab. Dis. 24 Suppl 2, 47–51; discussion 45-46. https://doi.org/10.1023/a:1012463605992

Bellesso, S., Salvalaio, M., Lualdi, S., Tognon, E., Costa, R., Braghetta, P., Giraudo, C., Stramare, R., Rigon, L., Filocamo, M., Tomanin, R., Moro, E., 2018. FGF signaling deregulation is associated with early developmental skeletal defects in animal models for mucopolysaccharidosis type II (MPSII).

Berendsen, A.D., Olsen, B.R., 2015. Bone development. Bone 80, 14–18. https://doi.org/10.1016/j.bone.2015.04.035

Bernardo, M.E., Aiuti, A., 2016. The Role of Conditioning in Hematopoietic Stem-Cell Gene Therapy. Hum. Gene Ther. 27, 741–748. https://doi.org/10.1089/hum.2016.103

Bertolin, J., Sánchez, V., Ribera, A., Jaén, M.L., Garcia, M., Pujol, A., Sánchez, X., Muñoz, S., Marcó, S., Pérez, J., Elias, G., León, X., Roca, C., Jimenez, V., Otaegui, P., Mulero, F., Navarro, M., Ruberte, J., Bosch, F., 2021. Treatment of skeletal and non-skeletal alterations of Mucopolysaccharidosis type IVA by AAV-mediated gene therapy. Nat. Commun. 12, 5343. https://doi.org/10.1038/s41467-021-25697-y

Bidchol, A.M., Dalal, A., Shah, H., S, S., Nampoothiri, S., Kabra, M., Gupta, N., Danda, S., Gowrishankar, K., Phadke, S.R., Kapoor, S., Kamate, M., Verma, I.C., Puri, R.D., Sankar, V.H., Devi, A.R.R., Patil, S.J., Ranganath, P., Jain, S.J.M.N., Agarwal, M., Singh, A., Mishra, P., Tamhankar, P.M., Gopinath, P.M., Nagarajaram, H.A., Satyamoorthy, K., Girisha, K.M., 2014. GALNS mutations in Indian patients with mucopolysaccharidosis IVA. Am. J. Med. Genet. A. 164A, 2793–2801. https://doi.org/10.1002/ajmg.a.36735

Biffi, A., Bartolomae, C.C., Cesana, D., Cartier, N., Aubourg, P., Ranzani, M., Cesani, M., Benedicenti, F., Plati, T., Rubagotti, E., Merella, S., Capotondo, A.,

Sgualdino, J., Zanetti, G., von Kalle, C., Schmidt, M., Naldini, L., Montini, E., 2011. Lentiviral vector common integration sites in preclinical models and a clinical trial reflect a benign integration bias and not oncogenic selection. Blood 117, 5332–5339. https://doi.org/10.1182/blood-2010-09-306761

Biffi, A., Capotondo, A., Fasano, S., del Carro, U., Marchesini, S., Azuma, H., Malaguti, M.C., Amadio, S., Brambilla, R., Grompe, M., Bordignon, C., Quattrini, A., Naldini, L., 2006. Gene therapy of metachromatic leukodystrophy reverses neurological damage and deficits in mice. J. Clin. Invest. 116, 3070–3082. https://doi.org/10.1172/JCI28873

Biffi, A., De Palma, M., Quattrini, A., Del Carro, U., Amadio, S., Visigalli, I., Sessa, M., Fasano, S., Brambilla, R., Marchesini, S., Bordignon, C., Naldini, L., 2004. Correction of metachromatic leukodystrophy in the mouse model by transplantation of genetically modified hematopoietic stem cells. J. Clin. Invest. 113, 1118–1129. https://doi.org/10.1172/JCI19205

Biswas, S.N., Patra, S., Chakraborty, P.P., Barman, H., 2017. Mucopolysaccharidosis type IVA (Morquio A): a close differential diagnosis of spondylo-epiphyseal dysplasia. BMJ Case Rep. 2017, bcr2017221156. https://doi.org/10.1136/bcr-2017-221156

Bochernitsan, A.N., Brusius-Facchin, A.C., Couto, R.R., Kubaski, F., dos Santos Lopes, S.S., Gondim, C.E., de Medeiros, P.F.V., de Souza, C.F.M., Giugliani, R., Leistner-Segal, S., 2018. Spectrum of GALNS mutations and haplotype study in Brazilian patients with Mucopolysaccharidosis type IVA. Meta Gene 16, 77–84. https://doi.org/10.1016/j.mgene.2018.01.008

Boelens, J.J., Aldenhoven, M., Purtill, D., Ruggeri, A., Defor, T., Wynn, R., Wraith, E., Cavazzana-Calvo, M., Rovelli, A., Fischer, A., Tolar, J., Prasad, V.K., Escolar, M., Gluckman, E., O'Meara, A., Orchard, P.J., Veys, P., Eapen, M., Kurtzberg, J., Rocha, V., Eurocord, Inborn Errors Working Party of European Blood and Marrow Transplant group, Duke University Blood and Marrow Transplantation Program, Centre for International Blood and Marrow Research, 2013. Outcomes of transplantation using various hematopoietic cell sources in children with Hurler syndrome after myeloablative conditioning. Blood 121, 3981–3987. https://doi.org/10.1182/blood-2012-09-455238

Boelens, J.J., Orchard, P.J., Wynn, R.F., 2014. Transplantation in inborn errors of metabolism: current considerations and future perspectives. Br. J. Haematol. 167, 293–303. https://doi.org/10.1111/bjh.13059

Boelens, J.J., Wynn, R.F., O'Meara, A., Veys, P., Bertrand, Y., Souillet, G., Wraith, J.E., Fischer, A., Cavazzana-Calvo, M., Sykora, K.W., Sedlacek, P., Rovelli, A.,

Uiterwaal, C.S.P.M., Wulffraat, N., 2007. Outcomes of hematopoietic stem cell transplantation for Hurler's syndrome in Europe: a risk factor analysis for graft failure. Bone Marrow Transplant. 40, 225–233. https://doi.org/10.1038/sj.bmt.1705718

Brailsford, J.F., 1929. The classics: Chondro-osteo-dystrophy. roentgenographic and clinical features of a child with dislocation of vertebrae, James F. Brailsford, M.D.: Am. J. Surg. Clin. Orthop. 404–410.

Braulke, T., Bonifacino, J.S., 2009. Sorting of lysosomal proteins. Biochim. Biophys. Acta 1793, 605–614. https://doi.org/10.1016/j.bbamcr.2008.10.016

Brunetti, G., Oranger, A., Carbone, C., Mori, G., Sardone, F.R., Mori, C., Celi, M., Faienza, M.F., Tarantino, U., Zallone, A., Grano, M., Colucci, S., 2013. Osteoblasts Display Different Responsiveness to TRAIL-Induced Apoptosis During Their Differentiation Process. Cell Biochem. Biophys. 67, 1127–1136. https://doi.org/10.1007/s12013-013-9616-6

Buckwalter, J.A., Mankin, H.J., Grodzinsky, A.J., 2005. Articular cartilage and osteoarthritis. Instr. Course Lect. 54, 465–480.

Caciotti, A., Tonin, R., Rigoldi, M., Ferri, L., Catarzi, S., Cavicchi, C., Procopio, E., Donati, M.A., Ficcadenti, A., Fiumara, A., Barone, R., Garavelli, L., Rocco, M.D., Filocamo, M., Antuzzi, D., Scarpa, M., Mooney, S.D., Li, B., Skouma, A., Bianca, S., Concolino, D., Casalone, R., Monti, E., Pantaleo, M., Giglio, S., Guerrini, R., Parini, R., Morrone, A., 2015. Optimizing the Molecular Diagnosis of GALNS: Novel Methods to Define and Characterize Morquio—A Syndrome-Associated Mutations. Hum. Mutat. 36, 357–368. https://doi.org/10.1002/humu.22751

Caterson, B., Melrose, J., 2018. Keratan sulfate, a complex glycosaminoglycan with unique functional capability. Glycobiology 28, 182–206. https://doi.org/10.1093/glycob/cwy003

Celik, B., Tomatsu, S.C., Tomatsu, S., Khan, S.A., 2021. Epidemiology of Mucopolysaccharidoses Update. Diagnostics 11, 273. https://doi.org/10.3390/diagnostics11020273

Chen, C.-L., Huang, S.S., Huang, J.S., 2006. Cellular heparan sulfate negatively modulates transforming growth factor-beta1 (TGF-beta1) responsiveness in epithelial cells. J. Biol. Chem. 281, 11506–11514. https://doi.org/10.1074/jbc.M512821200

Chen, H., Khan, S., Celik, B., Suzuki, Y., Ago, Y., Tomatsu, S., 2021. Activity of daily living in mucopolysaccharidosis IVA patients: Evaluation of therapeutic

efficacy. Mol. Genet. Genomic Med. 9, e1806. https://doi.org/10.1002/mgg3.1806

Chinen, Y., Higa, T., Tomatsu, S., Suzuki, Y., Orii, T., Hyakuna, N., 2014. Long-term therapeutic efficacy of allogenic bone marrow transplantation in a patient with mucopolysaccharidosis IVA. Mol. Genet. Metab. Rep. 1, 31–41. https://doi.org/10.1016/j.ymgmr.2013.11.002

Choi, H.U., Meyer, K., 1975. The structure of keratan sulphates from various sources. Biochem. J. 151, 543–553. https://doi.org/10.1042/bj1510543

Conrad, A.H., Zhang, Y., Tasheva, E.S., Conrad, G.W., 2010. Proteomic analysis of potential keratan sulfate, chondroitin sulfate A, and hyaluronic acid molecular interactions. Invest. Ophthalmol. Vis. Sci. 51, 4500–4515. https://doi.org/10.1167/iovs.09-4914

Cosma, M.P., Pepe, S., Annunziata, I., Newbold, R.F., Grompe, M., Parenti, G., Ballabio, A., 2003. The multiple sulfatase deficiency gene encodes an essential and limiting factor for the activity of sulfatases. Cell 113, 445–456. https://doi.org/10.1016/s0092-8674(03)00348-9

Coutinho, M.F., Lacerda, L., Alves, S., 2012. Glycosaminoglycan Storage Disorders: A Review. Biochem. Res. Int. 2012, 471325. https://doi.org/10.1155/2012/471325

De Duve, C., Pressman, B.C., Gianetto, R., Wattiaux, R., Appelmans, F., 1955. Tissue fractionation studies. 6. Intracellular distribution patterns of enzymes in rat-liver tissue. Biochem. J. 60, 604–617. https://doi.org/10.1042/bj0600604

de Oliveira, P.G., Baldo, G., Mayer, F.Q., Martinelli, B., Meurer, L., Giugliani, R., Matte, U., Xavier, R.M., 2013. Characterization of joint disease in mucopolysaccharidosis type I mice. Int. J. Exp. Pathol. 94, 305–311. https://doi.org/10.1111/iep.12033

de Ru, M.H., Boelens, J.J., Das, A.M., Jones, S.A., van der Lee, J.H., Mahlaoui, N., Mengel, E., Offringa, M., O'Meara, A., Parini, R., Rovelli, A., Sykora, K.-W., Valayannopoulos, V., Vellodi, A., Wynn, R.F., Wijburg, F.A., 2011. Enzyme replacement therapy and/or hematopoietic stem cell transplantation at diagnosis in patients with mucopolysaccharidosis type I: results of a European consensus procedure. Orphanet J. Rare Dis. 6, 55. https://doi.org/10.1186/1750-1172-6-55

Dede, O., Thacker, M.M., Rogers, K.J., Oto, M., Belthur, M.V., Baratela, W., Mackenzie, W.G., 2013. Upper cervical fusion in children with Morquio syndrome: intermediate to long-term results. J. Bone Joint Surg. Am. 95, 1228–1234. https://doi.org/10.2106/JBJS.J.01135

Dempster, D.W., Compston, J.E., Drezner, M.K., Glorieux, F.H., Kanis, J.A., Malluche, H., Meunier, P.J., Ott, S.M., Recker, R.R., Parfitt, A.M., 2013. Standardized nomenclature, symbols, and units for bone histomorphometry: a 2012 update of the report of the ASBMR Histomorphometry Nomenclature Committee. J. Bone Miner. Res. Off. J. Am. Soc. Bone Miner. Res. 28, 2–17. https://doi.org/10.1002/jbmr.1805

Dhawale, A.A., Thacker, M.M., Belthur, M.V., Rogers, K., Bober, M.B., Mackenzie, W.G., 2012. The lower extremity in Morquio syndrome. J. Pediatr. Orthop. 32, 534–540. https://doi.org/10.1097/BPO.0b013e318259fe57

Di Natale, P., Villani, G.R.D., Parini, R., Scarpa, M., Parenti, G., Pontarelli, G., Grosso, M., Sersale, G., Tomanin, R., Sibilio, M., Barone, R., Fiumara, A., 2008. Molecular markers for the follow-up of enzyme-replacement therapy in mucopolysaccharidosis type VI disease. Biotechnol. Appl. Biochem. 49, 219–223. https://doi.org/10.1042/BA20070093

Dierks, T., Schmidt, B., Borissenko, L.V., Peng, J., Preusser, A., Mariappan, M., von Figura, K., 2003. Multiple sulfatase deficiency is caused by mutations in the gene encoding the human C(alpha)-formylglycine generating enzyme. Cell 113, 435–444. https://doi.org/10.1016/s0092-8674(03)00347-7

Dinarello, C.A., 1997. Interleukin-1. Cytokine Growth Factor Rev. 8, 253–265. https://doi.org/10.1016/s1359-6101(97)00023-3

Dinarello, C.A., 1996. Biologic basis for interleukin-1 in disease. Blood 87, 2095–2147.

DiRosario, J., Divers, E., Wang, C., Etter, J., Charrier, A., Jukkola, P., Auer, H., Best, V., Newsom, D.L., McCarty, D.M., Fu, H., 2009. Innate and adaptive immune activation in the brain of MPS IIIB mouse model. J. Neurosci. Res. 87, 978–990. https://doi.org/10.1002/jnr.21912

Do Cao, J., Wiedemann, A., Quinaux, T., Battaglia-Hsu, S.F., Mainard, L., Froissart, R., Bonnemains, C., Ragot, S., Leheup, B., Journeau, P., Feillet, F., 2016. 30 months follow-up of an early enzyme replacement therapy in a severe Morquio A patient: About one case. Mol. Genet. Metab. Rep. 9, 42–45. https://doi.org/10.1016/j.ymgmr.2016.10.001

Doherty, C., Stapleton, M., Piechnik, M., Mason, R.W., Mackenzie, W.G., Yamaguchi, S., Kobayashi, H., Suzuki, Y., Tomatsu, S., 2019. Effect of enzyme replacement therapy on the growth of patients with Morquio A. J. Hum. Genet. 64, 625–635. https://doi.org/10.1038/s10038-019-0604-6

Donida, B., Marchetti, D.P., Biancini, G.B., Deon, M., Manini, P.R., da Rosa, H.T., Moura, D.J., Saffi, J., Bender, F., Burin, M.G., Coitinho, A.S., Giugliani, R.,

Vargas, C.R., 2015. Oxidative stress and inflammation in mucopolysaccharidosis type IVA patients treated with enzyme replacement therapy. Biochim. Biophys. Acta BBA - Mol. Basis Dis. 1852, 1012–1019. https://doi.org/10.1016/j.bbadis.2015.02.004

Dũng, V.C., Tomatsu, S., Montaño, A.M., Gottesman, G., Bober, M.B., Mackenzie, W., Maeda, M., Mitchell, G.A., Suzuki, Y., Orii, T., 2013. Mucopolysaccharidosis IVA: Correlation between genotype, phenotype and keratan sulfate levels. Mol. Genet. Metab., Special Issue: Diagnosis 110, 129–138. https://doi.org/10.1016/j.ymgme.2013.06.008

Dunham, N.W., Miya, T.S., 1957. A Note on a Simple Apparatus for Detecting Neurological Deficit in Rats and Mice**College of Pharmacy, University of Nebraska, Lincoln 8. J. Am. Pharm. Assoc. Sci. Ed 46, 208–209. https://doi.org/10.1002/jps.3030460322

Erazo-Narváez, A.F., Muñoz-Vidal, J.M., Rodríguez-Vélez, G.H., Acosta-Aragón, M.A., 2020. Clinical outcomes in elderly patients with Morquio a syndrome receiving enzyme replacement therapy - experience in a Colombian center. Mol. Genet. Metab. Rep. 25, 100679. https://doi.org/10.1016/j.ymgmr.2020.100679

Eriksen, E.F., 2010. Cellular mechanisms of bone remodeling. Rev. Endocr. Metab. Disord. 11, 219–227. https://doi.org/10.1007/s11154-010-9153-1

Feuerherm A.J., Børset, M., Seidel, C., Sundan, A., Leistad, L., Østensen, M., Faxvaag, A., 2001. Elevated levels of osteoprotegerin (OPG) and hepatocyte growth factor (HGF) in rheumatoid arthritis. Scand. J. Rheumatol. 30, 229–234. https://doi.org/10.1080/030097401316909585

Ficicioglu, C., Matalon, D.R., Luongo, N., Menello, C., Kornafel, T., Degnan, A.J., 2020. Diagnostic journey and impact of enzyme replacement therapy for mucopolysaccharidosis IVA: a sibling control study. Orphanet J. Rare Dis. 15, 336. https://doi.org/10.1186/s13023-020-01618-y

Filippon, L., Vanzin, C.S., Biancini, G.B., Pereira, I.N., Manfredini, V., Sitta, A., Peralba, M. do C.R., Schwartz, I.V.D., Giugliani, R., Vargas, C.R., 2011. Oxidative stress in patients with mucopolysaccharidosis type II before and during enzyme replacement therapy. Mol. Genet. Metab. 103, 121–127. https://doi.org/10.1016/j.ymgme.2011.02.016

Filocamo, M., Morrone, A., 2011. Lysosomal storage disorders: molecular basis and laboratory testing. Hum. Genomics 5, 156–169. https://doi.org/10.1186/1479-7364-5-3-156

Filocamo, M., Tomanin, R., Bertola, F., Morrone, A., 2018. Biochemical and molecular analysis in mucopolysaccharidoses: what a paediatrician must know. Ital. J. Pediatr. 44, 129. https://doi.org/10.1186/s13052-018-0553-2

Fujitsuka, H., Sawamoto, K., Peracha, H., Mason, R.W., Mackenzie, W., Kobayashi, H., Yamaguchi, S., Suzuki, Y., Orii, K., Orii, T., Fukao, T., Tomatsu, S., 2019. Biomarkers in patients with mucopolysaccharidosis type II and IV. Mol. Genet. Metab. Rep. 19, 100455. https://doi.org/10.1016/j.ymgmr.2019.100455

Fukuda, S., Tomatsu, S., Masuno, M., Ogawa, T., Yamagishi, A., Rezvi, G.M., Sukegawa, K., Shimozawa, N., Suzuki, Y., Kondo, N., Imaizumi, K., Kuroki, Y., Okabe, T., Orii, T., 1996. Mucopolysaccharidosis IVA: submicroscopic deletion of 16q24.3 and a novel R386C mutation of N-acetylgalactosamine-6-sulfate sulfatase gene in a classical Morquio disease. Hum. Mutat. 7, 123–134. https://doi.org/10.1002/(SICI)1098-1004(1996)7:2<123::AID-HUMU6>3.0.CO;2-D

Funderburgh, J.L., 2002. Keratan Sulfate Biosynthesis. IUBMB Life 54, 187–194. https://doi.org/10.1080/15216540214932

Funderburgh, J.L., 2000. Keratan sulfate: structure, biosynthesis, and function. Glycobiology 10, 951–958. https://doi.org/10.1093/glycob/10.10.951

Futrega, K., Robey, P.G., Klein, T.J., Crawford, R.W., Doran, M.R., 2021. A single day of TGF-β1 exposure activates chondrogenic and hypertrophic differentiation pathways in bone marrow-derived stromal cells. Commun. Biol. 4, 1–12. https://doi.org/10.1038/s42003-020-01520-0

Gaffke, L., Pierzynowska, K., Podlacha, M., Brokowska, J., Węgrzyn, G., 2021. Changes in cellular processes occurring in mucopolysaccharidoses as underestimated pathomechanisms of these diseases. Cell Biol. Int. 45, 498–506. https://doi.org/10.1002/cbin.11275

Galimberti, C., Madeo, A., Di Rocco, M., Fiumara, A., 2018. Mucopolysaccharidoses: early diagnostic signs in infants and children. Ital. J. Pediatr. 44, 133. https://doi.org/10.1186/s13052-018-0550-5

Ganesh, A., Bruwer, Z., Al-Thihli, K., 2013. An update on ocular involvement in mucopolysaccharidoses. Curr. Opin. Ophthalmol. 24, 379–388. https://doi.org/10.1097/ICU.0b013e3283644ea1

Garantziotis, S., Savani, R.C., 2019. Hyaluronan biology: A complex balancing act of structure, function, location and context. Matrix Biol., Hyaluronan Biology 78–79, 1–10. https://doi.org/10.1016/j.matbio.2019.02.002

Gardner, C.J., Robinson, N., Meadows, T., Wynn, R., Will, A., Mercer, J., Church, H.J., Tylee, K., Wraith, J.E., Clayton, P.E., 2011. Growth, final height and endocrine

sequelae in a UK population of patients with Hurler syndrome (MPS1H). J. Inherit. Metab. Dis. 34, 489–497. https://doi.org/10.1007/s10545-010-9262-8

Gentner, B., Tucci, F., Galimberti, S., Fumagalli, F., De Pellegrin, M., Silvani, P., Camesasca, C., Pontesilli, S., Darin, S., Ciotti, F., Sarzana, M., Consiglieri, G., Filisetti, C., Forni, G., Passerini, L., Tomasoni, D., Cesana, D., Calabria, A., Spinozzi, G., Cicalese, M.-P., Calbi, V., Migliavacca, M., Barzaghi, F., Ferrua, F., Gallo, V., Miglietta, S., Zonari, E., Cheruku, P.S., Forni, C., Facchini, M., Corti, A., Gabaldo, M., Zancan, S., Gasperini, S., Rovelli, A., Boelens, J.-J., Jones, S.A., Wynn, R., Baldoli, C., Montini, E., Gregori, S., Ciceri, F., Valsecchi, M.G., la Marca, G., Parini, R., Naldini, L., Aiuti, A., Bernardo, M.-E., 2021. Hematopoietic Stem- and Progenitor-Cell Gene Therapy for Hurler Syndrome. N. Engl. J. Med. 385, 1929–1940. https://doi.org/10.1056/NEJMoa2106596

Ghiselli, G., 2017. Drug-Mediated Regulation of Glycosaminoglycan Biosynthesis. Med. Res. Rev. 37, 1051–1094. https://doi.org/10.1002/med.21429

Ghosh, A., Jana, M., Modi, K., Gonzalez, F.J., Sims, K.B., Berry-Kravis, E., Pahan, K., 2015. Activation of peroxisome proliferator-activated receptor α induces lysosomal biogenesis in brain cells: implications for lysosomal storage disorders. J. Biol. Chem. 290, 10309–10324. https://doi.org/10.1074/jbc.M114.610659

Ghosh, P., Shimmon, S., Whitehouse, M.W., 2006. Arthritic disease suppression and cartilage protection with glycosaminoglycan polypeptide complexes (Peptacans) derived from the cartilage extracellular matrix: a novel approach to therapy. Inflammopharmacology 14, 155–162. https://doi.org/10.1007/s10787-006-1522-8

Giugliani, R., Carvalho, C.G., Herber, S., de Camargo Pinto, L.L., 2011. Recent Advances in Treatment Approaches of Mucopolysaccharidosis VI. Curr. Pharm. Biotechnol. 12, 956–962. https://doi.org/10.2174/138920111795542688

Goldberg, A., Mitchell, K., Soans, J., Kim, L., Zaidi, R., 2017. The use of mesenchymal stem cells for cartilage repair and regeneration: a systematic review. J. Orthop. Surg. 12, 39. https://doi.org/10.1186/s13018-017-0534-y

Goldring, M.B., 2012. Articular cartilage degradation in osteoarthritis. HSS J. Musculoskelet. J. Hosp. Spec. Surg. 8, 7–9. https://doi.org/10.1007/s11420-011-9250-z

Gonzalez, E.A., Martins, G.R., Tavares, A.M.V., Viegas, M., Poletto, E., Giugliani, R., Matte, U., Baldo, G., 2018. Cathepsin B inhibition attenuates cardiovascular

pathology in mucopolysaccharidosis I mice. Life Sci. 196, 102–109. https://doi.org/10.1016/j.lfs.2018.01.020

Goodall, K.J., Poon, I.K.H., Phipps, S., Hulett, M.D., 2014. Soluble heparan sulfate fragments generated by heparanase trigger the release of pro-inflammatory cytokines through TLR-4. PloS One 9, e109596. https://doi.org/10.1371/journal.pone.0109596

Gritti, A., Parati, E.A., Cova, L., Frolichsthal, P., Galli, R., Wanke, E., Faravelli, L., Morassutti, D.J., Roisen, F., Nickel, D.D., Vescovi, A.L., 1996. Multipotential stem cells from the adult mouse brain proliferate and self-renew in response to basic fibroblast growth factor. J. Neurosci. Off. J. Soc. Neurosci. 16, 1091–1100. https://doi.org/10.1523/JNEUROSCI.16-03-01091.1996

Guo, N., DeAngelis, V., Zhu, C., Schuchman, E.H., Simonaro, C.M., 2019. Pentosan Polysulfate Treatment of Mucopolysaccharidosis Type IIIA Mice. JIMD Rep. 43, 37–52. https://doi.org/10.1007/8904_2018_96

Haeussler, M., Schönig, K., Eckert, H., Eschstruth, A., Mianné, J., Renaud, J.-B., Schneider-Maunoury, S., Shkumatava, A., Teboul, L., Kent, J., Joly, J.-S., Concordet, J.-P., 2016. Evaluation of off-target and on-target scoring algorithms and integration into the guide RNA selection tool CRISPOR. Genome Biol. 17, 148. https://doi.org/10.1186/s13059-016-1012-2

Hannon, R., Blumsohn, A., Naylor, K., Eastell, R., 1998. Response of biochemical markers of bone turnover to hormone replacement therapy: impact of biological variability. J. Bone Miner. Res. Off. J. Am. Soc. Bone Miner. Res. 13, 1124–1133. https://doi.org/10.1359/jbmr.1998.13.7.1124

Hardin, J.A., Cobelli, N., Santambrogio, L., 2015. Consequences of metabolic and oxidative modifications of cartilage tissue. Nat. Rev. Rheumatol. 11, 521–529. https://doi.org/10.1038/nrrheum.2015.70

Harmatz, P., Shediac, R., 2017. Mucopolysaccharidosis VI: pathophysiology, diagnosis and treatment. Front. Biosci. Landmark Ed. 22, 385–406. https://doi.org/10.2741/4490

Hayashi, M., Kadomatsu, K., Kojima, T., Ishiguro, N., 2011. Keratan sulfate and related murine glycosylation can suppress murine cartilage damage in vitro and in vivo. Biochem. Biophys. Res. Commun. 409, 732–737. https://doi.org/10.1016/j.bbrc.2011.05.077

Hayes, Anthony J., Melrose, J., 2020. Keratan Sulphate in the Tumour Environment, in: Birbrair, A. (Ed.), Tumor Microenvironment: Extracellular Matrix Components – Part A, Advances in Experimental Medicine and Biology.

Springer International Publishing, Cham, pp. 39–66. https://doi.org/10.1007/978-3-030-40146-7_2

Hayes, Anthony J, Melrose, J., 2020. Aggrecan, the Primary Weight-Bearing Cartilage Proteoglycan, Has Context-Dependent, Cell-Directive Properties in Embryonic Development and Neurogenesis: Aggrecan Glycan Side Chain Modifications Convey Interactive Biodiversity. Biomolecules 10, 1244. https://doi.org/10.3390/biom10091244

Hendriksz, C.J., Burton, B., Fleming, T.R., Harmatz, P., Hughes, D., Jones, S.A., Lin, S.-P., Mengel, E., Scarpa, M., Valayannopoulos, V., Giugliani, R., STRIVE Investigators, Slasor, P., Lounsbury, D., Dummer, W., 2014. Efficacy and safety of enzyme replacement therapy with BMN 110 (elosulfase alfa) for Morquio A syndrome (mucopolysaccharidosis IVA): a phase 3 randomised placebo-controlled study. J. Inherit. Metab. Dis. 37, 979–990. https://doi.org/10.1007/s10545-014-9715-6

Hendriksz, C.J., Giugliani, R., Harmatz, P., Mengel, E., Guffon, N., Valayannopoulos, V., Parini, R., Hughes, D., Pastores, G.M., Lau, H.A., Al-Sayed, M.D., Raiman, J., STRIVE Investigators, Yang, K., Mealiffe, M., Haller, C., 2015. Multi-domain impact of elosufase alfa in Morquio A syndrome in the pivotal phase III trial. Mol. Genet. Metab. 114, 178–185. https://doi.org/10.1016/j.ymgme.2014.08.012

Hendriksz, C.J., Harmatz, P., Beck, M., Jones, S., Wood, T., Lachman, R., Gravance, C.G., Orii, T., Tomatsu, S., 2013. Review of clinical presentation and diagnosis of mucopolysaccharidosis IVA. Mol. Genet. Metab., Special Issue: Diagnosis 110, 54–64. https://doi.org/10.1016/j.ymgme.2013.04.002

Hengartner, N.-E., Fiedler, J., Ignatius, A., Brenner, R.E., 2013. IL-1β Inhibits Human Osteoblast Migration. Mol. Med. 19, 36–42. https://doi.org/10.2119/molmed.2012.00058

Hers, H.G., 1963. alpha-Glucosidase deficiency in generalized glycogenstorage disease (Pompe's disease). Biochem. J. 86, 11–16. https://doi.org/10.1042/bj0860011

Hintze, J.P., Tomatsu, S., Fujii, T., Montaño, A.M., Yamaguchi, S., Suzuki, Y., Fukushi, M., Ishimaru, T., Orii, T., 2011. Comparison of Liquid Chromatography–Tandem Mass Spectrometry and Sandwich ELISA for Determination of Keratan Sulfate in Plasma and Urine. Biomark. Insights 6, 69–78. https://doi.org/10.4137/BMI.S7451

Hobbs, J.R., Hugh-Jones, K., Barrett, A.J., Byrom, N., Chambers, D., Henry, K., James, D.C., Lucas, C.F., Rogers, T.R., Benson, P.F., Tansley, L.R., Patrick,

A.D., Mossman, J., Young, E.P., 1981. Reversal of clinical features of Hurler's disease and biochemical improvement after treatment by bone-marrow transplantation. Lancet Lond. Engl. 2, 709–712. https://doi.org/10.1016/s0140-6736(81)91046-1

Holley, R.J., Ellison, S.M., Fil, D., O'Leary, C., McDermott, J., Senthivel, N., Langford-Smith, A.W.W., Wilkinson, F.L., D'Souza, Z., Parker, H., Liao, A., Rowlston, S., Gleitz, H.F.E., Kan, S.-H., Dickson, P.I., Bigger, B.W., 2018. Macrophage enzyme and reduced inflammation drive brain correction of mucopolysaccharidosis IIIB by stem cell gene therapy. Brain J. Neurol. 141, 99–116. https://doi.org/10.1093/brain/awx311

Hoogerbrugge, P.M., Brouwer, O.F., Bordigoni, P., Ringden, O., Kapaun, P., Ortega, J.J., O'Meara, A., Cornu, G., Souillet, G., Frappaz, D., 1995. Allogeneic bone marrow transplantation for lysosomal storage diseases. The European Group for Bone Marrow Transplantation. Lancet Lond. Engl. 345, 1398–1402. https://doi.org/10.1016/s0140-6736(95)92597-x

Ho-Pham, L.T., Ho-Le, T.P., Mai, L.D., Do, T.M., Doan, M.C., Nguyen, T.V., 2018. Sex-difference in bone architecture and bone fragility in Vietnamese. Sci. Rep. 8, 7707. https://doi.org/10.1038/s41598-018-26053-9

Hopkins, P.V., Klug, T., Vermette, L., Raburn-Miller, J., Kiesling, J., Rogers, S., 2018. Incidence of 4 Lysosomal Storage Disorders From 4 Years of Newborn Screening. JAMA Pediatr. 172, 696–697. https://doi.org/10.1001/jamapediatrics.2018.0263

Hopwood, J.J., Ballabio, A., 2001. Mutation and polymorphism spectrum of the GALNS gene in mucopolysaccharidosis IVA (Morquio A) - PubMed [WWW Document]. URL https://pubmed.ncbi.nlm.nih.gov/16287098/ (accessed 6.5.23).

Hsu, P.D., Scott, D.A., Weinstein, J.A., Ran, F.A., Konermann, S., Agarwala, V., Li, Y., Fine, E.J., Wu, X., Shalem, O., Cradick, T.J., Marraffini, L.A., Bao, G., Zhang, F., 2013. DNA targeting specificity of RNA-guided Cas9 nucleases. Nat. Biotechnol. 31, 827–832. https://doi.org/10.1038/nbt.2647

Huang, C., Zheng, Y., Bai, J., Shi, C., Shi, X., Shan, H., Zhou, X., 2020. Hepatocyte growth factor overexpression promotes osteoclastogenesis and exacerbates bone loss in CIA mice. J. Orthop. Transl. 27, 9–16. https://doi.org/10.1016/j.jot.2020.10.011

Iozzo, R.V., Schaefer, L., 2015. Proteoglycan form and function: A comprehensive nomenclature of proteoglycans. Matrix Biol. 42, 11–55. https://doi.org/10.1016/j.matbio.2015.02.003

Itoh, T., Matsuda, H., Tanioka, M., Kuwabara, K., Itohara, S., Suzuki, R., 2002. The Role of Matrix Metalloproteinase-2 and Matrix Metalloproteinase-9 in Antibody-Induced Arthritis. J. Immunol. 169, 2643–2647. https://doi.org/10.4049/jimmunol.169.5.2643

Jakobkiewicz-Banecka, J., Gabig-Ciminska, M., Kloska, A., Malinowska, M., Piotrowska, E., Banecka-Majkutewicz, Z., Banecki, B., Wegrzyn, A., Wegrzyn, G., 2016. Glycosaminoglycans and mucopolysaccharidosis type III. Front. Biosci. Landmark Ed. 21, 1393–1409. https://doi.org/10.2741/4463

Jiang, N., An, J., Yang, K., Liu, J., Guan, C., Ma, C., Tang, X., 2021. NLRP3 Inflammasome: A New Target for Prevention and Control of Osteoporosis? Front. Endocrinol. 12.

Jiang, Y., Tuan, R.S., 2015. Origin and function of cartilage stem/progenitor cells in osteoarthritis. Nat. Rev. Rheumatol. 11, 206–212. https://doi.org/10.1038/nrrheum.2014.200

Karamanos, N.K., Piperigkou, Z., Theocharis, A.D., Watanabe, H., Franchi, M., Baud, S., Brézillon, S., Götte, M., Passi, A., Vigetti, D., Ricard-Blum, S., Sanderson, R.D., Neill, T., Iozzo, R.V., 2018. Proteoglycan Chemical Diversity Drives Multifunctional Cell Regulation and Therapeutics. Chem. Rev. 118, 9152–9232. https://doi.org/10.1021/acs.chemrev.8b00354

Kecskemethy, H.H., Kubaski, F., Harcke, H.T., Tomatsu, S., 2016. Bone mineral density in MPS IV A (Morquio syndrome type A). Mol. Genet. Metab. 117, 144–149. https://doi.org/10.1016/j.ymgme.2015.11.013

Kenth, J.J., Thompson, G., Fullwood, C., Wilkinson, S., Jones, S., Bruce, I.A., 2019. The characterisation of pulmonary function in patients with mucopolysaccharidoses IVA: A longitudinal analysis. Mol. Genet. Metab. Rep. 20, 100487. https://doi.org/10.1016/j.ymgmr.2019.100487

Khan, S., Alméciga-Díaz, C.J., Sawamoto, K., Mackenzie, W.G., Theroux, M.C., Pizarro, C., Mason, R.W., Orii, T., Tomatsu, S., 2017. Mucopolysaccharidosis IVA and glycosaminoglycans. Mol. Genet. Metab. 120, 78–95. https://doi.org/10.1016/j.ymgme.2016.11.007

Khan, S.A., Mason, R.W., Giugliani, R., Orii, K., Fukao, T., Suzuki, Y., Yamaguchi, S., Kobayashi, H., Orii, T., Tomatsu, S., 2018. Glycosaminoglycans analysis in blood and urine of patients with mucopolysaccharidosis. Mol. Genet. Metab. 125, 44–52. https://doi.org/10.1016/j.ymgme.2018.04.011

Khan, S.A., Peracha, H., Ballhausen, D., Wiesbauer, A., Rohrbach, M., Gautschi, M., Mason, R.W., Giugliani, R., Suzuki, Y., Orii, K.E., Orii, T., Tomatsu, S., 2017.

Epidemiology of mucopolysaccharidoses. Mol. Genet. Metab. 121, 227–240. https://doi.org/10.1016/j.ymgme.2017.05.016

Khedhiri, S., Chkioua, L., Ferchichi, S., Miled, A., Laradi, S., 2011. Polymorphisms in Tunisian patients with N-acetylgalactosamine-6-sulfate sulfatase gene deficiency: Implication in Morquio A disease. Diagn. Pathol. 6, 11. https://doi.org/10.1186/1746-1596-6-11

Killedar, S., DiRosario, J., Divers, E., Popovich, P.G., McCarty, D.M., Fu, H., 2010. RMeseuarcchopolysaccharidosis IIIB, a lysosomal storage disease, triggers a pathogenic CNS autoimmune response.

Kim, S.-J., Zhang, Z., Hitomi, E., Lee, Y.-C., Mukherjee, A.B., 2006. Endoplasmic reticulum stress-induced caspase-4 activation mediates apoptosis and neurodegeneration in INCL. Hum. Mol. Genet. 15, 1826–1834. https://doi.org/10.1093/hmg/ddl105

Kingma, S.D.K., Wagemans, T., IJlst, L., Bronckers, A.L.J.J., van Kuppevelt, T.H., Everts, V., Wijburg, F.A., van Vlies, N., 2016. Altered interaction and distribution of glycosaminoglycans and growth factors in mucopolysaccharidosis type I bone disease. Bone 88, 92–100. https://doi.org/10.1016/j.bone.2016.01.029

Kiykim, E., Barut, K., Cansever, M.S., Zeybek, C.A., Zubarioglu, T., Aydin, A., Kasapcopur, O., 2015. Screening Mucopolysaccharidosis Type IX in Patients with Juvenile Idiopathic Arthritis. JIMD Rep. 25, 21–24. https://doi.org/10.1007/8904_2015_467

Klüppel, M., Wight, T.N., Chan, C., Hinek, A., Wrana, J.L., 2005. Maintenance of chondroitin sulfation balance by chondroitin-4-sulfotransferase 1 is required for chondrocyte development and growth factor signaling during cartilage morphogenesis. Dev. Camb. Engl. 132, 3989–4003. https://doi.org/10.1242/dev.01948

Koehler, L., Samsonov, S., Rother, S., Vogel, S., Köhling, S., Moeller, S., Schnabelrauch, M., Rademann, J., Hempel, U., Pisabarro, M.T., Scharnweber, D., Hintze, V., 2017. Sulfated Hyaluronan Derivatives Modulate TGF-β1:Receptor Complex Formation: Possible Consequences for TGF-β1 Signaling. Sci. Rep. 7, 1210. https://doi.org/10.1038/s41598-017-01264-8

Kontny, E., Prochorec-Sobieszek, M., 2013. Articular adipose tissue resident macrophages in rheumatoid arthritis patients: potential contribution to local abnormalities. Rheumatol. Oxf. Engl. 52, 2158–2167. https://doi.org/10.1093/rheumatology/ket287

Kroos, M., Hoogeveen-Westerveld, M., van der Ploeg, A., Reuser, A.J.J., 2012. The genotype–phenotype correlation in Pompe disease. Am. J. Med. Genet. C Semin. Med. Genet. 160C, 59–68. https://doi.org/10.1002/ajmg.c.31318

Kubaski, F., Yabe, H., Suzuki, Y., Seto, T., Hamazaki, T., Mason, R.W., Xie, L., Onsten, T.G.H., Leistner-Segal, S., Giugliani, R., Dũng, V.C., Ngoc, C.T.B., Yamaguchi, S., Montaño, A.M., Orii, K.E., Fukao, T., Shintaku, H., Orii, T., Tomatsu, S., 2017. Hematopoietic Stem Cell Transplantation for Patients with Mucopolysaccharidosis II. Biol. Blood Marrow Transplant. J. Am. Soc. Blood Marrow Transplant. 23, 1795–1803. https://doi.org/10.1016/j.bbmt.2017.06.020

Langereis, E.J., van Vlies, N., Church, H.J., Geskus, R.B., Hollak, C.E.M., Jones, S.A., Kulik, W., van Lenthe, H., Mercer, J., Schreider, L., Tylee, K.L., Wagemans, T., Wijburg, F.A., Bigger, B.W., 2015. Biomarker responses correlate with antibody status in mucopolysaccharidosis type I patients on long-term enzyme replacement therapy. Mol. Genet. Metab. 114, 129–137. https://doi.org/10.1016/j.ymgme.2014.10.012

Latz, E., Xiao, T.S., Stutz, A., 2013. Activation and regulation of the inflammasomes. Nat. Rev. Immunol. 13, 397–411. https://doi.org/10.1038/nri3452

Lavery, C., Hendriksz, C., 2014. Mortality in Patients with Morquio Syndrome A. JIMD Rep. 15, 59–66. https://doi.org/10.1007/8904_2014_298

Leadley, R.M., Lang, S., Misso, K., Bekkering, T., Ross, J., Akiyama, T., Fietz, M., Giugliani, R., Hendriksz, C.J., Hock, N.L., McGill, J., Olaye, A., Jain, M., Kleijnen, J., 2014. A systematic review of the prevalence of Morquio A syndrome: challenges for study reporting in rare diseases. Orphanet J. Rare Dis. 9, 173. https://doi.org/10.1186/s13023-014-0173-x

Lee, C.-L., Chuang, C.-K., Chiu, H.-C., Tu, R.-Y., Lo, Y.-T., Chang, Y.-H., Lin, S.-P., Lin, H.-Y., 2022. Clinical Utility of Elosulfase Alfa in the Treatment of Morquio A Syndrome. Drug Des. Devel. Ther. 16, 143–154. https://doi.org/10.2147/DDDT.S219433

Lee, Y.-M., Fujikado, N., Manaka, H., Yasuda, H., Iwakura, Y., 2010. IL-1 plays an important role in the bone metabolism under physiological conditions. Int. Immunol. 22, 805–816. https://doi.org/10.1093/intimm/dxq431

Li, H.H., Zhao, H.-Z., Neufeld, E.F., Cai, Y., Gómez-Pinilla, F., 2002. Attenuated plasticity in neurons and astrocytes in the mouse model of Sanfilippo syndrome type B. J. Neurosci. Res. 69, 30–38. https://doi.org/10.1002/jnr.10278

Li, L., Ly, M., Linhardt, R.J., 2012. Proteoglycan sequence. Mol. Biosyst. 8, 1613–1625. https://doi.org/10.1039/c2mb25021g

Lin, H.-Y., Chuang, C.-K., Chen, M.-R., Lin, S.-M., Hung, C.-L., Chang, C.-Y., Chiu, P.C., Tsai, W.-H., Niu, D.-M., Tsai, F.-J., Lin, S.J., Hwu, W.-L., Lin, J.-L., Lin, S.-P., 2016. Cardiac structure and function and effects of enzyme replacement therapy in patients with mucopolysaccharidoses I, II, IVA and VI. Mol. Genet. Metab. 117, 431–437. https://doi.org/10.1016/j.ymgme.2016.02.003

Lin, H.-Y., Shih, S.-C., Chuang, C.-K., Chen, M.-R., Niu, D.-M., Lin, S.-P., 2013. Assessment of bone mineral density by dual energy x-ray absorptiometry in patients with mucopolysaccharidoses. Orphanet J. Rare Dis. 8, 71. https://doi.org/10.1186/1750-1172-8-71

Liu, E.T., Bolcun-Filas, E., Grass, D.S., Lutz, C., Murray, S., Shultz, L., Rosenthal, N., 2017. Of mice and CRISPR. EMBO Rep. 18, 187–193. https://doi.org/10.15252/embr.201643717

Long, B., Tompkins, T., Decker, C., Jesaitis, L., Khan, S., Slasor, P., Harmatz, P., O'Neill, C.A., Schweighardt, B., 2017. Long-term Immunogenicity of Elosulfase Alfa in the Treatment of Morquio A Syndrome: Results From MOR-005, a Phase III Extension Study. Clin. Ther. 39, 118-129.e3. https://doi.org/10.1016/j.clinthera.2016.11.017

Lowry, R.B., Applegarth, D.A., Toone, J.R., MacDonald, E., Thunem, N.Y., 1990. An update on the frequency of mucopolysaccharide syndromes in British Columbia. Hum. Genet. 85, 389–390. https://doi.org/10.1007/BF00206770

Lum, S.H., Miller, W.P., Jones, S., Poulton, K., Ogden, W., Lee, H., Logan, A., Bonney, D., Lund, T.C., Orchard, P.J., Wynn, R.F., 2017. Changes in the incidence, patterns and outcomes of graft failure following hematopoietic stem cell transplantation for Hurler syndrome. Bone Marrow Transplant. 52, 846–853. https://doi.org/10.1038/bmt.2017.5

Luzio, J.P., Pryor, P.R., Bright, N.A., 2007. Lysosomes: fusion and function. Nat. Rev. Mol. Cell Biol. 8, 622–632. https://doi.org/10.1038/nrm2217

Luzio, J.P., Pryor, P.R., Gray, S.R., Gratian, M.J., Piper, R.C., Bright, N.A., 2005. Membrane traffic to and from lysosomes. Biochem. Soc. Symp. 77–86. https://doi.org/10.1042/bss0720077

Ma, N., Teng, X., Zheng, Q., Chen, P., 2019. The regulatory mechanism of p38/MAPK in the chondrogenic differentiation from bone marrow mesenchymal stem cells. J. Orthop. Surg. 14, 434. https://doi.org/10.1186/s13018-019-1505-2

Ma, X., Tittiger, M., Knutsen, R.H., Kovacs, A., Schaller, L., Mecham, R.P., Ponder, K.P., 2008. Upregulation of elastase proteins results in aortic dilatation in

mucopolysaccharidosis I mice. Mol. Genet. Metab. 94, 298–304. https://doi.org/10.1016/j.ymgme.2008.03.018

Madani, R., Kozlov, S., Akhmedov, A., Cinelli, P., Kinter, J., Lipp, H.-P., Sonderegger, P., Wolfer, D.P., 2003. Impaired explorative behavior and neophobia in genetically modified mice lacking or overexpressing the extracellular serine protease inhibitor neuroserpin. Mol. Cell. Neurosci. 23, 473–494. https://doi.org/10.1016/S1044-7431(03)00077-0

Martel-Pelletier, J., Lajeunesse, D., Fahmi, H., Tardif, G., Pelletier, J.-P., 2006. New thoughts on the pathophysiology of osteoarthritis: one more step toward new therapeutic targets. Curr. Rheumatol. Rep. 8, 30–36. https://doi.org/10.1007/s11926-006-0022-6

Martinon, F., Chen, X., Lee, A.-H., Glimcher, L.H., 2010. TLR activation of the transcription factor XBP1 regulates innate immune responses in macrophages. Nat. Immunol. 11, 411–418. https://doi.org/10.1038/ni.1857

Martins, A.S., Alves, I., Helguero, L., Domingues, M.R., Neves, B.M., 2016. The Unfolded Protein Response in Homeostasis and Modulation of Mammalian Immune Cells. Int. Rev. Immunol. 35, 457–476. https://doi.org/10.3109/08830185.2015.1110151

McClure, J., Smith, P.S., Sorby-Adams, G., Hopwood, J., 1986. The histological and ultrastructural features of the epiphyseal plate in morquio type a syndrome (Mucopolysaccharidosis type IVA). Pathology (Phila.) 18, 217–221. https://doi.org/10.3109/00313028609059462

Mehta, A., Beck, M., Sunder-Plassmann, G. (Eds.), 2006. Fabry Disease: Perspectives from 5 Years of FOS. Oxford PharmaGenesis, Oxford.

Melrose, J., 2019. Keratan sulfate (KS)-proteoglycans and neuronal regulation in health and disease: the importance of KS-glycodynamics and interactive capability with neuroregulatory ligands. J. Neurochem. 149, 170–194. https://doi.org/10.1111/jnc.14652

Meyer, K., Linker, A., Davidson, E.A., Weissmann, B., 1953. The mucopolysaccharides of bovine cornea. J. Biol. Chem. 205, 611–616.

Mikles, M., Stanton, R.P., 1997. A review of Morquio syndrome. Am. J. Orthop. Belle Mead NJ 26, 533–540.

Mizukami, H., Mi, Y., Wada, R., Kono, M., Yamashita, T., Liu, Y., Werth, N., Sandhoff, R., Sandhoff, K., Proia, R.L., 2002. Systemic inflammation in glucocerebrosidase-deficient mice with minimal glucosylceramide storage. J. Clin. Invest. 109, 1215–1221. https://doi.org/10.1172/JCI14530

Mizushima, N., Yoshimori, T., Levine, B., 2010. Methods in Mammalian Autophagy Research. Cell 140, 313–326. https://doi.org/10.1016/j.cell.2010.01.028

Montaño, A.M., Lock-Hock, N., Steiner, R.D., Graham, B.H., Szlago, M., Greenstein, R., Pineda, M., Gonzalez-Meneses, A., Çoker, M., Bartholomew, D., Sands, M.S., Wang, R., Giugliani, R., Macaya, A., Pastores, G., Ketko, A.K., Ezgü, F., Tanaka, A., Arash, L., Beck, M., Falk, R.E., Bhattacharya, K., Franco, J., White, K.K., Mitchell, G.A., Cimbalistiene, L., Holtz, M., Sly, W.S., 2016. Original article: Clinical course of sly syndrome (mucopolysaccharidosis type VII). J. Med. Genet. 53, 403. https://doi.org/10.1136/jmedgenet-2015-103322

Montaño, A.M., Tomatsu, S., Gottesman, G.S., Smith, M., Orii, T., 2007. International Morquio A Registry: clinical manifestation and natural course of Morquio A disease. J. Inherit. Metab. Dis. 30, 165–174. https://doi.org/10.1007/s10545-007-0529-7

Moreno Giraldo, L.J., Escudero Rodríguez, Á.M., Sánchez Gómez, A., Satizabal Soto, J.M., 2018. Clinical and molecular characteristics of colombian patients with mucopolysaccharidosis IVA, and description of a new galns gene mutation. Mol. Genet. Metab. Rep. 16, 53–56. https://doi.org/10.1016/j.ymgmr.2018.06.008

Morla, S., 2019. Glycosaminoglycans and Glycosaminoglycan Mimetics in Cancer and Inflammation. Int. J. Mol. Sci. 20, 1963. https://doi.org/10.3390/ijms20081963

Morquio, L., 1929. Sur une forme de dystrophie osseusse familiale. Arch Med Enfants 32, 129–40.

Morrone, A., Caciotti, A., Atwood, R., Davidson, K., Du, C., Francis-Lyon, P., Harmatz, P., Mealiffe, M., Mooney, S., Oron, T.R., Ryles, A., Zawadzki, K.A., Miller, N., 2014. Morquio A Syndrome-Associated Mutations: A Review of Alterations in the GALNS Gene and a New Locus-Specific Database. Hum. Mutat. 35, 1271–1279. https://doi.org/10.1002/humu.22635

Muenzer, J., 2004. The mucopolysaccharidoses: a heterogeneous group of disorders with variable pediatric presentations. J. Pediatr. 144, S27-34. https://doi.org/10.1016/j.jpeds.2004.01.052

Mundy, G.R., 2007. Osteoporosis and inflammation. Nutr. Rev. 65, S147-151. https://doi.org/10.1111/j.1753-4887.2007.tb00353.x

Muralidharan, S., Mandrekar, P., 2013. Cellular stress response and innate immune signaling: integrating pathways in host defense and inflammation. J. Leukoc. Biol. 94, 1167–1184. https://doi.org/10.1189/jlb.0313153

Mynarek, M., Tolar, J., Albert, M.H., Escolar, M.L., Boelens, J.J., Cowan, M.J., Finnegan, N., Glomstein, A., Jacobsohn, D.A., Kühl, J.S., Yabe, H., Kurtzberg, J., Malm, D., Orchard, P.J., Klein, C., Lücke, T., Sykora, K.-W., 2012. Allogeneic hematopoietic SCT for alpha-mannosidosis: an analysis of 17 patients. Bone Marrow Transplant. 47, 352–359. https://doi.org/10.1038/bmt.2011.99

Nagase, H., Visse, R., Murphy, G., 2006. Structure and function of matrix metalloproteinases and TIMPs. Cardiovasc. Res. 69, 562–573. https://doi.org/10.1016/j.cardiores.2005.12.002

Nagpal, R., Goyal, R.B., Priyadarshini, K., Kashyap, S., Sharma, M., Sinha, R., Sharma, N., 2022. Mucopolysaccharidosis: A broad review. Indian J. Ophthalmol. 70, 2249–2261. https://doi.org/10.4103/ijo.IJO_425_22

Nakae, S., Horai, R., Komiyama, Y., Nambu, A., Asano, M., Nakane, A., Iwakura, Y., 2003. The Role of IL-1 in the Immune System, in: Fantuzzi, G. (Ed.), Cytokine Knockouts, Contemporary Immunology. Humana Press, Totowa, NJ, pp. 95–109. https://doi.org/10.1007/978-1-59259-405-4_6

Nakamura-Utsunomiya, A., 2021. Bone Biomarkers in Mucopolysaccharidoses. Int. J. Mol. Sci. 22, 12651. https://doi.org/10.3390/ijms222312651

Nakashima, T., Kobayashi, Y., Yamasaki, S., Kawakami, A., Eguchi, K., Sasaki, H., Sakai, H., 2000. Protein expression and functional difference of membrane-bound and soluble receptor activator of NF-kappaB ligand: modulation of the expression by osteotropic factors and cytokines. Biochem. Biophys. Res. Commun. 275, 768–775. https://doi.org/10.1006/bbrc.2000.3379

Nakashima, Y., Tomatsu, S., Hori, T., Fukuda, S., Sukegawa, K., Kondo, N., Suzuki, Y., Shimozawa, N., Orii, T., 1994. Mucopolysaccharidosis IV A: Molecular Cloning of the Human N-Acetylgalactosamine-6-sulfatase Gene (GALNS) and Analysis of the 5′-Flanking Region. Genomics 20, 99–104. https://doi.org/10.1006/geno.1994.1132

Nakayama, Y., Narita, T., Mori, A., Uesaka, S., Miyazaki, K., Ito, H., 2002. The effects of age and sex on chondroitin sulfates in normal synovial fluid. Arthritis Rheum. 46, 2105–2108. https://doi.org/10.1002/art.10424

Nelson, J., Crowhurst, J., Carey, B., Greed, L., 2003. Incidence of the mucopolysaccharidoses in Western Australia. Am. J. Med. Genet. A. 123A, 310–313. https://doi.org/10.1002/ajmg.a.20314

Neufeld, E.F., 1980. The uptake of enzymes into lysosomes: an overview. Birth Defects Orig. Artic. Ser. 16, 77–84.

Nijmeijer, S.C.M., van den Born, L.I., Kievit, A.J.A., Stepien, K.M., Langendonk, J., Marchal, J.P., Roosing, S., Wijburg, F.A., Wagenmakers, M.A.E.M., 2019. The attenuated end of the phenotypic spectrum in MPS III: from late-onset stable cognitive impairment to a non-neuronopathic phenotype. Orphanet J. Rare Dis. 14, 249. https://doi.org/10.1186/s13023-019-1232-0

Noh, H., Lee, J.I., 2014. Current and potential therapeutic strategies for mucopolysaccharidoses. J. Clin. Pharm. Ther. 39, 215–224. https://doi.org/10.1111/jcpt.12136

Novikoff, A.B., Beaufay, H., De Duve, C., 1956. Electron microscopy of lysosomerich fractions from rat liver. J. Biophys. Biochem. Cytol. 2, 179–184.

O'Gradaigh, D., Bord, S., Ireland, D., Compston, J.E., 2003. Osteoclastic bone resorption in rheumatoid arthritis and the acute-phase response. Rheumatol. Oxf. Engl. 42, 1429–1430. https://doi.org/10.1093/rheumatology/keg375

Ornitz, D.M., Itoh, N., 2001. Fibroblast growth factors. Genome Biol. 2, REVIEWS3005. https://doi.org/10.1186/gb-2001-2-3-reviews3005

Ornitz, D.M., Marie, P.J., 2015. Fibroblast growth factor signaling in skeletal development and disease. Genes Dev. 29, 1463. https://doi.org/10.1101/gad.266551.115

Oslowski, C.M., Urano, F., 2011. Measuring ER stress and the unfolded protein response using mammalian tissue culture system. Methods Enzymol. 490, 71–92. https://doi.org/10.1016/B978-0-12-385114-7.00004-0

Oslowski, C.M., Urano, F., 2010. The binary switch between life and death of endoplasmic reticulum-stressed beta cells. Curr. Opin. Endocrinol. Diabetes Obes. 17, 107–112. https://doi.org/10.1097/MED.0b013e3283372843

Ott, S.M., 2018. Cortical or Trabecular Bone: What's the Difference? Am. J. Nephrol. 47, 373–375. https://doi.org/10.1159/000489672

Ozkinay, F., Emecen, D.A., Kose, M., Isik, E., Bozaci, A.E., Canda, E., Tuysuz, B., Zubarioglu, T., Atik, T., Onay, H., 2021. Clinical and genetic features of 13 patients with mucopolysaccarhidosis type IIIB: Description of two novel NAGLU gene mutations. Mol. Genet. Metab. Rep. 27, 100732. https://doi.org/10.1016/j.ymgmr.2021.100732

Pan, C., Nelson, M.S., Reyes, M., Koodie, L., Brazil, J.J., Stephenson, E.J., Zhao, R.C., Peters, C., Selleck, S.B., Stringer, S.E., Gupta, P., 2005. Functional abnormalities of heparan sulfate in mucopolysaccharidosis-I are associated with defective biologic activity of FGF-2 on human multipotent progenitor cells. Blood 106, 1956–1964. https://doi.org/10.1182/blood-2005-02-0657

Panicker, L.M., Miller, D., Awad, O., Bose, V., Lun, Y., Park, T.S., Zambidis, E.T., Sgambato, J.A., Feldman, R.A., 2014. Gaucher iPSC-derived macrophages produce elevated levels of inflammatory mediators and serve as a new platform for therapeutic development. Stem Cells Dayt. Ohio 32, 2338–2349. https://doi.org/10.1002/stem.1732

Parenti, G., Medina, D.L., Ballabio, A., 2021. The rapidly evolving view of lysosomal storage diseases. EMBO Mol. Med. 13, e12836. https://doi.org/10.15252/emmm.202012836

Parini, R., Deodato, F., Di Rocco, M., Lanino, E., Locatelli, F., Messina, C., Rovelli, A., Scarpa, M., 2017. Open issues in Mucopolysaccharidosis type I-Hurler. Orphanet J. Rare Dis. 12, 112. https://doi.org/10.1186/s13023-017-0662-9

Parker, H., Bigger, B.W., 2019. The role of innate immunity in mucopolysaccharide diseases. J. Neurochem. 148, 639–651. https://doi.org/10.1111/jnc.14632

Parker, H., Ellison, S.M., Holley, R.J., O'Leary, C., Liao, A., Asadi, J., Glover, E., Ghosh, A., Jones, S., Wilkinson, F.L., Brough, D., Pinteaux, E., Boutin, H., Bigger, B.W., 2020. Haematopoietic stem cell gene therapy with IL-1Ra rescues cognitive loss in mucopolysaccharidosis IIIA. EMBO Mol. Med. 12, e11185. https://doi.org/10.15252/emmm.201911185

Pastores, G.M., Torres, P.A., Zeng, B.-J., 2013. Animal models for lysosomal storage disorders. Biochem. Biokhimiia 78, 721–725. https://doi.org/10.1134/S0006297913070043

Peracha, H., Sawamoto, K., Averill, L., Kecskemethy, H., Theroux, M., Thacker, M., Nagao, K., Pizarro, C., Mackenzie, W., Kobayashi, H., Yamaguchi, S., Suzuki, Y., Orii, K., Orii, T., Fukao, T., Tomatsu, S., 2018. Molecular Genetics and Metabolism Special Edition: Diagnosis Diagnosis and Prognosis of Mucopolysaccharidosis IVA. Mol. Genet. Metab. 125, 18–37. https://doi.org/10.1016/j.ymgme.2018.05.004

Pereira, V.G., Martins, A.M., Micheletti, C., D'Almeida, V., 2008. Mutational and oxidative stress analysis in patients with mucopolysaccharidosis type I undergoing enzyme replacement therapy. Clin. Chim. Acta 387, 75–79. https://doi.org/10.1016/j.cca.2007.09.008

Perera, R.M., Zoncu, R., 2016. The Lysosome as a Regulatory Hub. Annu. Rev. Cell Dev. Biol. 32, 223–253. https://doi.org/10.1146/annurev-cellbio-111315-125125

Peters, C., Shapiro, E.G., Anderson, J., Henslee-Downey, P.J., Klemperer, M.R., Cowan, M.J., Saunders, E.F., deAlarcon, P.A., Twist, C., Nachman, J.B., Hale, G.A., Harris, R.E., Rozans, M.K., Kurtzberg, J., Grayson, G.H., Williams, T.E.,

Lenarsky, C., Wagner, J.E., Krivit, W., 1998. Hurler syndrome: II. Outcome of HLA-genotypically identical sibling and HLA-haploidentical related donor bone marrow transplantation in fifty-four children. The Storage Disease Collaborative Study Group. Blood 91, 2601–2608.

Pizarro, C., Davies, R.R., Theroux, M., Spurrier, E.A., Averill, L.W., Tomatsu, S., 2016. Surgical Reconstruction for Severe Tracheal Obstruction in Morquio A Syndrome. Ann. Thorac. Surg. 102, e329-331. https://doi.org/10.1016/j.athoracsur.2016.02.113

Platt, F.M., d'Azzo, A., Davidson, B.L., Neufeld, E.F., Tifft, C.J., 2018. Lysosomal storage diseases. Nat. Rev. Dis. Primer 4, 1–25. https://doi.org/10.1038/s41572-018-0025-4

Pomin, V.H., 2015. Keratan sulfate: An up-to-date review. Int. J. Biol. Macromol. 72, 282–289. https://doi.org/10.1016/j.ijbiomac.2014.08.029

Pomin, V.H., Mulloy, B., 2018. Glycosaminoglycans and Proteoglycans. Pharmaceuticals 11. https://doi.org/10.3390/ph11010027

Qu, Y., Liu, Hao, Wei, L., Nie, S., Ding, W., Liu, S., Liu, Haiyan, Jiang, H., 2022. The Outcome of Allogeneic Hematopoietic Stem Cell Transplantation From Different Donors in Recipients With Mucopolysaccharidosis. Front. Pediatr. 10, 877735. https://doi.org/10.3389/fped.2022.877735

Quijada-Fraile, P., Arranz Canales, E., Martín-Hernández, E., Ballesta-Martínez, M.J., Guillén-Navarro, E., Pintos-Morell, G., Moltó-Abad, M., Moreno-Martínez, D., García Morillo, S., Blasco-Alonso, J., Couce, M.L., Gil Sánchez, R., Cortès-Saladelafont, E., López Rodríguez, M.A., García-Silva, M.T., Morales Conejo, M., 2021. Clinical features and health-related quality of life in adult patients with mucopolysaccharidosis IVA: the Spanish experience. Orphanet J. Rare Dis. 16, 464. https://doi.org/10.1186/s13023-021-02074-y

Rabquer, B.J., Koch, A.E., 2013. NK4 therapy: a new approach to target angiogenesis and inflammation in rheumatoid arthritis. Arthritis Res. Ther. 15, 119. https://doi.org/10.1186/ar4320

Raisz, L.G., Rodan, G.A., 2003. Pathogenesis of osteoporosis. Endocrinol. Metab. Clin. North Am. 32, 15–24. https://doi.org/10.1016/s0889-8529(02)00055-5

Rajpar, I., Kumar, G., Fortina, P., Tomlinson, R.E., 2023. Toll-like receptor 4 signaling in osteoblasts is required for load-induced bone formation in mice. iScience 26, 106304. https://doi.org/10.1016/j.isci.2023.106304

Regier, D.S., Tifft, C.J., Rothermel, C.E., 1993. GLB1-Related Disorders, in: Adam, M.P., Everman, D.B., Mirzaa, G.M., Pagon, R.A., Wallace, S.E., Bean, L.J.,

Gripp, K.W., Amemiya, A. (Eds.), GeneReviews®. University of Washington, Seattle, Seattle (WA).

Richard, M., Arfi, A., Rhinn, H., Gandolphe, C., Scherman, D., 2008. Identification of new markers for neurodegeneration process in the mouse model of Sly disease as revealed by expression profiling of selected genes. J. Neurosci. Res. 86, 3285–3294. https://doi.org/10.1002/jnr.21779

Rivera-Colón, Y., Schutsky, E.K., Kita, A.Z., Garman, S.C., 2012. The structure of human GALNS reveals the molecular basis for mucopolysaccharidosis IV A. J. Mol. Biol. 423, 736. https://doi.org/10.1016/j.jmb.2012.08.020

Romas, E., Gillespie, M.T., Martin, T.J., 2002. Involvement of receptor activator of NFkappaB ligand and tumor necrosis factor-alpha in bone destruction in rheumatoid arthritis. Bone 30, 340–346. https://doi.org/10.1016/s8756-3282(01)00682-2

Rustad, C.F., Prescott, T.E., Merckoll, E., Kristensen, E., Salvador, C.L., Nordgarden, H., Tveten, K., 2022. Phenotypic expansion of ARSK-related mucopolysaccharidosis. Am. J. Med. Genet. A. 188, 3369–3373. https://doi.org/10.1002/ajmg.a.62934

Sachse, M., Urbé, S., Oorschot, V., Strous, G.J., Klumperman, J., 2002. Bilayered clathrin coats on endosomal vacuoles are involved in protein sorting toward lysosomes. Mol. Biol. Cell 13, 1313–1328. https://doi.org/10.1091/mbc.01-10-0525

Saftig, P., Klumperman, J., 2009. Lysosome biogenesis and lysosomal membrane proteins: trafficking meets function. Nat. Rev. Mol. Cell Biol. 10, 623–635. https://doi.org/10.1038/nrm2745

Saitoh, T., Fujita, N., Jang, M.H., Uematsu, S., Yang, B.-G., Satoh, T., Omori, H., Noda, T., Yamamoto, N., Komatsu, M., Tanaka, K., Kawai, T., Tsujimura, T., Takeuchi, O., Yoshimori, T., Akira, S., 2008. Loss of the autophagy protein Atg16L1 enhances endotoxin-induced IL-1beta production. Nature 456, 264–268. https://doi.org/10.1038/nature07383

Sardiello, M., Palmieri, M., di Ronza, A., Medina, D.L., Valenza, M., Gennarino, V.A., Di Malta, C., Donaudy, F., Embrione, V., Polishchuk, R.S., Banfi, S., Parenti, G., Cattaneo, E., Ballabio, A., 2009. A gene network regulating lysosomal biogenesis and function. Science 325, 473–477. https://doi.org/10.1126/science.1174447

Sasarman, F., Maftei, C., Campeau, P.M., Brunel-Guitton, C., Mitchell, G.A., Allard, P., 2016. Biosynthesis of glycosaminoglycans: associated disorders and

biochemical tests. J. Inherit. Metab. Dis. 39, 173–188. https://doi.org/10.1007/s10545-015-9903-z

Sawamoto, K., Álvarez González, J.V., Piechnik, M., Otero, F.J., Couce, M.L., Suzuki, Y., Tomatsu, S., 2020. Mucopolysaccharidosis IVA: Diagnosis, Treatment, and Management. Int. J. Mol. Sci. 21, 1517. https://doi.org/10.3390/ijms21041517

Sawamoto, K., Suzuki, Y., Mackenzie, W.G., Theroux, M.C., Pizarro, C., Yabe, H., Orii, K.E., Mason, R.W., Orii, T., Tomatsu, S., 2016. Current therapies for Morquio A syndrome and their clinical outcomes. Expert Opin. Orphan Drugs 4, 941–951. https://doi.org/10.1080/21678707.2016.1214572

Schmidt, B., Selmer, T., Ingendoh, A., Figurat, K.V., 1995. A novel amino acid modification in sulfatases that is defective in multiple sulfatase deficiency. Cell 82, 271–278. https://doi.org/10.1016/0092-8674(95)90314-3

Schulze, H., Kolter, T., Sandhoff, K., 2009. Principles of lysosomal membrane degradation: Cellular topology and biochemistry of lysosomal lipid degradation. Biochim. Biophys. Acta 1793, 674–683. https://doi.org/10.1016/j.bbamcr.2008.09.020

Schweighardt, B., Tompkins, T., Lau, K., Jesaitis, L., Qi, Y., Musson, D.G., Farmer, P., Haller, C., Shaywitz, A.J., Yang, K., O'Neill, C.A., 2015. Immunogenicity of Elosulfase Alfa, an Enzyme Replacement Therapy in Patients With Morquio A Syndrome: Results From MOR-004, a Phase III Trial. Clin. Ther. 37, 1012-1021.e6. https://doi.org/10.1016/j.clinthera.2014.11.005

Settembre, C., De Cegli, R., Mansueto, G., Saha, P.K., Vetrini, F., Visvikis, O., Huynh, T., Carissimo, A., Palmer, D., Klisch, T.J., Wollenberg, A.C., Di Bernardo, D., Chan, L., Irazoqui, J.E., Ballabio, A., 2013a. TFEB controls cellular lipid metabolism through a starvation-induced autoregulatory loop. Nat. Cell Biol. 15, 647–658. https://doi.org/10.1038/ncb2718

Settembre, C., Di Malta, C., Polito, V.A., Arencibia, M.G., Vetrini, F., Erdin, S., Erdin, S.U., Huynh, T., Medina, D., Colella, P., Sardiello, M., Rubinsztein, D.C., Ballabio, A., 2011. TFEB Links Autophagy to Lysosomal Biogenesis. Science 332, 1429–1433. https://doi.org/10.1126/science.1204592

Settembre, C., Fraldi, A., Jahreiss, L., Spampanato, C., Venturi, C., Medina, D., de Pablo, R., Tacchetti, C., Rubinsztein, D.C., Ballabio, A., 2008. A block of autophagy in lysosomal storage disorders. Hum. Mol. Genet. 17, 119–129. https://doi.org/10.1093/hmg/ddm289

Settembre, C., Fraldi, A., Medina, D.L., Ballabio, A., 2013b. Signals from the lysosome: a control centre for cellular clearance and energy metabolism. Nat. Rev. Mol. Cell Biol. 14, 283–296. https://doi.org/10.1038/nrm3565

Settembre, C., Zoncu, R., Medina, D.L., Vetrini, F., Erdin, Serkan, Erdin, SerpilUckac, Huynh, T., Ferron, M., Karsenty, G., Vellard, M.C., Facchinetti, V., Sabatini, D.M., Ballabio, A., 2012. A lysosome-to-nucleus signalling mechanism senses and regulates the lysosome via mTOR and TFEB. EMBO J. 31, 1095–1108. https://doi.org/10.1038/emboj.2012.32

Simonaro, C.M., D'Angelo, M., Haskins, M.E., Schuchman, E.H., 2005. Joint and Bone Disease in Mucopolysaccharidoses VI and VII: Identification of New Therapeutic Targets and BioMarkers Using Animal Models. Pediatr. Res. 57, 701–707. https://doi.org/10.1203/01.PDR.0000156510.96253.5A

Simonaro, C.M., D'Angelo, M., He, X., Eliyahu, E., Shtraizent, N., Haskins, M.E., Schuchman, E.H., 2008. Mechanism of glycosaminoglycan-mediated bone and joint disease: implications for the mucopolysaccharidoses and other connective tissue diseases. Am. J. Pathol. 172, 112–122. https://doi.org/10.2353/ajpath.2008.070564

Simonaro, C.M., Ge, Y., Eliyahu, E., He, X., Jepsen, K.J., Schuchman, E.H., 2010. Involvement of the Toll-like receptor 4 pathway and use of TNF-alpha antagonists for treatment of the mucopolysaccharidoses. Proc. Natl. Acad. Sci. U. S. A. 107, 222–227. https://doi.org/10.1073/pnas.0912937107

Simonaro, C.M., Haskins, M.E., Schuchman, E.H., 2001. Articular chondrocytes from animals with a dermatan sulfate storage disease undergo a high rate of apoptosis and release nitric oxide and inflammatory cytokines: a possible mechanism underlying degenerative joint disease in the mucopolysaccharidoses. Lab. Investig. J. Tech. Methods Pathol. 81, 1319–1328. https://doi.org/10.1038/labinvest.3780345

Sleat, D.E., Lackland, H., Wang, Y., Sohar, I., Xiao, G., Li, H., Lobel, P., 2005. The human brain mannose 6-phosphate glycoproteome: a complex mixture composed of multiple isoforms of many soluble lysosomal proteins. Proteomics 5, 1520–1532. https://doi.org/10.1002/pmic.200401054

Sly, W.S., Fischer, H.D., 1982. The phosphomannosyl recognition system for intracellular and intercellular transport of lysosomal enzymes. J. Cell. Biochem. 18, 67–85. https://doi.org/10.1002/jcb.1982.240180107

Song, L., Pei, L., Yao, S., Wu, Y., Shang, Y., 2017. NLRP3 Inflammasome in Neurological Diseases, from Functions to Therapies. Front. Cell. Neurosci. 11, 63. https://doi.org/10.3389/fncel.2017.00063

Spada, M., Pagliardini, S., Yasuda, M., Tukel, T., Thiagarajan, G., Sakuraba, H., Ponzone, A., Desnick, R.J., 2006. High incidence of later-onset fabry disease revealed by newborn screening. Am. J. Hum. Genet. 79, 31–40. https://doi.org/10.1086/504601

Standal, T., Abildgaard, N., Fagerli, U.-M., Stordal, B., Hjertner, Ø., Borset, M., Sundan, A., 2007. HGF inhibits BMP-induced osteoblastogenesis: possible implications for the bone disease of multiple myeloma. Blood 109, 3024–3030. https://doi.org/10.1182/blood-2006-07-034884

Sun, X., Chang, R., Tang, Y., Luo, S., Jiang, C., Jia, H., Xu, Q., Dong, Z., Liang, Y., Loor, J.J., Xu, C., 2021. Transcription factor EB (TFEB)-mediated autophagy protects bovine mammary epithelial cells against H2O2-induced oxidative damage in vitro. J. Anim. Sci. Biotechnol. 12, 35. https://doi.org/10.1186/s40104-021-00561-7

Suzuki, M., 1939. Biochemical Studies on Carbohydrates. J. Biochem. (Tokyo) 30, 185–191.

Takaishi, H., Kimura, T., Dalal, S., Okada, Y., D'Armiento, J., 2008. Joint Diseases and Matrix Metalloproteinases: A Role for MMP-13. Curr. Pharm. Biotechnol. 9, 47–54.

Taylor, M., Khan, S., Stapleton, M., Wang, J., Chen, J., Wynn, R., Yabe, H., Chinen, Y., Boelens, J.J., Mason, R.W., Kubaski, F., Horovitz, D.D.G., Barth, A.L., Serafini, M., Bernardo, M.E., Kobayashi, H., Orii, K.E., Suzuki, Y., Orii, T., Tomatsu, S., 2019. Hematopoietic stem cell transplantation for mucopolysaccharidoses; past, present, and future. Biol. Blood Marrow Transplant. J. Am. Soc. Blood Marrow Transplant. 25, e226–e246. https://doi.org/10.1016/j.bbmt.2019.02.012

Taylor, R.M., Kashima, T.G., Knowles, H.J., Athanasou, N.A., 2012. VEGF, FLT3 ligand, PlGF and HGF can substitute for M-CSF to induce human osteoclast formation: implications for giant cell tumour pathobiology. Lab. Investig. J. Tech. Methods Pathol. 92, 1398–1406. https://doi.org/10.1038/labinvest.2012.108

Terai, H., Nakamura, H., 2020. Surgical Management of Spinal Disorders in People with Mucopolysaccharidoses. Int. J. Mol. Sci. 21, 1171. https://doi.org/10.3390/ijms21031171

Termeer, C., Benedix, F., Sleeman, J., Fieber, C., Voith, U., Ahrens, T., Miyake, K., Freudenberg, M., Galanos, C., Simon, J.C., 2002. Oligosaccharides of Hyaluronan activate dendritic cells via toll-like receptor 4. J. Exp. Med. 195, 99–111. https://doi.org/10.1084/jem.20001858

Terzioglu, M., Tokatli, A., Coskun, T., Emre, S., 2002. Molecular analysis of Turkish mucopolysaccharidosis IVA (Morquio A) patients: identification of novel mutations in the N-acetylgalactosamine-6-sulfate sulfatase (GALNS) gene. Hum. Mutat. 20, 477–478. https://doi.org/10.1002/humu.9088

Tessitore, A., del P Martin, M., Sano, R., Ma, Y., Mann, L., Ingrassia, A., Laywell, E.D., Steindler, D.A., Hendershot, L.M., d'Azzo, A., 2004. GM1-ganglioside-mediated activation of the unfolded protein response causes neuronal death in a neurodegenerative gangliosidosis. Mol. Cell 15, 753–766. https://doi.org/10.1016/j.molcel.2004.08.029

Tessitore, A., Pirozzi, M., Auricchio, A., 2009. Abnormal autophagy, ubiquitination, inflammation and apoptosis are dependent upon lysosomal storage and are useful biomarkers of mucopolysaccharidosis VI. PathoGenetics 2, 4. https://doi.org/10.1186/1755-8417-2-4

Thümler, A., Miebach, E., Lampe, C., Pitz, S., Kamin, W., Kampmann, C., Link, B., Mengel, E., 2012. Clinical characteristics of adults with slowly progressing mucopolysaccharidosis VI: a case series. J. Inherit. Metab. Dis. 35, 1071–1079. https://doi.org/10.1007/s10545-012-9474-1

Tillerson, J.L., Miller, G.W., 2003. Grid performance test to measure behavioral impairment in the MPTP-treated-mouse model of parkinsonism. J. Neurosci. Methods 123, 189–200. https://doi.org/10.1016/S0165-0270(02)00360-6

Tomatsu, S., Averill, L.W., Sawamoto, K., Mackenzie, W.G., Bober, M.B., Pizarro, C., Goff, C.J., Xie, L., Orii, T., Theroux, M., 2016. Obstructive airway in Morquio A syndrome, the past, the present and the future. Mol. Genet. Metab. 117, 150–156. https://doi.org/10.1016/j.ymgme.2015.09.007

Tomatsu, S., Filocamo, M., Orii, K.O., Sly, W.S., Gutierrez, M.A., Nishioka, T., Serrato, O.P., Di Natale, P., Montaño, A.M., Yamaguchi, S., Kondo, N., Orii, T., Noguchi, A., 2004. Mucopolysaccharidosis IVA (Morquio A): identification of novel common mutations in the N-acetylgalactosamine-6-sulfate sulfatase (GALNS) gene in Italian patients. Hum. Mutat. 24, 187–188. https://doi.org/10.1002/humu.9265

Tomatsu, S., Fukuda, S., Cooper, A., Wraith, J.E., Rezvi, G.Md.M., Yamagishi, A., Yamada, N., Kato, Z., Isogai, K., Sukegawa, K., Kondo, N., Suzuki, Y., Shimozawa, N., Orii, T., 1995. Mucopolysaccharidosis IVA: Identification of a Common Missense Mutation I113F in the N-Acetylgalactosamine-6-Sulfate Sulfatase Gene. Am. J. Hum. Genet. 57, 556–563.

Tomatsu, S., Gutierrez, M., Nishioka, T., Yamada, Masamichi, Yamada, Mana, Tosaka, Y., Grubb, J.H., Montaño, A.M., Vieira, M.B., Trandafirescu, G.G.,

Peña, O.M., Yamaguchi, S., Orii, K.O., Orii, T., Noguchi, A., Laybauer, L., 2005. Development of MPS IVA mouse (Galnstm(hC79S·mC76S)slu) tolerant to human N-acetylgalactosamine-6-sulfate sulfatase. Hum. Mol. Genet. 14, 3321–3335. https://doi.org/10.1093/hmg/ddi364

Tomatsu, S., Montaño, A.M., Dung, V.C., Ohashi, A., Oikawa, H., Oguma, T., Orii, T., Barrera, L., Sly, W.S., 2010. Enhancement of Drug Delivery: Enzyme-replacement Therapy for Murine Morquio A Syndrome. Mol. Ther. 18, 1094–1102. https://doi.org/10.1038/mt.2010.32

Tomatsu, S., Montaño, A.M., Oikawa, H., Smith, M., Barrera, L., Chinen, Y., Thacker, M.M., Mackenzie, W.G., Suzuki, Y., Orii, T., 2011. Mucopolysaccharidosis type IVA (Morquio A disease): clinical review and current treatment. Curr. Pharm. Biotechnol. 12, 931–945. https://doi.org/10.2174/138920111795542615

Tomatsu, S., Orii, K.O., Vogler, C., Nakayama, J., Levy, B., Grubb, J.H., Gutierrez, M.A., Shim, S., Yamaguchi, S., Nishioka, T., Montano, A.M., Noguchi, A., Orii, T., Kondo, N., Sly, W.S., 2003. Mouse model of N-acetylgalactosamine-6-sulfate sulfatase deficiency (Galns-/-) produced by targeted disruption of the gene defective in Morquio A disease. Hum. Mol. Genet. 12, 3349–3358. https://doi.org/10.1093/hmg/ddg366

Tomatsu, S., Pitz, S., Hampel, U., 2019. Ophthalmological Findings in Mucopolysaccharidoses. J. Clin. Med. 8, 1467. https://doi.org/10.3390/jcm8091467

Tomatsu, S., Sawamoto, K., Alméciga-Díaz, C.J., Shimada, T., Bober, M.B., Chinen, Y., Yabe, H., Montaño, A.M., Giugliani, R., Kubaski, F., Yasuda, E., Rodríguez-López, A., Espejo-Mojica, A.J., Sánchez, O.F., Mason, R.W., Barrera, L.A., Mackenzie, W.G., Orii, T., 2015a. Impact of enzyme replacement therapy and hematopoietic stem cell transplantation in patients with Morquio A syndrome. Drug Des. Devel. Ther. 9, 1937–1953. https://doi.org/10.2147/DDDT.S68562

Tomatsu, S., Sawamoto, K., Shimada, T., Bober, M.B., Kubaski, F., Yasuda, E., Mason, R.W., Khan, S., Alméciga-Díaz, C.J., Barrera, L.A., Mackenzie, W.G., Orii, T., 2015b. Enzyme replacement therapy for treating mucopolysaccharidosis type IVA (Morquio A syndrome): effect and limitations. Expert Opin. Orphan Drugs 3, 1279–1290. https://doi.org/10.1517/21678707.2015.1086640

Tomatsu, S., Vogler, C., Montaño, A.M., Gutierrez, M., Oikawa, H., Dung, V.C., Orii, T., Noguchi, A., Sly, W.S., 2007. Murine model (Galns(tm(C76S)slu)) of MPS IVA with missense mutation at the active site cysteine conserved among

sulfatase proteins. Mol. Genet. Metab. 91, 251–258. https://doi.org/10.1016/j.ymgme.2007.02.009

Tomatsu, S., Yasuda, E., Patel, P., Ruhnke, K., Shimada, T., Mackenzie, W.G., Mason, R., Thacker, M.M., Theroux, M., Montaño, A.M., Alméciga-Díaz, C.J., Barrera, L.A., Chinen, Y., Sly, W.S., Rowan, D., Suzuki, Y., Orii, T., 2014. Morquio A syndrome: diagnosis and current and future therapies. Pediatr. Endocrinol. Rev. PER 12 Suppl 1, 141–151.

Tonomura, H., Nagae, M., Takatori, R., Ishibashi, H., Itsuji, T., Takahashi, K., 2020. The Potential Role of Hepatocyte Growth Factor in Degenerative Disorders of the Synovial Joint and Spine. Int. J. Mol. Sci. 21, 8717. https://doi.org/10.3390/ijms21228717

Trivedi, P.C., Bartlett, J.J., Pulinilkunnil, T., 2020. Lysosomal Biology and Function: Modern View of Cellular Debris Bin. Cells 9, 1131. https://doi.org/10.3390/cells9051131

Tsubaki, M., Seki, S., Takeda, T., Chihara, A., Arai, Y., Morii, Y., Imano, M., Satou, T., Shimomura, K., Nishida, S., 2020. The HGF/Met/NF-κB Pathway Regulates RANKL Expression in Osteoblasts and Bone Marrow Stromal Cells. Int. J. Mol. Sci. 21, 7905. https://doi.org/10.3390/ijms21217905

Uchimura, K., 2015. Keratan sulfate: biosynthesis, structures, and biological functions. Methods Mol. Biol. Clifton NJ 1229, 389–400. https://doi.org/10.1007/978-1-4939-1714-3_30

Uesaka, S., Miyazaki, K., Ito, H., 2004. Age-related changes and sex differences in chondroitin sulfate isomers and hyaluronic acid in normal synovial fluid. Mod. Rheumatol. 14, 470–475. https://doi.org/10.3109/s10165-004-0351-0

van den Broek, B.T.A., Lindemans, C.A., Boelens, J.J., Delemarre, E.M., Drylewicz, J., Verhoeven-Duif, N., van Hasselt, P.M., Nierkens, S., 2021. Long-term effect of hematopoietic cell transplantation on systemic inflammation in patients with mucopolysaccharidoses. Blood Adv. 5, 3092–3101. https://doi.org/10.1182/bloodadvances.2020003824

van Hoof, F., 1974. Mucopolysaccharidoses and mucolipidoses. J. Clin. Pathol. 27, 64–93. https://doi.org/10.1136/jcp.27.Suppl_8.64

van Meel, E., Klumperman, J., 2008. Imaging and imagination: understanding the endo-lysosomal system. Histochem. Cell Biol. 129, 253–266. https://doi.org/10.1007/s00418-008-0384-0

Vellodi, A., Young, E., Cooper, A., Lidchi, V., Winchester, B., Wraith, J.E., 1999. Long-term follow-up following bone marrow transplantation for Hunter disease. J. Inherit. Metab. Dis. 22, 638–648. https://doi.org/10.1023/A:1005525931994

Venn, G., Mason, R.M., 1985. Absence of keratan sulphate from skeletal tissues of mouse and rat. Biochem. J. 228, 443–450. https://doi.org/10.1042/bj2280443

Verheyen, S., Blatterer, J., Speicher, M.R., Bhavani, G.S., Boons, G.-J., Ilse, M.-B., Andrae, D., Sproß, J., Vaz, F.M., Kircher, S.G., Posch-Pertl, L., Baumgartner, D., Lübke, T., Shah, H., Kaissi, A.A., Girisha, K.M., Plecko, B., 2022. Novel subtype of mucopolysaccharidosis caused by arylsulfatase K (ARSK) deficiency. J. Med. Genet. 59, 957–964. https://doi.org/10.1136/jmedgenet-2021-108061

Villani, G.R.D., Chierchia, A., Di Napoli, D., Di Natale, P., 2012. Unfolded protein response is not activated in the mucopolysaccharidoses but protein disulfide isomerase 5 is deregulated. J. Inherit. Metab. Dis. 35, 479–493. https://doi.org/10.1007/s10545-011-9403-8

Visigalli, I., Delai, S., Politi, L.S., Di Domenico, C., Cerri, F., Mrak, E., D'Isa, R., Ungaro, D., Stok, M., Sanvito, F., Mariani, E., Staszewsky, L., Godi, C., Russo, I., Cecere, F., del Carro, U., Rubinacci, A., Brambilla, R., Quattrini, A., Di Natale, P., Ponder, K., Naldini, L., Biffi, A., 2010. Gene therapy augments the efficacy of hematopoietic cell transplantation and fully corrects mucopolysaccharidosis type I phenotype in the mouse model. Blood 116, 5130–5139. https://doi.org/10.1182/blood-2010-04-278234

Vitner, E.B., Farfel-Becker, T., Ferreira, N.S., Leshkowitz, D., Sharma, P., Lang, K.S., Futerman, A.H., 2016. Induction of the type I interferon response in neurological forms of Gaucher disease. J. Neuroinflammation 13, 104. https://doi.org/10.1186/s12974-016-0570-2

Vitner, E.B., Platt, F.M., Futerman, A.H., 2010. Common and Uncommon Pathogenic Cascades in Lysosomal Storage Diseases. J. Biol. Chem. 285, 20423–20427. https://doi.org/10.1074/jbc.R110.134452

Voskoboeva, E., Semyachkina, A., Miklyaev, O., Gamzatova, A., Mikhaylova, S., Vashakmadze, N., Baydakova, G., Omzar, O., Pichkur, N., Zakharova, E., Kutsev, S., 2022. Epidemiology and Genetics of Mucopolysaccharidosis Type VI in Russia. Front. Mol. Biosci. 8.

Wagner, V.F., Northrup, H., 1993. Mucopolysaccharidosis Type III, in: Adam, M.P., Mirzaa, G.M., Pagon, R.A., Wallace, S.E., Bean, L.J., Gripp, K.W., Amemiya, A. (Eds.), GeneReviews®. University of Washington, Seattle, Seattle (WA).

Walkley, S.U., 2004. Secondary accumulation of gangliosides in lysosomal storage disorders. Semin. Cell Dev. Biol. 15, 433–444. https://doi.org/10.1016/j.semcdb.2004.03.002

Wang, J.Y., Roehrl, M.H., 2002. Glycosaminoglycans are a potential cause of rheumatoid arthritis. Proc. Natl. Acad. Sci. 99, 14362–14367. https://doi.org/10.1073/pnas.222536599

Wang, W., Rigueur, D., Lyons, K.M., 2014. TGFβ Signaling in Cartilage Development and Maintenance. Birth Defects Res. Part C Embryo Today Rev. 102, 37–51. https://doi.org/10.1002/bdrc.21058

Wasserstein, M.P., Caggana, M., Bailey, S.M., Desnick, R.J., Edelmann, L., Estrella, L., Holzman, I., Kelly, N.R., Kornreich, R., Kupchik, S.G., Martin, M., Nafday, S.M., Wasserman, R., Yang, A., Yu, C., Orsini, J.J., 2019. The New York pilot newborn screening program for lysosomal storage diseases: Report of the First 65,000 Infants. Genet. Med. Off. J. Am. Coll. Med. Genet. 21, 631–640. https://doi.org/10.1038/s41436-018-0129-y

Wei, H., Kim, S.-J., Zhang, Z., Tsai, P.-C., Wisniewski, K.E., Mukherjee, A.B., 2008. ER and oxidative stresses are common mediators of apoptosis in both neurodegenerative and non-neurodegenerative lysosomal storage disorders and are alleviated by chemical chaperones. Hum. Mol. Genet. 17, 469–477. https://doi.org/10.1093/hmg/ddm324

Wei, X., Gao, J., Messner, K., 1996. Concentrations of proteoglycan fragments in relation to maturation, sex and time of day: physiologic variations in knee joint fluid of rabbits. Acta Orthop. Scand. 67, 185–188. https://doi.org/10.3109/17453679608994669

Wen, C.-Y., Wu, C.-B., Tang, B., Wang, T., Yan, C.-H., Lu, W.W., Pan, H., Hu, Y., Chiu, K.-Y., 2012. Collagen fibril stiffening in osteoarthritic cartilage of human beings revealed by atomic force microscopy. Osteoarthritis Cartilage 20, 916–922. https://doi.org/10.1016/j.joca.2012.04.018

Weyers, A., Yang, B., Solakyildirim, K., Yee, V., Li, L., Zhang, F., Linhardt, R.J., 2013. Isolation of bovine corneal keratan sulfate and its growth factor and morphogen binding. FEBS J. 280, 2285–2293. https://doi.org/10.1111/febs.12165

Wiesinger, A.-M., Bigger, B., Giugliani, R., Scarpa, M., Moser, T., Lampe, C., Kampmann, C., Lagler, F.B., 2022. The Inflammation in the Cytopathology of Patients With Mucopolysaccharidoses- Immunomodulatory Drugs as an Approach to Therapy. Front. Pharmacol. 13, 863667. https://doi.org/10.3389/fphar.2022.863667

Wilkinson, F.L., Holley, R.J., Langford-Smith, K.J., Badrinath, S., Liao, A., Langford-Smith, A., Cooper, J.D., Jones, S.A., Wraith, J.E., Wynn, R.F., Merry, C.L.R., Bigger, B.W., 2012. Neuropathology in mouse models of

mucopolysaccharidosis type I, IIIA and IIIB. PloS One 7, e35787. https://doi.org/10.1371/journal.pone.0035787

Wood, T.C., Harvey, K., Beck, M., Burin, M.G., Chien, Y.-H., Church, H.J., D'Almeida, V., van Diggelen, O.P., Fietz, M., Giugliani, R., Harmatz, P., Hawley, S.M., Hwu, W.-L., Ketteridge, D., Lukacs, Z., Miller, N., Pasquali, M., Schenone, A., Thompson, J.N., Tylee, K., Yu, C., Hendriksz, C.J., 2013. Diagnosing mucopolysaccharidosis IVA. J. Inherit. Metab. Dis. 36, 293–307. https://doi.org/10.1007/s10545-013-9587-1

Woychik, N.A., Cardelli, J.A., Dimond, R.L., 1986. A conformationally altered precursor to the lysosomal enzyme alpha-mannosidase accumulates in the endoplasmic reticulum in a mutant strain of Dictyostelium discoideum. J. Biol. Chem. 261, 9595–9602.

Wraith, J.E., Scarpa, M., Beck, M., Bodamer, O.A., De Meirleir, L., Guffon, N., Meldgaard Lund, A., Malm, G., Van der Ploeg, A.T., Zeman, J., 2008. Mucopolysaccharidosis type II (Hunter syndrome): a clinical review and recommendations for treatment in the era of enzyme replacement therapy. Eur. J. Pediatr. 167, 267–277. https://doi.org/10.1007/s00431-007-0635-4

Xue, M., McKelvey, K., Shen, K., Minhas, N., March, L., Park, S.-Y., Jackson, C.J., 2014. Endogenous MMP-9 and not MMP-2 promotes rheumatoid synovial fibroblast survival, inflammation and cartilage degradation. Rheumatology 53, 2270–2279. https://doi.org/10.1093/rheumatology/keu254

Yabe, H., Tanaka, A., Chinen, Y., Kato, S., Sawamoto, K., Yasuda, E., Shintaku, H., Suzuki, Y., Orii, T., Tomatsu, S., 2016. Hematopoietic stem cell transplantation for Morquio A syndrome. Mol. Genet. Metab. 117, 84–94. https://doi.org/10.1016/j.ymgme.2015.09.011

Yamada, Y., Kato, K., Sukegawa, K., Tomatsu, S., Fukuda, S., Emura, S., Kojima, S., Matsuyama, T., Sly, W.S., Kondo, N., Orii, T., 1998. Treatment of MPS VII (Sly disease) by allogeneic BMT in a female with homozygous A619V mutation. Bone Marrow Transplant. 21, 629–634. https://doi.org/10.1038/sj.bmt.1701141

Yang, J., LeBlanc, F.R., Dighe, S.A., Hamele, C.E., Olson, T.L., Feith, D.J., Loughran, T.P., 2018. TRAIL mediates and sustains constitutive NF-κB activation in LGL leukemia. Blood 131, 2803–2815. https://doi.org/10.1182/blood-2017-09-808816

Yasuda, E., Mackenzie, W., Ruhnke, K., Shimada, T., Mason, R.W., Zustin, J., Martin, P.L., Thacker, M., Orii, T., Sai, Y., Tomatsu, S., 2015. Molecular Genetics and Metabolism Report Long-term follow-up of post hematopoietic stem cell

transplantation for Hurler syndrome: clinical, biochemical, and pathological improvements. Mol. Genet. Metab. Rep. 2, 65–76. https://doi.org/10.1016/j.ymgmr.2014.12.006

Yasuda, E., Suzuki, Y., Shimada, T., Sawamoto, K., Mackenzie, W.G., Theroux, M.C., Pizarro, C., Xie, L., Miller, F., Rahman, T., Kecskemethy, H.H., Nagao, K., Morlet, T., Shaffer, T.H., Chinen, Y., Yabe, H., Tanaka, A., Shintaku, H., Orii, K.E., Orii, K.O., Mason, R.W., Montaño, A.M., Fukao, T., Orii, T., Tomatsu, S., 2016. Activity of daily living for Morquio A syndrome. Mol. Genet. Metab. 118, 111–122. https://doi.org/10.1016/j.ymgme.2016.04.005

Yogalingam, G., Hopwood, J.J., 2001. Molecular genetics of mucopolysaccharidosis type IIIA and IIIB: Diagnostic, clinical, and biological implications. Hum. Mutat. 18, 264–281. https://doi.org/10.1002/humu.1189

Yoshihara, Y., Nakamura, H., Obata, K., Yamada, H., Hayakawa, T., Fujikawa, K., Okada, Y., 2000. Matrix metalloproteinases and tissue inhibitors of metalloproteinases in synovial fluids from patients with rheumatoid arthritis or osteoarthritis. Ann. Rheum. Dis. 59, 455–461. https://doi.org/10.1136/ard.59.6.455

Zanetti, A., D'Avanzo, F., AlSayed, M., Brusius-Facchin, A.C., Chien, Y., Giugliani, R., Izzo, E., Kasper, D.C., Lin, H., Lin, S., Pollard, L., Singh, A., Tonin, R., Wood, T., Morrone, A., Tomanin, R., 2021. Molecular basis of mucopolysaccharidosis IVA (Morquio A syndrome): A review and classification of GALNS gene variants and reporting of 68 novel variants. Hum. Mutat. 42, 1384–1398. https://doi.org/10.1002/humu.24270

Zhang, Y.-P., Liu, Y.-Z., Guo, Y., Liu, X.-G., Xu, X.-H., Guo, Y.-F., Chen, Y., Zhang, F., Pan, F., Zhu, X.-Z., Deng, H.-W., 2011. Pathway-Based Association Analyses Identified TRAIL Pathway for Osteoporotic Fractures. PLOS ONE 6, e21835. https://doi.org/10.1371/journal.pone.0021835

Zhou, J., Lin, J., Leung, W.T., Wang, L., 2020. A basic understanding of mucopolysaccharidosis: Incidence, clinical features, diagnosis, and management. Intractable Rare Dis. Res. 9, 1–9. https://doi.org/10.5582/irdr.2020.01011

Zilberman, U., Bibi, H., 2016. The Effect of Multiple Sulfatase Deficiency (MSD) on Dental Development: Can We Use the Teeth as an Early Diagnostic Tool? JIMD Rep. 30, 95–101. https://doi.org/10.1007/8904_2015_523

